CHALMERS
UNIVERSITY OF TECHNOLOGY

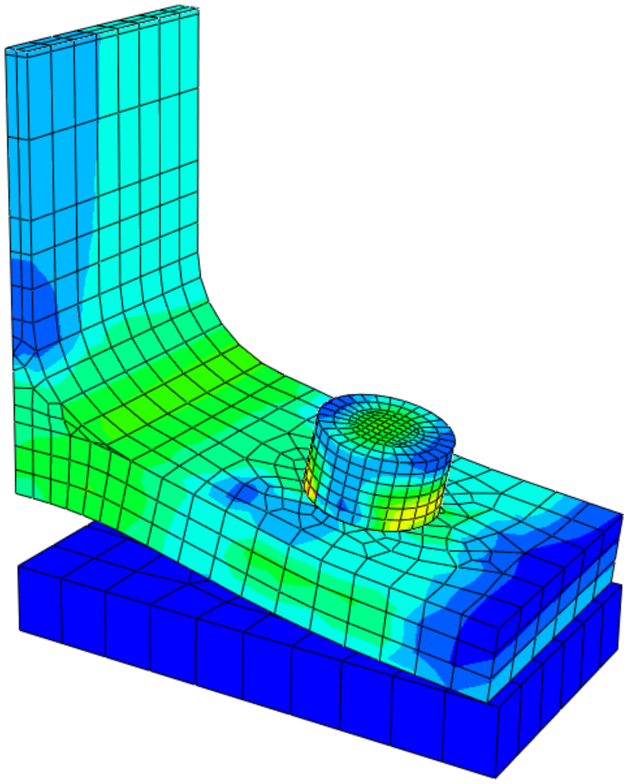

Finite Element Analysis of T-stub Components in Tension

A study of model parameters and their influence on time and accuracy

Master's Thesis in Master Program Structural Engineering and Building Technology

FELIX DUBREFJORD
OLE NETEK

Department of Architecture and Civil Engineering
CHALMERS UNIVERSITY OF TECHNOLOGY
Master's thesis ACEX30-19-43
Gothenburg, Sweden 2019

MASTER'S THESIS ACEX30-19-43

Finite Element Analysis of T-stub Components in Tension

A study of model parameters and their influence on time and accuracy

Master's Thesis in Master's Programme Structural Engineering and Building Technology

FELIX DUBREFJORD
OLE NETEK

Department of Architecture and Civil Engineering
Division of Structural Engineering
Lightweight Structures
CHALMERS UNIVERSITY OF TECHNOLOGY
Gothenburg, Sweden 2019

Finite Element Analysis of T-stub Components in Tension
A study of model parameters and their influence on time and accuracy
Master's Thesis in Master's Programme Structural Engineering and Building Technology
FELIX DUBREFJORD
OLE NETEK

Supervisor: David Wesley, Structural Engineer at ÅF Infrastructure AB - Buildings
Examiner: Professor Mohammad Al-Emrani, Department of Architecture and Civil Engineering

Master's Thesis ACEX30-19-43
Department of Architecture and Civil Engineering
Division of Structural Engineering
Lightweight Structures
Chalmers University of Technology
SE-412 96 Gothenburg
Telephone +46 31 772 22 58

Cover: An illustration of a T-stub in tension modelled in Abaqus/CAE.

Typeset in LaTeX

Department of Architecture and Civil Engineering
Gothenburg, Sweden 2019

Finite Element Analysis of T-stub Components in Tension
A study of model parameters and their influence on time and accuracy
Master's Thesis in Master's Programme Structural Engineering and Building Technology
FELIX DURBREFJORD
OLE NETEK

Structural Engineering and Building Technology
Chalmers University of Technology

Abstract

Connections are essential in every kind of structure. For the tension-zone of a bolted steel joint, most interesting to assess is the ultimate load capacity. Moreover, does the choice of design procedure depend on the time effort and thereby to the designers preference. A finite element analysis can be used, but can also be required, during the design of bolted steel joints. It can help to examine local effects further within a joint and can be a counterpoise to the lack of experimental results. Nevertheless, no clear guidance exists in the present EN 1993 about the setup of such a FE-model.

This degree project should give an insight into finite element modelling of bolted steel joints, more precisely T-stub components in tension, and the corresponding theoretical background. It should provide greater knowledge about FE-parameters in general, their influence on computational time and ultimate load, as well as how geometrical changes affect the computational time and the T-stubs behavior.

A scientific literature review is performed w.r.t. finite element modelling of bolted steel connections. Followed by, remodelling of two existing models from literature according to the corresponding set-up of geometry and FE-parameters. Continuing with a study of FE-parameters w.r.t. running time and load accuracy. Finally, the influence of geometrical changes on running time are compared with dimensional adjustments of the original specimen and simultaneously the failure mode progression in the FE-models are studied and compared to EC-formulation.

Results are presented in form of load-displacement curves, displaying relevant events, accompanied with more details in tables about the FE-model's running time and ultimate load accuracy. Through this, an insight for further modelling of components in tension is provided. While different FE-parameters have a significant influence on computational time, the collapse load is barely affected.

Keywords: Steel structures, Bolted steel connections, Equivalent T-stub method, FE-modelling, FE-implementation, FE-parameters, EN 1993-1-8, Failure mode transition, Ultimate capacity, Time efficiency

Finita Elementanalys av T-stycke-komponenter utsatta för Drag
En studie av modellparametrar och deras inverkan på tid och exakthet
Examensarbete inom masterprogrammet för Konstruktionsteknik och Byggnadsteknologi

FELIX DURBREFJORD
OLE NETEK

Structural Engineering and Building Technology
Chalmers Tekniska Högskola

Sammanfattning

Anslutningar är nödvändiga i alla slags strukturer. För området belastad av drag hos en bultad anslutning, är det mest intressanta att bedöma lastkapaciteten. Vidare beror valet av beräkningsmetod på tidsåtgången och därför med hänsyn till ingenjörens preferens. En finit elementanalys kan användas men också krävas för beräkning av bultade stålanslutningar. Den kan visa lokala effekter i anslutningen och väga upp för bristen av experimentella resultat. Trots detta finns det ingen tydlig vägledning i nuvarande version av EN 1993 gällande upprättandet av en sådan modell.

Detta examensarbete ska ge insikt i finit elementmodellering av bultade anslutningar, i form av T-stycken, belastade med dragspänning. Det bör ge ökad kunskap om FE-parametrar i allmänhet, deras inflytande på beräkningstid och maximal kapacitet samt hur geometriska förändringar påverkar beräkningstiden och mekaniska beteendet.

En vetenskaplig litteraturstudie utförs med hänsyn till modellering av bultade stålanslutningar i FEM. Därefter sker en återuppbyggnad av två existerande modeller från litteratur enligt motsvarande geometri och FE-parametrar. Fortsatt med en studie av FE-parametrar med hänsyn till beräkningstid och kapacitet. Slutligen jämförs inverkan av geometriska förändringar på körtid med hänsyn till originalmodellen och samtidigt jämförs brottmodernas förändring i modellerna med formulering enligt Eurocode.

Resultaten presenteras i form av last-förskjutningsgrafer med relevanta händelser tillsammans med ytterligare detaljer i tabeller berörande FE-modellens körtid och ultimata kapacitet. Genom detta tillhandahålls en inblick i vidare modellering av komponenter i drag. Medan olika FE-parametrar har en stor effekt på beräkningstiden, påverkas knappt lastkapaciteten.

Keywords: Stålkonstruktioner, Bultade stålanslutningar, Ekvivalent T-stycke, FE-modellering, FE-realisering, FE-parametrar, EN 1993-1-8, Brottmodsövergång, Maximal bärförmåga, Tidseffektivitet

Contents

Preface

This master's thesis, with main purpose to investigate time influence of FE-parameters, was carried out with the Division of Structural Engineering at Chalmers University of Technology in co-operation with the Division of Structural Building Engineering at ÅF. The work was mainly carried out at the ÅF office in Gothenburg with a start in January 2019. Project progressed for five months and corresponds to 30 higher education credits.

We especially would like to thank our supervisor David Wesley for his great and continuous support over the whole project. His helpful suggestions and curiosity helped the work develop and also gave us increased understanding of practical implementation. Furthermore, we would also like to thank Mohammad Al-Emrani, supervisor and examiner, for his precise comments regarding the project's progress as well as the provided research documentation.

In addition, we would like to thank Malin Holmström Ivarsson and Jenny Berglund for their constructive criticism of our thesis so that it can be perceived more clearly for an external reader.

Felix Dubrefjord & Ole Netek, Gothenburg, June 2019

Nomenclature

The list describes letters, abbreviations and regulations mentioned in the document.

Upper case letters

$\tilde{S}$	Stress tensor for a certain point
A_c	Gross cross-sectional area for bolt shank
A_s	Effective cross-sectional area for threaded bolt shank
B_s	Bolt thread stripping capacity
C_{WH}	Work hardening coefficient
E	Modulus of elasticity of steel
E_d	Internal dissipated energy
F_v	Shear resistance per shear plane
$F_{T.Rd}$	Design moment of a T-stub flange
$F_{t.Rd}$	Tension resistance for bolt
I_i	Second moment of area of member i
K_i	Bolt geometry parameters
L_i	System length of member i
L_{bolt}	Agerskov's effective length of bolt
$M_{j,Rd}$	Design moment resistance of a joint
$M_{pl.Rd}$	Plastic resistance moment
P	General load
Q	Prying force
S_j	Rotational stiffness for joint
W	External energy
W_{pl}	Plastic moment resistance

Lower case letters

b_i	General notation of width for member i
d_1	Effective diameter of bolt shank

e_1	Distance between bolt axis and outer end in direction of load
e_2	Distance between bolt axis and outer edge perpendicular to load direction
f_u	Material's ultimate strength
f_y	Material's yield strength
f_{ub}	Bolt's ultimate strength
f_{yb}	Bolt's yield strength
g	Gravitational Constant
k_i	General stiffness factor for member i
l	Length of the respective yield-line
l_i	Length of different components related Agerskov's expression
l_{eff}	Effective length of an equivalent T-stub
m	Distance between bolt axis and flange-to-web connection
m_f	Plastic field moment of resistance
m_s	Plastic support moment of resistance
m_{pl}	Plastic moment resistance per width
n	Distance between bolt axis and flange edge
n_i	Normal vector with index
p	Distance between bolt axis' for multiple bolt rows
p_t	Bolt's thread pitch
q	Uniform load
r	Radius
t_f	Flange thickness
z	Amount of active threads

Greek letters

β	Circular angle
δ	Displacement
ϵ	Conventional strain
ϵ_y	Strain at yield point
ϵ_{true}	True strain
γ_{M0}	Partial safety factor
γ_{M2}	Partial safety factor - Resistance of bolts, rivets, pins & welds
ν	Poisson's ratio
ϕ	Angle of rotation at joint
ρ	Material density
σ	Nominal stress
σ_i	Normal stress in i-direction
$\sigma_{e,VM}$	Von Mises stress from stress components

σ_{true}	True stress
σ_{VM}	Von Mises stress from principal stress
τ_i	Shear stress in i-direction
θ	Rotation angle

Abbreviations

FE	Finite element
FEA	Finite element analysis
FEM	Finite element method
SLS	Serviceability limit state
ULS	Ultimate limit state
VPN	Virtual private network
F-d	Force-deflection
C3D8	8-node linear brick in Abaqus/CAE
C3D8R	8-node linear brick, reduced integration, hourglass control
C3D8I	8-node linear brick, incompatible modes
C3D20	20-node quadratic brick
C3D20R	20-node quadratic brick, reduced integration

Codes and regulations

EN 1993-1-1 Design of steel structures - General rules and rules for buildings
EN 1993-1-5 Design of steel structures - Plated structural elements
EN 1993-1-8 Design of steel structures - Design of joints

List of Figures

List of Tables

1 Introduction

Several design procedures exist to acquire the ultimate capacity of a bolted steel connection. The choice of design procedure depends on the time effort and thereby to the designers preference. Finite element models are widely used and can be applicable to several engineering problems. In particular, where a 2D visualization of a problem does not fully represent reality or when the amount of analyses are extensive (Díaz et al., 2011).

Moreover, finite element analyses should represent the reality in an accurate way while not being too time consuming to be set up and run. That means appropriate parameters and phenomena, such as element types or loading procedure, should be compiled in a way suitable to the problem at hand, so that the discrepancy between reality and model is sufficiently small. An oversimplified FE-model might give miss-leading results, which makes the accuracy of the FE-model very much dependent on the user's expertise (Shah, 2002). A FE-model with wrong representation of reality (such as boundary conditions) can be solved correctly with FEA, but will thereby provide inaccurate results. Therefore one needs understanding about FE-parameters and their influence on time to execute the procedure effectively. When these conditions are met, the possibility to analyze larger amount of T-stubs with less user modification opens up.

For the tension zone of bolted steel connections analytical approaches, provided by Eurocode or tabulated values, are mostly used to get the ultimate tensile capacity. EN 1993-1-5 (CEN, 2006) presents brief information about few parameters to be considered when performing a FEA. However, when a finite element analysis is demanded, no comprehensive regulations exist for how such FE-model should be set up to obtain an accurate outcome within a reasonable time.

1.1 Background

Connections are essential in every kind of structure. McLain (1998) states, ”A structure is a constructed assembly of joints separated by members” which implies the importance of connections. Joints enable force paths between structural members, such as a ”simple” beam-column connection or a more advanced 3D space truss. The isotropic property of steel empowers joints with higher flexibility and thereby a broader area of application.

For the tension-zone of a bolted steel joint, the most interesting to assess is the ultimate load capacity. There exist different design approaches to obtain the ultimate capacity of a tension-zone of a steel joint, both numerical and analytical methods. Depending on the joint configuration, different approaches can be favourable in terms of time.

One analytic method provided in chapter 6 of EN 1993-1-8 (CEN, 2005), ”Equivalent T-stub in tension”, determines the capacity of a T-stub in the tension-zone of a bolted steel joint. Failure by this method is described by yield-line models depending on geometry of plates and bolts. Additionally, design resistance values of entire joints, with respect to moment and shear, can be extracted from tables provided by e.g. the Swedish organization ”Stålbyggnadsinstitutet”. The pre-calculated values provided are limited to standard connections and are calculated according to EN 1993-1-8.

Furthermore, a finite element analysis can be used, but can also be required, during the design of bolted steel joints. According to Díaz et al. (2011) FE-models are frequently used to assess the mechanical behaviour of steel joints. They can help to examine local effects further within a joint and can be a counterpoise to the lack of experimental results for such steel connections. Errors in FEA can broadly be categorized as user errors, representation errors and errors caused by insufficient mesh discretization (Shah, 2002).

The Annex C of EN 1993-1-5 presents brief information about the use of FEM for plated structures, such as material properties and partial factors to be used for FEA. Nevertheless, no clear guidance exists in the present EN 1993 about the set-up of such a model, i.e. information about how to use different FE-parameters, such as element discretization.

1.2 Goal

This degree project aims to give an insight into finite element modelling of bolted steel connections, more precisely T-stub components in tension, and the corresponding theoretical background. It should provide greater knowledge about FE-parameters in general, their influence on computational time and ultimate load. Additionally, it is investigated how geometrical changes affects the running time with consistent FE-parameters and how geometry influences the overall behavior of a T-stub.

Hence, the objectives of this project are the following:

- Identify research progress i.e. what recommendations in scientific literature exist for FE-application of bolted steel joints
- Gain knowledge about FE-modelling of bolted steel joints in general (by re-modelling existing benchmarks)
- Analyze the influence of different FE-parameters on running time and ultimate load (accuracy).
- Investigate influence of geometrical changes on computational time and ultimate load.
- Study influence of changes in geometry on the failure mode progression within a T-stub.

1.3 Method

The degree project can be divided into several parts, and the goal to reach more understanding regarding finite elements, their influence on time and ultimate load is reached by doing literature study, benchmarks and parameter study of time. Additionally, geometrical adjustments are performed to see the effect on running time and failure mode progression of different specimens. The steps are further described below in chronological order:

To start with, a scientific literature review is performed with respect to finite element modelling of bolted steel connections. Experimental validations with FEA are examined, but in particular, previous research regarding finite element parameters and their implementation.

Parallel to the initial literature study, EN 1993 are interpreted and a calculation sheet for bolted joints is created with respect to the ”Equivalent T-stub”-method. This sheet is made as general as possible, to be adjusted for several particular cases and is used as validation for all upcoming models.

As next step, two models existing from literature by O. Bursi and C. Gantes is remodelled according to the corresponding set-up of geometry and FE-parameters.

These are validated with hand calculations for each paper respectively.

Continuing with a parameter study of FE-parameters for one chosen model with respect to running time and accuracy. Deviations of collapse load are registered for each parameter setting with the original set-up according to author as reference. A time efficient model is created based on the output to see how much lower the running time can be with a marginal load accuracy.

Finally, the influence of geometrical changes on running time are compared with dimensional adjustments of the remodelled specimen. Simultaneously the ultimate capacity is extracted and transition between failure modes in the FE-models are compared to EC-formulation.

1.4 Limitations

First of all, this thesis work is restricted to non-pretensioned steel connections of bolted type in form of T-stubs in tension. Variation of flange representation is investigated and reduced capacity from bending in bolts are accounted for but not further investigated. Strength class of all bolts are chosen to be 8.8 with reference to standard DIN 931. Steel strength of plates are presented in each section in form of stress-strain curves.

Furthermore, the output of the analysis is to determine the ultimate load or respectively the collapse load. In other words the maximum load a connection or plate can take before collapse. The Ultimate Limit State (ULS) or Service Limit State (SLS) are not considered. As regulatory, EN 1993 for steel structures is used with parts extracted from EN 1993-1-1 (CEN, 2009) but the majority from chapters associated with EN 1993-1-5 and EN 1993-1-8.

Geometrical nor structural imperfections are considered throughout the analysis in accordance with table C.1 in EN-1993-1-5. Exposure class is not treated as the joints are assumed to be indoor with no risk of corrosion and design with respect to fatigue are not performed due to static loading of the joints.

Analyses preformed are made in Abaqus/CAE (Dassault Systèmes, 2016) using a stationary computer with an Intel(R) Xeon(R) processor with 4 cores, 3.40GHz together with 16 GB RAM and a hard disk drive (HDD). Licence are provided by Chalmers University of Technology using a virtual private network. No additional software packages regarding contact interactions are used.

2
Theory

The upcoming chapter provides the reader with fundamental theory behind bolted steel connections regarding design procedures and failure modes.

First, general steel connections are presented with a short historical perspective followed by existing type of connections. Their classification types by stiffness and strength are introduced before going into detail with bolted joints and their relevant failure modes.

Then, the infinitesimal strain theory or ”small deformation theory” is illustrated with an simple string example. Followed by a brief description of theory of plasticity, which is the basis for the upcoming analytical and numerical design methods. Moreover, the true stress-strain behaviour, principal stresses and yield stress criterion are further explained in Section 2.3. Additionally, the yield-line theory is presented, which is also the theoretical foundation for the upcoming section about the ”Equivalent T-stub method”.

The principle behind the different parameters and phenomena of a finite element model, are presented separately in Chapter 3.

2.1 Steel connections

In the construction sector, connections enable longer and larger structures from steel profiles. The most common connection methods for steel joints are welding, bolting and riveting. Connections are composed of components and their relative movements keep the connection together. The components are often used in different ways and can be of different strength which make no connection stronger than its weakest link.

Rivets were common in infrastructure projects as well as buildings in form of trusses, girders etc. but has decreased since the 1940's. Rivets consist, according to Francken (1910), of a cylindrical shank together with a rivet head. The rivet is put through the rivet hole so that the second rivet head can be formed. Rivets are permanent which provide joints with high stiffness. Collette et al. (2011) mention that rivets are relatively inexpensive but not easily disassembled which led to the reduction in usage.

Bolted connections are not far away from riveted, but provide much better flexibility, for instance for cases where large diameters or long shank lengths are required (Collette et al., 2011). These type of steel joints are normally used for the erection of components due to their favorable assembling simplicity and the linked lower labour costs (BCSA, 2003).

Welded connections open up possibilities for unique cross-sections where material can be maximally utilized. However, changing geometry too far away from standardized profiles might create instability phenomena, i.e. when plates are made too thin. Regulations for plate slenderness of different parts can be found in EN 1993-1-1 Table 5.2, and how an effective length of parts in cross-section class 4 are treated, can be seen in EN 1993-1-5 Tables 4.1-4.2.

In addition, welds accommodate an essential joining process. According to BCSA (2003) the majority of end-plates and fittings are welded to the respective connected component. Welding is mostly used within the production facility and less frequently on site due to more complex and altering weather conditions. Besides, welding is a challenging activity that requires qualified specialists, so that the weld quality can be assured. In general, two different types of welds exist: butt and fillet welds.

2.1.1 Joint classification

Moreover, the EN 1993-1-8 classifies steel joints by their rotational stiffness (or flexibility) and their strength. Figure 2.1 illustrates the joint stiffness classification and the bending moment dependence on the rotation for three different zones. In steel design it is common to either assume a rigid or a pinned connection, but the actual behavior is often something in between. Jaspart and Demonceau (2008) implies, "joints which are traditionally considered as a hinge do not fulfill the stiffness and/or strength limitations required by Eurocode 3 for nominally pinned joints." This also indicate that even the simplest pinned connection actually is a semi-rigid join per definition. Normally pinned joints are capable of transmitting internal forces, without development of moments. They accept rotations under design loads and are easiest explained by a hinge. Rigid joins, on the other hand provide sufficient rotational stiffness to achieve full continuity, therefore keeping internal forces unaffected. Definition of semi-rigid connection are the ones that does not fulfill the pinned nor the rigid criteria. They provide a degree of interaction between members, based on design moment-rotation characteristics. Criterion for pinned respectively rigid joints, according to EN 1993-1-8; Figure 5.4, are seen in Equation 2.1 and 2.2, where definition of variables can be found in the same figure in Eurocode.

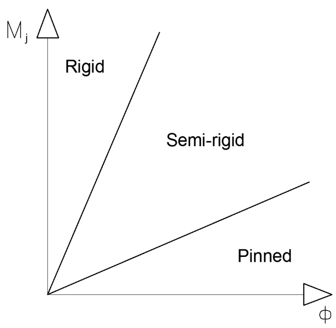

$$S_{j,ini} \geq k_b \cdot EI_b/L_b \tag{2.1}$$

$$S_{j,ini} \leq 0.5 \cdot EI_b/L_b \tag{2.2}$$

Figure 2.1: Joint classification by stiffness - Dependence of bending moment M_j and rotation ϕ.

Additionally, EN 1993-1-8 categorize joints also by their strength, i.e. how the design moment resistance differ between the joint and its connected members. Pinned joints are classified when the design moment resistance, $M_{j,Rd}$, is smaller than a fourth of the moment resistance required for a full-strength joint. The resistance of full-strength joints should not be less than the connected members, meaning that it needs to be larger than two times the plastic moment resistance of a column and two times the plastic moment resistance of a beam, in a double-sided symmetric joint. Conditions for classification are seen in Equation 2.3 and 2.4. Joints with strength in between these two conditions are classified as partial-strength joints.

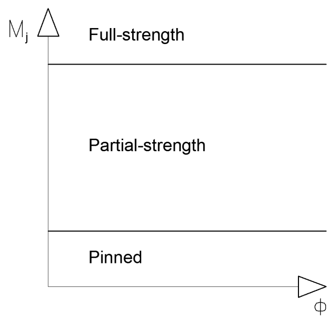

$$M_{j,Rd} \geq M_{full-strength} \tag{2.3}$$

$$M_{j,Rd} \leq 0.25 \cdot M_{full-strength} \tag{2.4}$$

Figure 2.2: Joint classification by strength - Dependence of bending moment M_j on the rotation ϕ.

2.1.2 Bolted steel connections

Bolted connections are flexible in terms of mounting and dismantling. The quick erection time is competitive which also provide easy replacement of damaged pieces and is why bolted connections are commonly used (Pisarek and Koz, 2008). Swanson and Leon (2000) also mentions that bolted connections have higher redundancy compared to fully welded connections.

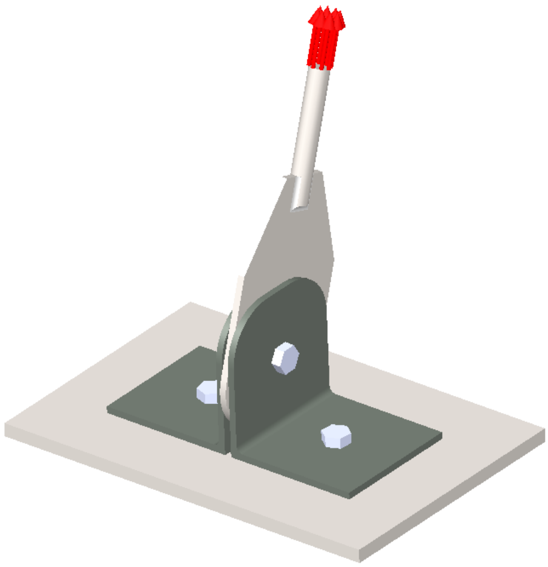

Figure 2.3: Load capabilities of bolts - Two bolts mainly loaded in tension and one in pure shear.

Furthermore bolts ideally provide two types of force transfers within connections. They can be used either perpendicular or parallel to the force direction, i.e. they are loaded in shear or respectively in tension, illustrated in Figure 2.3. During plastic deformations or at unfavourable loading they can also be subjected to bending. Design procedure for individual fasteners can be seen in EN 1993-1-8, Chapter 3.4. Combination of shear force and tensile force are designed with an interaction formula seen in Equation 2.5, taken from EN 1993-1-8 Table 3.4, where F_v is related to shear and F_t to tension.

$$\frac{F_{v,Ed}}{F_{v,Rd}} + \frac{F_{t,Ed}}{1.4F_{t,Rd}} \leq 1.0 \tag{2.5}$$

The amount of bolts, steel strength, diameter and plate thickness are factors that affect the capacity of a connection. They can be adjusted to make yielding happen simultaneously which utilizes the material efficiency of components (Swanson et al., 2002). Increasing the flange thickness improves the connection's initial stiffness dramatically compared to increasing size of bolts or reducing bolt gauge (Leon and Swanson, 2000).

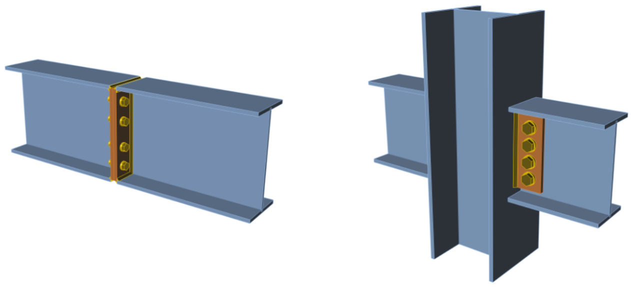

Figure 2.4: Simple connections.

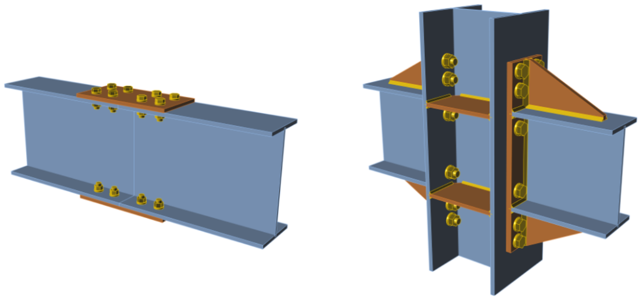

Figure 2.5: Moment-resisting connections.

Steel joints in general, are categorized into either simple connections as in Figure 2.4 or into moment-resisting joints as in Figure 2.5. These categorization is related to how much rotation the joints allow, i.e. their rotational stiffness, as mentioned in Section 2.1. Moment-resisting joints are commonly end-plate connections and used in continuous frames. Simple connections on the other hand are mainly carrying shear forces and can be used to connect beams to a column or to another beam.

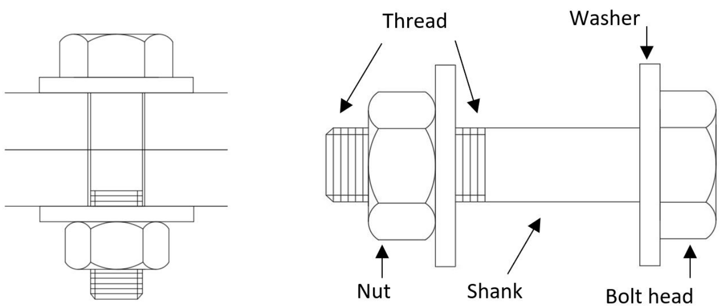

Figure 2.6: Bolt detail - Different components.

The different components of a bolt within a joint can be studied in Figure 2.6. The thread is the part where the nut sit and its length can differ depending on type of bolt used. Additionally, washers can be used both on the head and nut side in a joint.

2.1.3 Failure modes of bolted connections

A typical bolted connection consist of two or more plates attached together with a bolt and a nut. Normal forces, shear forces and moments can be carried by the connection depending on the shape. The failure mode change according to joint configuration which allows designers to choose mode from connection set-up and properties (Al-Emrani et al., 2011).

Figure 2.7 illustrates a beam-to-column connection with potential failure modes. Type of load, thickness and dimensions of components determines the type of failure. All failures are analyzed separately to confirm the total connection strength.

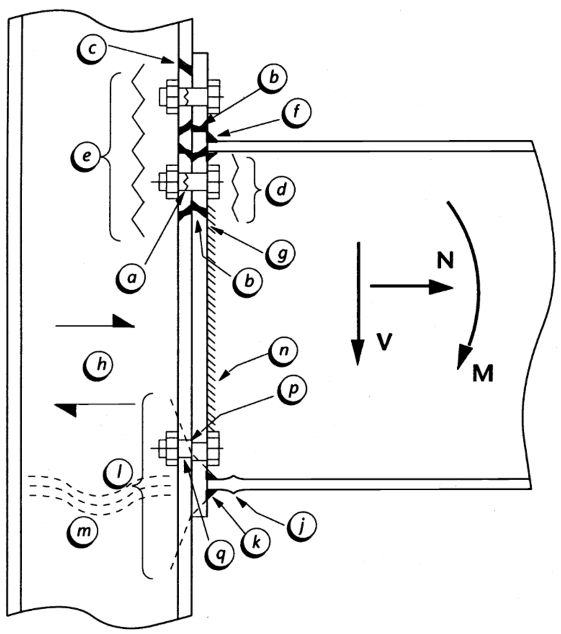

Index	Failure
a	Bolt tension
b	End plate bending
c	Column flange bending
d	Beam web tension
e	Column web tension
f	Flange to end plate weld
g	Web to end plate weld
h	Column web panel shear
j	Beam flange compression
k	Beam flange weld
l	Column web crushing
m	Column web buckling
n	Web to end plate weld
p	Bolt shear
q	Bolt bearing

Figure 2.7: Possible failure modes for beam-to-column connection (SCI and BCSA, 1995).

Plates or shells are, by definition, elements that have a small thickness in comparison to the other dimensions, which means that a simplification regarding stresses can be made. Applied loads on the plate, theoretically, only generate stresses in the in-plane directions. Plate strength are determined by yield capacity, f_y and ultimate capacity, f_u. However, plates subjected to compression may also suffer from buckling, which can be very decisive.

Strength of bolts are defined with two numbers e.g. 8.8 or 10.9. First number represents the ultimate tensile capacity, f_{ub}, expressed in hundred MPa. Second number gives the yield strength, f_{yb} as a percentage of f_{ub}.

Identical strength class for bolt and nut are recommended, which often governs a bolt failure before thread failure (Kirby, 1995). Although, thread failure can be forced by using different strength for bolt and nut. Grimsmo et al. (2016) mention that the cross sectional area of the shear failure is the governing factor and that failure typically occur from one of the following cases:

- Bolt thread failure from a high strength nut
- Nut thread failure from a high strength bolt
- Simultaneous failure of threads at the pitch line.

When the shank is stretched, the threads are subjected to bending and shear. The main failure of threads are threads being stripped at a certain load, which can be calculated according to Bursi and Jaspart (1997a) with the following equation:

$$B_s = \frac{5}{6}\frac{f_y b}{\sqrt{3}}\frac{7}{8} \cdot p_t \pi d_1 z \tag{2.6}$$

where p is the pitch, d_1 is the effective diameter and z is the amount of active threads (3-6). Shear area is therefore dependant on the length of the nut and by increasing the length, the lower probability of thread failure. Thread failure is prevented through ISO standards with proper thread engagement.

2.2 Infinitesimal Strain Theory

The infinitesimal strain theory or also known as ”small deformation theory” is a geometrical simplification for a solid body. It provides a description about that the displacement of a solid body is much smaller than the actual dimension of the body. In other words, one could say that the geometry of the respective body remain constant during the deformation takes place (Singulani, 2014). Thereby we can assume the following:

$$\tan(\theta) = \theta \tag{2.7}$$

For the case of a simple beam, the deformations in relation to beam's span are infinitesimal small, i.e ”small deformations”. Moreover, this above assumption serves a the basis for the yield-line method, explained further in Section 2.4.2.

The infinitesimal strain theory, i.e. the difference between ”small” and ”large” angles is visualized with an example of a simple string seen in Figure 2.8. The 3 kg weight is hung up in a string and would produce a bending moment of around 60 Nm. If the diameter of the circular string is assumed to be 5 mm, the area would be 19.64 mm^2 and the section modulus therefore, 12.27 mm^3. According to Naviers formula, stresses are generated from normal forces and moments. A normal force will not appear because of the perpendicular load direction and infinitesimal small deflection. Hence, the stress will only be generated from the bending moment, which can be solved as 60 Nm/12.27 mm^3 $\approx$ 4900 MPa. This is roughly 10 times the ultimate strength of steel class S355. For full calculations see Appendix IV.

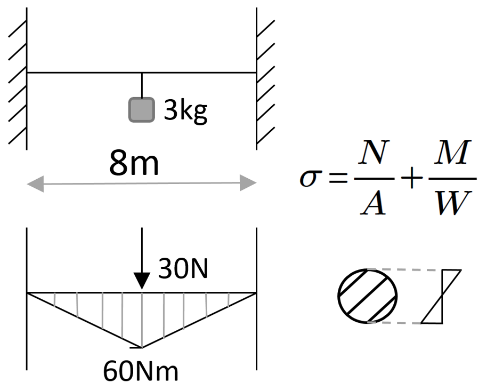

Figure 2.8: Example of string carrying bending moment.

Deflections for this weight can be calculated from an elementary case with fixed supports, which gives a deflection of 12.4 m. This deflection on a 8 m string does not seem right, and it isn't. In fact, for every millimeter deflection, parts of the applied vertical force will be resisted by normal force in the direction of the string due to the increasing inclination to keep equilibrium. That introduces non-linear geometry and a phenomena called ”rope action”, see Figure 2.9.

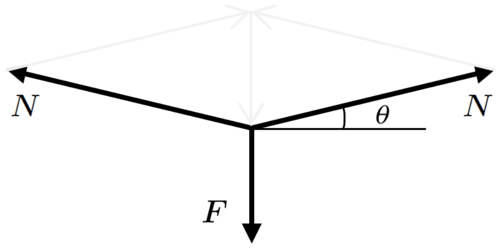

Figure 2.9: Force equilibrium between internal and external forces.

It is of importance, to mention the difference between carrying load via moment or normal force. A steel beam can simply be placed on top of two supports and still carry load in bending moment. A rope need some kind of anchorage at the edges for it to carry the load. The direction of the string determines the anchorage force that is required at each side. A steel beam is a typical example of a case where small deformations should be assumed, just as a nylon string is a good example for implementation of large deformations.

2.3 Theory of plasticity

2.3.1 Stress-strain behavior

This theory explains the behaviour of materials exposed to stress above their yield strength, f_y, and is based on experiments of metals exposed to combined stresses. Applied load generate stress, which in turn generate linear strains corresponding to the material's Young's modulus, E. As soon as f_y is reached somewhere in a object, a permanent deformation, also known as plastic deformation, will take place. Meaning that even if the stress disappear, the strain will not reach its original state (Lubliner, 2008). At that certain point, the crystalline microstructure in the metal change, creating an orientation in the former random oriented grains (Chakrabarty, 2006). The largest contribution to this are dislocation of planes, inside the grain lattice, which depend on the material's crystallographic system. This phenomenon is known as yielding and starts where the elastic capacity of the material is reached. Steel does not break because of its ductility, but it plasticizes. Redistribution of stresses happens internally until collapse. Distribution for a simple plate is illustrated in Figure 2.10.

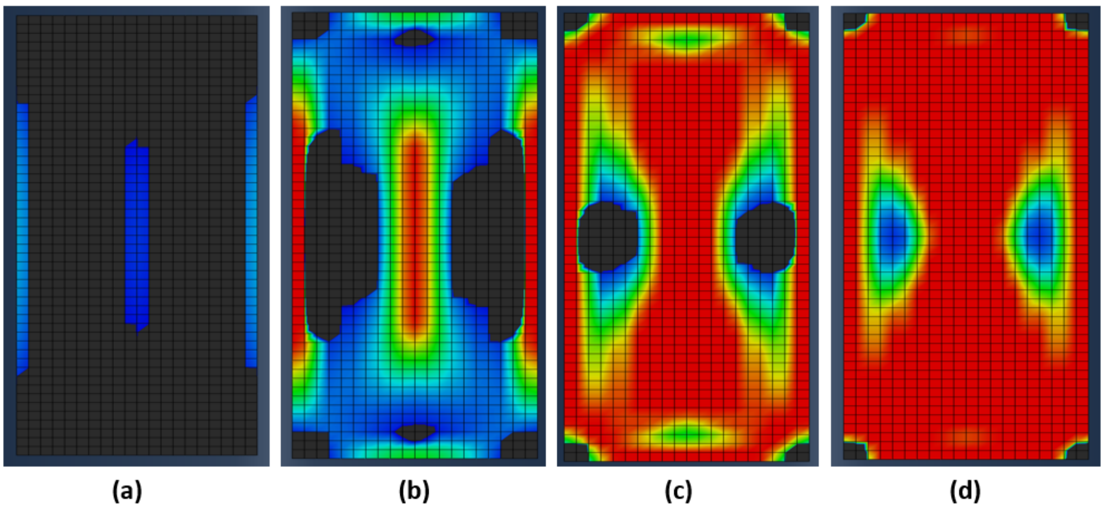

Figure 2.10: Stress redistribution at yielding - Simple plate with steel quality S355 and elastic-plastic material model with strain hardening.

The characteristic behaviour of steel can be seen in Figure 2.11. Elastic response until the point of yielding followed by plastic response, as mentioned. A Specimen loaded until "point A" will therefore be induced with a permanent plastic deformation. Strengthening of steel can be done by this procedure. When steel is unloaded before fracture, the capacity will be higher due to strain hardening. However, this occurs at the expense of ductile behavior and initial deformations (Lubliner, 2008).

The amount of energy an element can absorb before fracture is called toughness. Toughness is the combination of strength and ductility, which corresponds to the integral of area under the stress-strain curve at failure (BCSA, 2003).

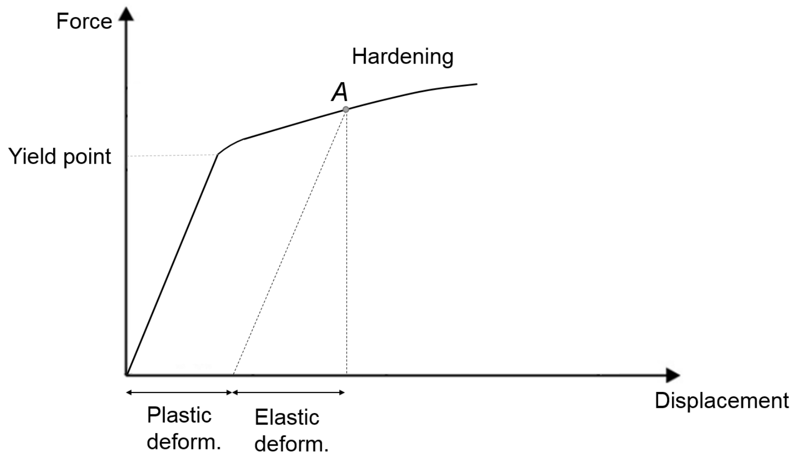

Figure 2.11: Characteristic properties of steel.

2.3.2 Yield stress criterion

For every point in space, stress components can be identified and represented by a stress-tensor, $\tilde{S}$ shown in Equation 2.8 below while Figure 2.12 illustrates how components are defined. Positive integers are defined in the normal direction. Moment equilibrium of this cube provide that shear components are coupled, $\tau_{xy} = \tau_{yx}$, which provides symmetry in the stress tensor and fulfills the condition $\tilde{S} = \tilde{S}^T$ (Lundh, 2000).

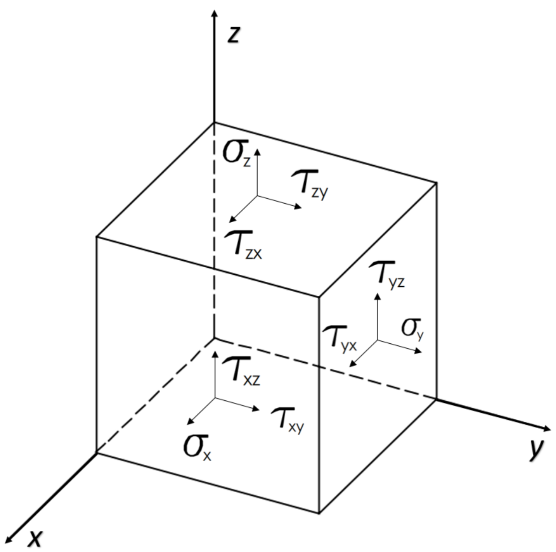

Figure 2.12: Components of stress tensor with directions.

$$\tilde{S} = \begin{bmatrix} \sigma_x & \tau_{xy} & \tau_{xz} \\ \tau_{yx} & \sigma_y & \tau_{yz} \\ \tau_{zx} & \tau_{zy} & \sigma_z \end{bmatrix}_{xyz} \tag{2.8}$$

Furthermore, Principal stresses are defined by stresses from the stress tensor. They occur when the normal stress ($\sigma_x, \sigma_y, \sigma_z$) reach their maximum or minimum value based on orientation (Chakrabarty, 2006). According to Equation 2.9, stress components can be rewritten into principal stresses with a corresponding normal vector. The notation for principal stresses are thereby; $\sigma_1, \sigma_2, \sigma_3$ with contribution of $\boldsymbol{n}_i$. For isotropic materials such as steel, the structural response is independent of material direction, and therefore normal stress direction, $\boldsymbol{n}_i$, does not need to be considered (Kelly, 2013).

$$\tilde{S}(\sigma_x, \tau_{xy}, \sigma_y, \tau_{yz}, \sigma_z, \tau_{zx}) = \tilde{S}(\sigma_1, \sigma_2, \sigma_3, \mathbf{n_i}) \tag{2.9}$$

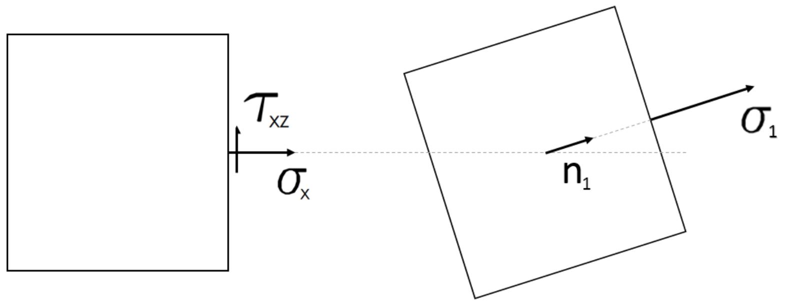

Figure 2.13: Illustration of principal stress σ_1.

Yield criterion is when stresses reach the strength capacity, f_y. This is the limit of elastic behaviour under any possible combination of stress. For uni-axial loading of a specimen in x direction, this is simple. σ_x and σ_1 will coincide and the principal stress is directly comparable with the strength capacity, as a result of σ_2 and σ_3 being absent. However, this is normally not the case and several stress components are present. Every component need to be considered since yielding does not happen in a certain direction, but in a point in the material.

Therefore, von Mises yield criterion define whether a material is yielding based on an equivalent stress which is representing the acting stress combination. This stress has no direction and acts locally in the point of interest (Chakrabarty, 2012). Lundh (2000) interprets that von Mises is frequently used in practice which Kelly (2013) confirms. Von Mises give accurate results for tri-dimensional problems. Equivalent stress according to von Mises are seen in Equation 2.10. The formulation can be expressed in terms of principal stresses, Equation 2.11.

$$\sigma_{e,VM} = \sqrt{\sigma_x^2 + \sigma_y^2 + \sigma_z^2 - \sigma_x\sigma_y - \sigma_y\sigma_z - \sigma_z\sigma_x + 3 \cdot (\tau_{xy}^2 + \tau_{yz}^2 + \tau_{zx}^2)} \tag{2.10}$$

$$\sigma_{VM} = \sqrt{\frac{1}{2}\Big((\sigma_1 - \sigma_2)^2 + (\sigma_2 - \sigma_3)^2 + (\sigma_3 - \sigma_1)^2\Big)} \tag{2.11}$$

2.4 Yield Line theory

The theory behind yield lines was initially introduced by the Russian, Ingerslev in 1920. About 20 years later, the Dane Johansen developed the theory further into what it is known for today. Moreover, various others confirmed its validity and complemented Johansen's theory (Kennedy and Goodchild, 2004).

Furthermore, within the design of reinforced concrete slabs, the application of yield-line theory or method is very common (Vrouwenvelder and Witteveen, 2003). Its theory is based on plastic analysis where sufficient ductility is assumed. Therefore, stress redistribution after yielding can take place, which is also a demand by the theory of plasticity as described in Section 2.3. Moreover, redistribution of stresses enables the development of a failure mechanism in plates (Meyboom, 2002).

Yield lines develop under collapse load in the part of the slab where the stress concentrations are critical. Continuous plastic hinges arise along these yield lines, which induces the global failure mechanism. Additionally, angle of rotation at the yield lines are assumed to be constant and the plate regions enclosed by its edges and yield lines behave rigidly (Vrouwenvelder and Witteveen, 2003).

The yield-line theory provides the basis for actual Yield-line method or work-method presented in Section 2.4.2. With that, the collapse load of a plate with prescribed plastic moment resistances can be determined. The method can be very useful within the design process of structures. Gilbert et al. (2015) mention that the application of this method can be used to diagnose additional capacity in existing structures, when they are assessed. On the other hand it can also help to develop a more economic slab.

2.4.1 Yield line pattern

Yield lines appear in certain patterns. In the Figure 2.14 different type of yield line formations can be identified, which restrain the failure mechanism of plates depending on geometry, type of load and boundary conditions.

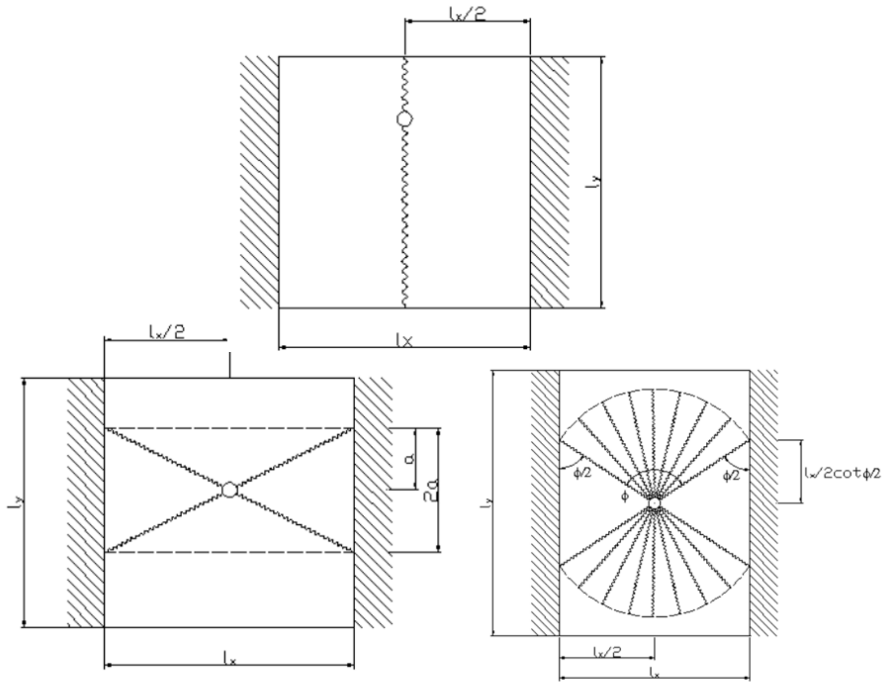

Figure 2.14: Different yield patterns for a concentrated load - linear & and circular (Alverne and Deus, 2012).

According to Kennedy and Goodchild (2004), following rules must be considered and they give a guidance on how to set up a valid yield line pattern:

- Axes of rotation generally lie along lines of support or alongside point supports.
- Yield lines are straight.
- Yield lines between adjacent rigid regions must pass through the point of intersection of the axes of rotation of those regions.
- Yield lines must end at a slab boundary.
- Continuous supports repel and simple supports attract yield lines.

A kinematic yield line pattern can now be established with the rules above. However, since there exists several possible collapse mechanisms, the engineer must find the most critical yield pattern, i.e. the pattern which gives the lowest load capacity for a plate at collapse. Furthermore Gilbert et al. (2015) state that the yield-line method requires sufficient competence by the user and is not made for routine use.

The circular pattern visualized in Figure 2.15 is an indicator of a phenomena termed fan effect i.e a continuous circular yield line. This occur around point loads e.g. a column support or for plates with a circular och triangular geometry (Bandyopadhyay, 2008). By looking at one segment of the circular pattern, using geometry and equilibrium one can derive the following equation:

$$(m_f + m_s)\beta r = \frac{\beta P r}{2\pi} \tag{2.12}$$

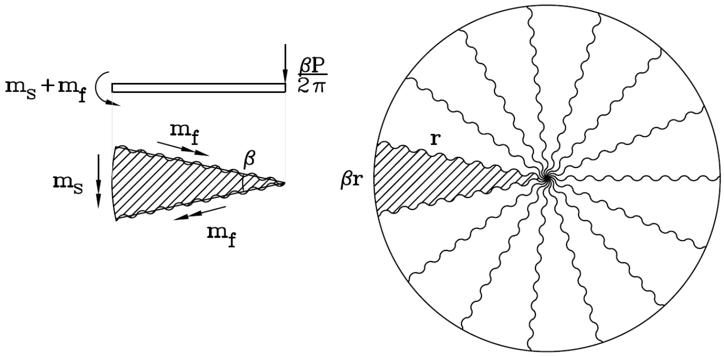

Figure 2.15: Fan effect with corresponding moments for one segment.

$$P = \frac{2\pi(m_f + m_s)\beta r}{\beta r} \tag{2.13}$$

Collapse load, P, in Equation 2.13, is independent of the fan radius, meaning that in the case with a concentrated force acing alone, a fan with any radius can be formed. Even though the radius in undefined, information regarding failure can still be identified. The critical load will determine whether punching shear failure occur before flexural failure. However, for the case with a circular plate with uniform load, the collapse load is dependent on boundary conditions and radius length (Bandyopadhyay, 2008).

A yield pattern of a relatively simple plate can be seen in Figure 2.16. The above rules are all true for this particular plate example and thereby a collapse mechanism is kinematically possible. When the plate deforms according to the collapse mechanism, the different parts should fit together. This is a requirement for a kinematically possible failure mechanism according to Engström (2014).

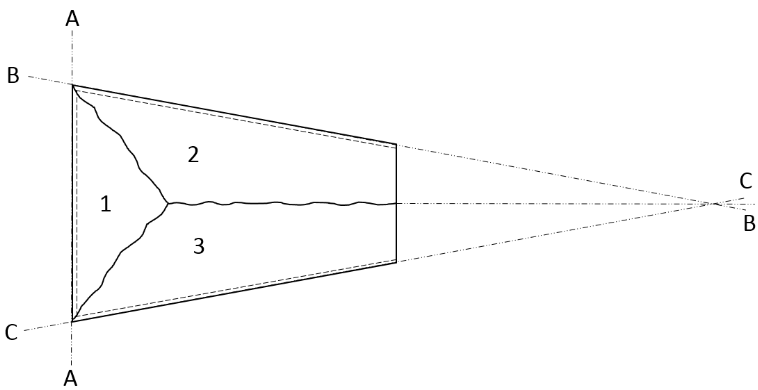

Figure 2.16: Yield-line pattern for simply supported plate with right edge free under uniformly distributed load.

2.4.2 The Yield-line method

This method can be used to determine the capacity of a bolted steel connection. Though, it's an upper-bound solution, which means that the solution might not be exact and slightly on the unsafe side. If used, an iterative procedure is required to find the critical pattern since other patterns provide a undesirable unsafe solution. To cover the uncertainty of the solution provided by the yield line method, the 10% rule is introduced. By that design can be assumed to be on the safe side (Kennedy and Goodchild, 2004).

When a valid yield pattern is chosen, the actual "Yield-line method" or so called "Work method" can be used for the respective plate problem at hand. The principle behind the work method is to set the external work, W exerted by applied loads equal to the internal dissipated energy, E_d along the yield-lines. The internal energy is represented by the magnitude of consumed energy for a chosen deflection δ at failure. The work equation can be set up according to Kennedy:

$$W = E_d \tag{2.14}$$

$$\sum P \cdot \delta = \sum m_{pl} \cdot l \cdot \theta \tag{2.15}$$

Where P is the load acting on the plate, either as point load or surface load $q \cdot A_i$ with A_i being the area of each rigid plate part. Then, δ represents the vertical centroid displacement of the respective plate region and m is the plastic resistance moment of the plate per metre. Additionally, l corresponds to the length of the chosen yield-line, i.e. the projected length on the rotation axis. And, θ is the rotation of the corresponding plate region about its rotation axis. In Figure 2.17 two rigid bodies are formed between the yield lines where the total rotation angle at the middle yield line is the sum of both angles at each fixed support.

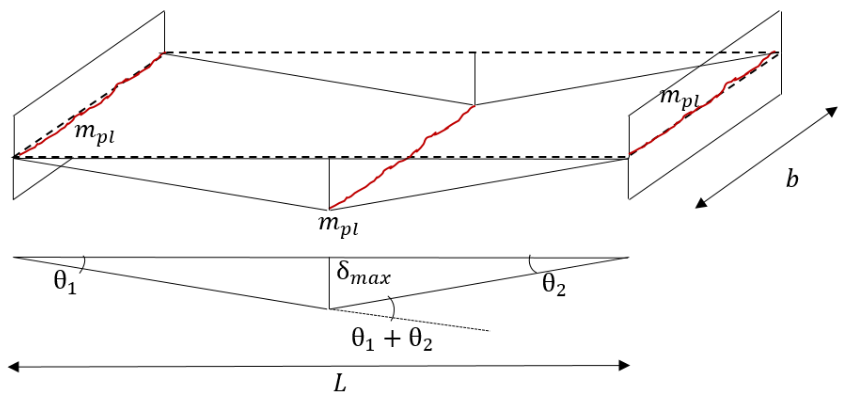

Figure 2.17: Fixed one-way plate with uniform load - Yield lines and deformations at collapse.

It has to be mentioned that Equation 2.15 is simplified to either to a point load or uniform surface load. For the case of not uniform loading Vrouwenvelder and

Witteveen (2003) present a more general equation accordingly:

$$W = \int\int q(x, y) \cdot \delta(x, y) dxdy \tag{2.16}$$

When using the work equation, the maximum deflection δ is assumed to be unity for simplicity. When the collapse load P is determined via the dissipated energy, the deformation δ will get cancelled out since the angle θ is δ-dependant. Moreover, a requirement for this to be applied is that the deflection angle θ is considered to be infinitesimal small, as explained in Section 2.2, so that following expression applies:

$$tan(\theta) = \theta \tag{2.17}$$

2.5 Equivalent T-stub method

When designing bolted structural joints consisting of I or H profiles, they are divided into basic components by the present EN 1993-1-8, also called component method, where Table 6.1 in EN 1993-1-8 provides a good overview of the different components. Most important components for bolted steel joints are the plates and the bolts which both are considered by the design of a T-stub through the ”Equivalent T-stub in tension”. The procedure uses yield line formulations to determine the resistance of the following basic components:

- Column flange in bending
- End-plate in bending
- Flange cleat in bending
- Base plate in bending under tension

A T-stub is an extracted part of a rolled I or H beam , as seen in Figure 2.18. The T-stubs flange is bolted, whereas the web can be either pulled in tension or compressed. Moreover, it is proven that the T-stub is a suitable model for the design of bolted steel joints under tension (Neves et al., 2001). The T-stub is then converted into a ”equivalent T-stub” that should represent the real T-stub. The equivalent one has a new width depending on the critical yield pattern, as can be studied in Figure 2.19. The new width is used to represent the failure in a two-dimensional way and the width corresponds to the length of the yield lines, the effective length.

Figure 2.18: T-stub idealization of a bolted connection.

2.5.1 Effective length

The term ”Effective length” of a T-stub is introduced by EN 1993-1-8 to be a notional dimension, which does not automatically have to represent a physical length of the components within the joint. The effective length, as said, is corresponding to the length of the plastic hinge, which gives an expression for the effective length for a inner bolt-row of an unstiffened column flange with a circular yield pattern according to Table 6.4 in EN 1993-1-8, as seen in Equation 2.18.

The effective length is mainly dependent on the joint configuration and expressions are provided in Tables 6.4-6.6 of EN 1993-1-8. It is distinguished whether a column flange or end-plate is considered as well as if a stiffener is present. Additionally, the length depends on the bolt-row position on the respective flange or plate, i.e. if it's an inner or outer bolt row. Another dependency is whether the bolt-rows are regarded as part of a group of bolt-rows or not, as seen in Figure 2.19. Furthermore, the yield pattern for the equivalent T-stub can occur in two different ways: circular and non-circular, as can be seen in Figures 2.19 and 2.20. They influence the T-tub resistance for each failure mode respectively.

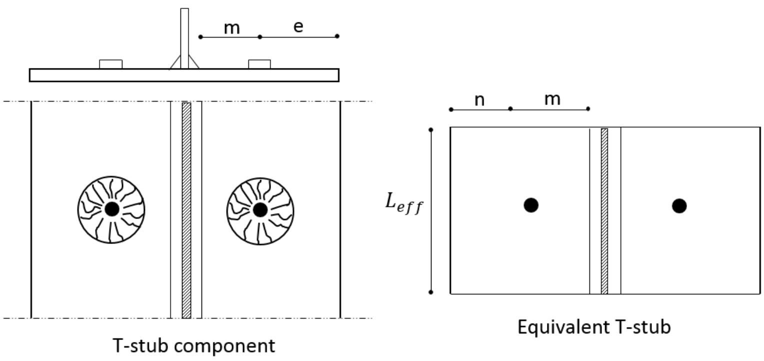

$$l_{eff.cp} = 2 \cdot \pi \cdot m \quad (2.18)$$

Figure 2.19: Circular yield pattern - Effective length of an equivalent T-stub for inner bolt-row.

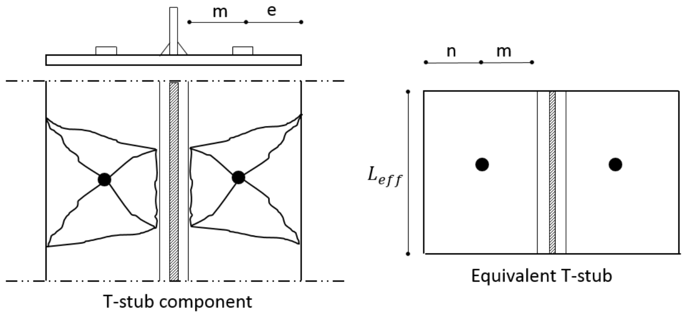

$$l_{eff.nc} = 4{\cdot}m{+}1.25{\cdot}e \quad (2.19)$$

Figure 2.20: Non-circular yield pattern - Effective length of an equivalent T-stub for inner bolt-row.

2.5.2 Failure modes

For a T-stub in tension there exist three different failure mechanism, which can be studied in the Figure 2.21. According to EN 1993-1-8 Table 6.2, there exist two additional methods to consider prying forces. Prying force, as symbolized with Q in Figure 2.21 is the resultant of contact pressure between flange and its connected plate due to deflection in the flange, which are induced by the pulling force $F_{T.Rd}$. The first method assumes that the force applied to the T-stub by the bolt is concentrated at the bolts centre line, whereas the second method assumes a uniform distribution of the applied force, as can be seen in Figure 2.22.

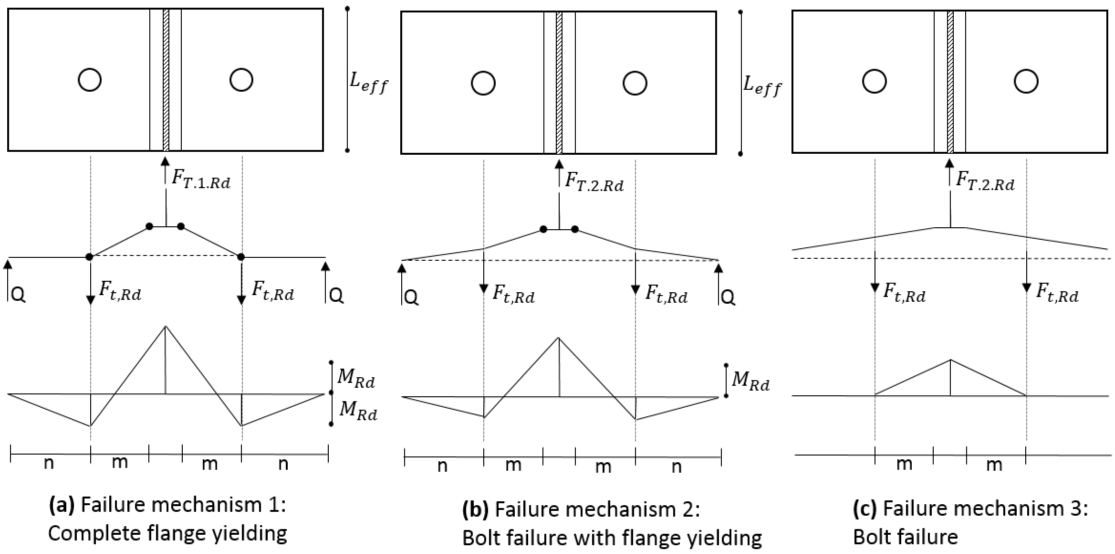

Figure 2.21: T-stub in tension - Three different failure modes corresponding to EN 1993-1-8 - Truncated plastic moments at flange to web connection.

The three different failure modes can be described as followed:

- The first failure mechanism arise due to a rather thin flange and sufficient tensile capacity of the bolts. Yielding occurs at four points in the flange and thereby plastic hinges are created.

- The second mechanism is characterized by a combined failure, where yielding in the flange and bolt rupture take place. After plastic hinges by the web are created, an additional increase of the prying forces will lead to tensile failure of the bolts.

- In case of a relatively strong flange of the T-stub, rupture of the bolts occur before yielding of the flange. Consequently, the bolt strength crucial and becomes governing for failure mechanism 3.

The balance between failure modes depend on geometrical and strength ratio between flange and bolt. The actual derivation of the failure modes, are based on the yield line theory i.e. theory of plasticity and can be seen subsequently.

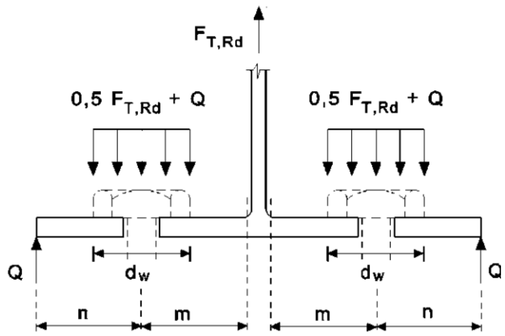

Figure 2.22: T-stub applied loads - Bolt forces applied uniformly (Method 2) - from Table 6.2 (CEN, 2005).

Derivation - Failure mode expressions

The derivation of the first and second failure mode is done with the help of the yield-line method or also called work-method, which was introduced in Section 2.4.2.

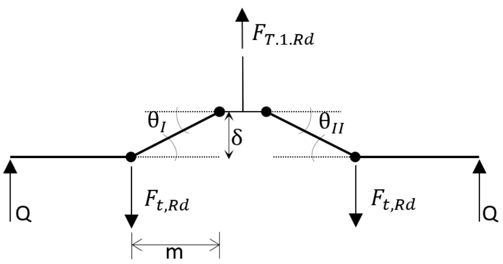

Figure 2.23: Failure mechanism 1 - Virtual work.

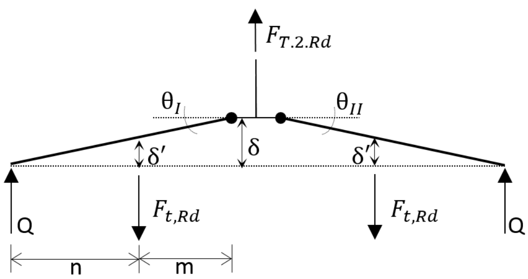

Figure 2.24: Failure mechanism 2 - Virtual work.

Failure mode 1: Complete yielding of the flange

First the external work W and internal dissipated energy E_d are stated with respect to Figure 2.23:

$$W = F_{T.1.Rd} \cdot \delta = F_{T.1.Rd} \cdot \theta_1 \cdot m \tag{2.20}$$

$$E_d = m_{pl} \cdot (2 \cdot \theta_1 \cdot l + 2 \cdot \theta_2 \cdot l) \tag{2.21}$$

Since the geometry of the T-stub is symmetric, the following expression is valid for the angles $\theta_1 = \theta_2 = \theta$ and thereby they can be eliminated. To determine the failure resistance, both energies from Equations 2.20 and 2.21 are equated, which leads to Equation 2.22:

$$F_{T.1.Rd} = \frac{4 \cdot m_{pl} \cdot l}{m} \tag{2.22}$$

$$F_{T.1.Rd} = \frac{4 \cdot M_{pl.1.Rd}}{m} \tag{2.23}$$

Whereas EN 1993-1-8 provides the Equation 2.23 for failure mode 1; without backing plates, considering ”Method 1” with an effective length taken into account in the Equation 2.24 for the plastic resistance moment $M_{pl.1.Rd}$.

$$M_{pl.1.Rd} = \frac{\sum l_{eff,1} \cdot t_f^2 \cdot f_y}{4 \cdot \gamma_{M0}} \tag{2.24}$$

Failure mode 2: Bolt failure with flange yielding

The energy equations with respect to the work method can be stated according to the Figure 2.24 as:

$$W = F_{T.2.Rd} \cdot \delta - \sum F_{t.Rd} \cdot \delta' = F_{T.2.Rd} \cdot \theta_1 \cdot m \tag{2.25}$$

$$E_d = m_{pl} \cdot (\theta_1 \cdot l + \theta_2 \cdot l) \tag{2.26}$$

Analog to above, external work W Equation 2.25 and internal energy E_d Equation 2.26 are equated to govern the T-stub failure resistance $F_{T.2.Rd}$. From the Figure 2.24 the relations $\theta_1 = \theta_2 = \theta$; $\delta = \theta \cdot (n + m)$ and $\delta' = \theta \cdot n$ can be derived.

$$F_{T.2.Rd} = \frac{2 \cdot m_{pl} \cdot l + n \cdot \sum F_{t.Rd}}{n + m} \tag{2.27}$$

Equation 2.27 can be now compared with the one provided by Eurocode in Equation 2.28. The flange length of the respective T-stub is considered in the equation for the plastic resistance moment $M_{pl.2.Rd}$, which also follows.

$$F_{T.2.Rd} = \frac{2 \cdot M_{pl.2.Rd} + n \cdot \sum F_{t.Rd}}{m + n} \tag{2.28}$$

$$M_{pl.2.Rd} = \frac{\sum l_{eff,2} \cdot t_f^2 \cdot f_y}{4 \cdot \gamma_{M0}} \tag{2.29}$$

Failure mode 3: Bolt failure

This particular failure mechanism occurs when the flange is strong enough, i.e. the thickness is sufficiently large, and thereby the bolt strength is governing. Eurocode provides the following Equation 2.30:

$$F_{T.3.Rd} = \sum F_{t.Rd} \tag{2.30}$$

Where the tension resistance $F_{t.Rd}$ of one bolt is determined according to Table 3.4 in EN 1993-1-8 with following equation:

$$F_{t.Rd} = \frac{k_2 \cdot f_{ub} \cdot A_s}{\gamma_{M2}} \tag{2.31}$$

Where k_2 is a factor for the design resistance for individual fasteners, found in Table 3.4 in EN 1993-1-8.

2.5.3 T-stub - Four bolts per row

The design approach ”Equivalent T-stub” in the present EN 1993-1-8 is valid for flanges, end-plates or base plates with two bolts per row. Eurocode states that in the case of four bolts per row, the T-stub should be simplified to two bolts per row. This is conservative and consequently, the results though differ a lot (Pisarek and Koz, 2008).

Furthermore, both Pisarek and Koz (2008) and Demonceau et al. (2010) introduce developed models based on plastic mechanisms for four bolts per row. They are derived in different ways and expressions differ for flange failure and combined flange failure modes.

Additionally, Santiago et al. (2013) performed a parametric study of several T-stubs with 4 bolts per row with FEM and Demonceau's model. Variable parameters were: plate dimensions, thickness, distances while M12 bolts of strength class 8.8 were retained during all tests. The second failure mode is most affected by the influence of the added bolts and the overall results correlate.

3

Finite element parameters

This chapter presents FE-parameters used in the set-up of a FE-model, this to provide knowledge of how phenomena are modelled and serve as basis for how their representation influence the overall behaviour of a joint. Moreover, recommendations for reasonable values, based on scientific research and experiments within this specific field, are presented.

3.1 General

In order to prevent errors in finite element analysis, user expertise must be increased and thereby lays the basis of understanding how representation of reality should be made. Without this, the outcome of a finite element model may be inaccurate and wrong.

Complexity of certain phenomena, such as material plasticity, has been researched and verified with experiments so that they can be relied and used accurately. Additionally, things in particular to consider when setting up a representative FE model are boundary conditions and application of load. Entire structures are rarely built up in softwares when a certain connection needs to be checked, due to computational effort. The parts of interest are often extracted and represented by boundary conditions and loads.

A 2D representation of a 3D problem can be used to save computational power and time but might not always be accurate enough (Gantes and Lemonis, 2003). Gantes describes how 2D bolts can't be projected in a 2D space and fully represent material non-linearity and friction. In the 1970's, Krishnamurthy and Durwood (1976) investigated 3D modelling with, at the time, modern computers. The long preparation and running time made 3D models inconvenient to use for parametric studies. Upon evaluating 13 end-plate connections with both 2D and 3D simulations, the results were correction factors for displacements, rotations and stresses. Conclusion were, that 3D analysis are required to model problems adequately and is more meaningful for comparison with experimental tests.

3.1.1 Load increment method

The general approach for executing a collapse analysis in finite-element programs is to add a small amount of load, in terms of load steps, continuously until failure, i.e. when equilibrium no longer can be reached. In other words the convergence of the numerical model is thereby obtained. Loading can be applied in terms of force or as displacement. For every applied load step, the stiffness matrix is used to calculate either deformations or forces. When either non-linear material or non-linear geometry are accounted for, the stiffness matrix is updated in every load step due to the change in geometry by deformation.

In FE-software it has to be chosen whether load (or displacement) steps/increments are applied automatically or set to a fixed length. Small steps are required to find a converged value with precision. This can for example be used by setting the fixed step sufficiently small to create a tolerance. The operating time will be long but the output as good as it's defined. Automatic stepping enables the software to choose a step length based on the previous length which naturally creates large steps in the beginning and very small steps at the converged value, see illustration in Figure 3.1. Fixed steps length, on the other hand, may hinder a converged solution and thereby is not recommended according to Dassault Systèmes (2016). For a typical linear analysis, the entire load can be applied in one step and then solved. While for e.g. a plastic analysis it is critical to repeat calculations with small load steps to recalculate the stiffness matrix and account for non-linear behaviour.

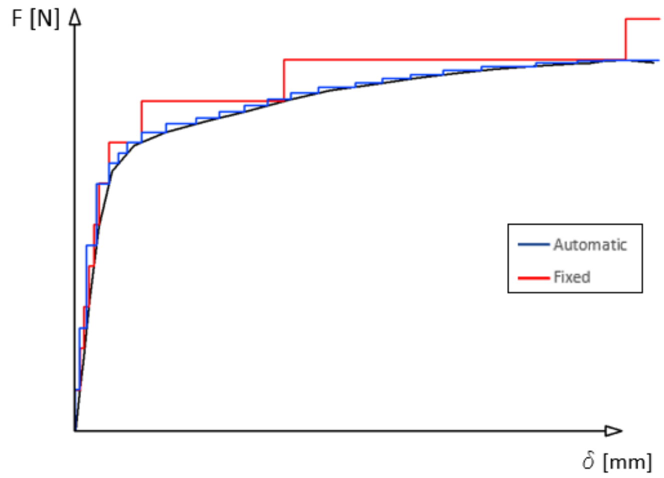

Figure 3.1: Example of automatic and fixed load increments.

Iteration methods

Additionally within each load step, when the solver iteratively approximates a solution, different methods can be used for the iteration. The update of stiffness matrix is also done within this process. There exists several iteration processes, such as Newton (Newton-Raphson), modified Newton-method or the Quasi-Newton method. The Newton iteration method is the fastest with a quadratic convergence rate, inverting and updating the stiffness matrix in every iteration step (Zienkiewicz and Taylor, 2003). By that, it usually reaches convergence in fewer amount of iteration steps, compared to other iteration methods with other updating techniques. However, this requires more computational power and thereby influences the running time, making the amount of elements in the specimen of interest when choosing iteration method Dassault Systèmes (2014). Moreover, the Quasi-Newton method inverts the stiffness matrix in the first load step and then updates based on the previous step rather than recalculating the inverse.

3.1.2 Non-linear geometry

In finite-element modelling it can be chosen whether non-linear geometry, i.e. enabling large deformations, is activated or not. The difference was explained in the previous Section 2.2. Whether it should be implemented or not depend on the type of problem analyzed. EN 1993-1-5 Table C.1 provides brief guidelines regarding situations where non-linear geometry should be used and can be summarized to; Buckling analysis and elastic-plastic resistance in ULS.

3.2 Material models

Material properties as f_y and f_u are provided for different steel classes, but how material behaviour, especially after the yield point, is interpreted in softwares, differs. Non-linearity of materials occurs in the plastic region which often is irreversible. A non-linear material model opens up for redistribution of stresses and an increased capacity. Researchers are proposing different models on how elastic and plastic behaviour can be merged together. These models are created to represent properties applicable to specific problems, rather than making one too complex and generalized material model (Prager, 1955). For example, stress-strain models can be simplified to neglect plastic capacity, suitable for cases where conditions are predominantly linear. The accuracy of such models should be validated before confirming the results.

Eurocode recommends certain models for FE-application in EN 1993-1-5 Annex C.6 which are redrawn and presented in Figure 3.2 - 3.5. All models start with a linearly dependant ratio governed by Hooke's Law until the yield strength. The material stiffness after yielding is what distinguishes the models.

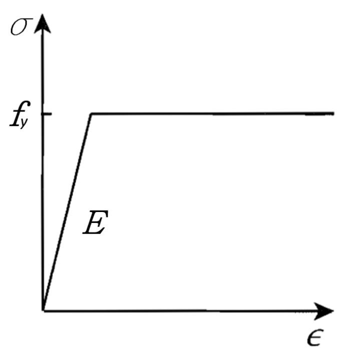

Figure 3.2: Elastic-plastic without strain hardening.

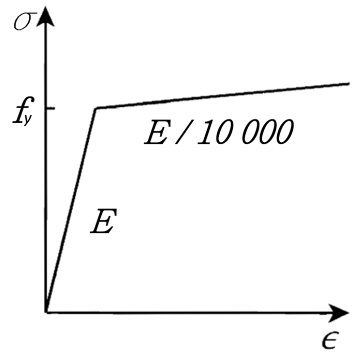

Figure 3.3: Elastic-plastic with nominal plateau slope.

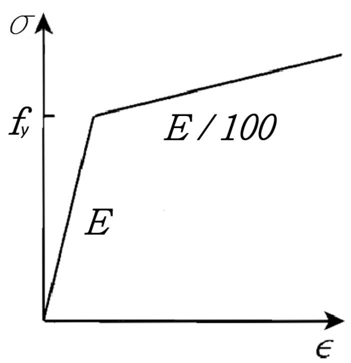

Figure 3.4: Elastic-plastic with linear strain hardening.

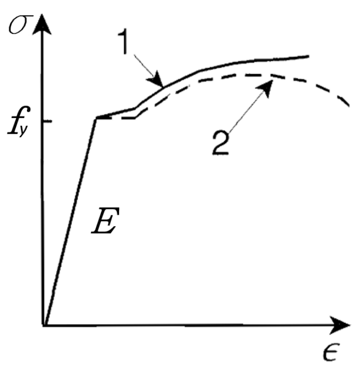

Figure 3.5: True stress-strain curve (1) modified from test results (2).

The true stress-strain curve, seen in Figure 3.5, is adopted from experiments which accounts for the reduced cross section that appears in a ductile material under tensile loading, more precisely the contraction in the cross-section plane governed by Poisson's ratio, giving the true stress a higher value than expected. True stress is calculated with Equation 3.1 when the nominal stress i.e. stress in an undeformed specimen is known. However, the true strain is computed directly from the conventional strain, see Equation 3.2.

$$\sigma_{true} = \sigma \cdot (\epsilon + 1) \tag{3.1}$$

$$\epsilon_{true} = \ln(\epsilon + 1) \tag{3.2}$$

Additionally, Díaz et al. (2011) is suggesting a modified material model based on the models in EN 1993-1-5 Annex C. The model is calibrated and validated with experimental results through a convergence study of moment resistance and rotational stiffness in his journal. The work hardening coefficient, $C_{WH} = 30$ was determined by the least error from an exhaustive search of work hardening coefficient and mesh size, in predicting the design moment resistance of the chosen beam-to-column connection including end-plate. The model has a tri-linear behaviour to account for both the isotropic strain hardening and prevent convergence problems in FE modelling. Figure 3.6 shows an illustration the model's properties.

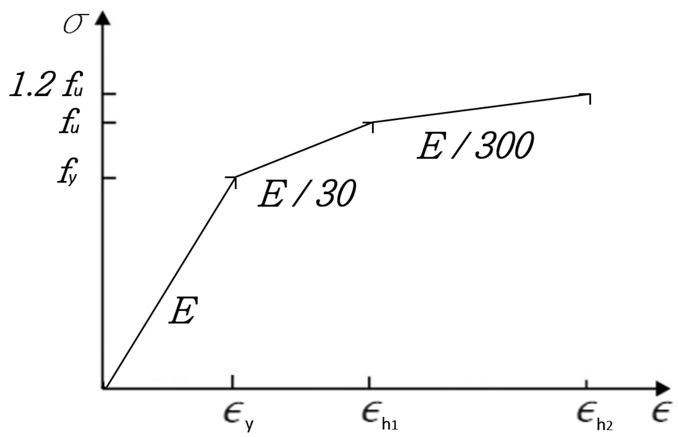

Figure 3.6: Tri-linear material model redrawn from Díaz et al. (2011).

3.3 Element discretization

There exists a strong need for a discretization of a FE model in order to represent the stress distribution and its changes over the different components in a bolted steel joint, in an accurate way. Both the element types and the meshing are decisive about the behaviour of the numerical model and thereby its exactness to reality.

3.3.1 Element type

Within the family of 3D stresses, element types can be further divided into geometrical shape, geometrical order and integration points. Element types are created in FE-programs to be able to choose how much and which kind of information that each element should provide. Stresses in a structure can be represented by one stress per element or one stress per element edge and be linear throughout the element as an example.

Geometrical shape

In general three different three-dimensional main element shapes within the 3D stress family can be identified: 8-node linear brick (hexahedron), 6-node linear triangular prism and a 4-node linear tetrahedron, as seen in the Figure 3.7. The shape should follow the geometrical shape of the part where they are applied, making particular shapes beneficial in different situations.

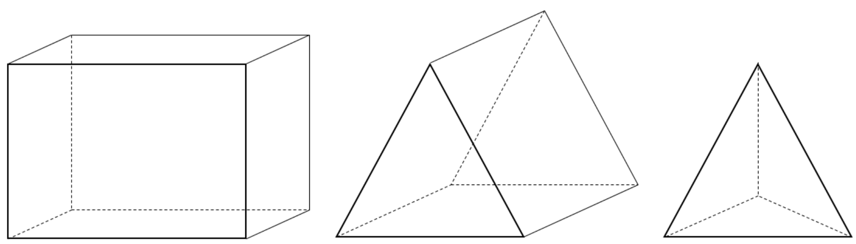

Figure 3.7: Different geometrical shapes of 3D elements (Hexahedron, prism and tetrahedron).

Geometrical order

The geometrical order of an element can be either linear or quadratic and it describes how the shape function looks like. The shape functions are required to estimate the behaviour between the degree of freedoms (DOFs) by interpolating, since FE-analyses solves only for nodal solutions. The difference between linear and quadratic order can be seen in Figure 3.8, e.g. when the displacement distribution over one element is quadratic, the behavior can then be either represented by a quadratic (b) or linear (a) shape function, see Figure 3.8. The linear approximation might give poor results and thereby require a finer mesh, i.e. more elements (c) is required for a linear shape function to obtain accurate results.

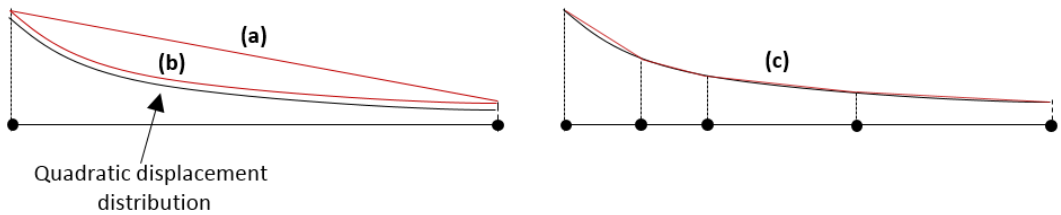

Figure 3.8: Element order of shape function - (a) linear, (b) quadratic approximation and (c) linear approximation with more elements.

Nodes and integration points

Based on the element shape, a certain amount of nodes can be selected to be used within that geometry. In Figure 3.9 a brick element is seen with different set-up of nodes. Integration points are placed inside each element and represent a piece of volume (in 3D) in the element so that distribution of stresses can be calculated through the elements. Amount of integration points are not visible, but can also vary. A 8-node brick element with full integration, seen to the left, contains eight integration points placed in a 2x2x2 pattern.

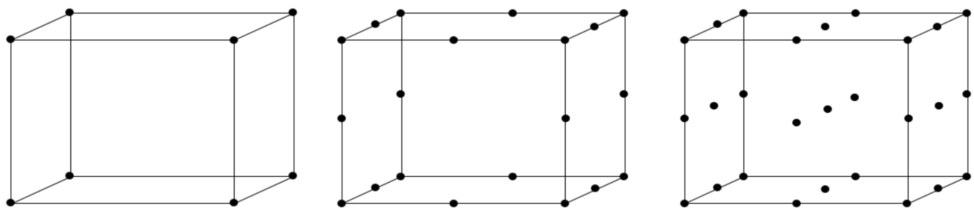

Figure 3.9: Different linear three-dimensional solid elements (bricks) with 8-nodes "C3D8", 20 nodes "C3D20" and 27 nodes "C3D27" (left to right).

Moreover, it is worth mentioning what the shear locking and hourglassing phenomena is. Linear solid elements with full integration under problems governed by bending, become extremely stiff or locked. This is due to the incapability of linear solid elements to adapt to curves when bending. Thereby an false artificial shear stress is added, which creates more shear than bending deformation. False displacement or stresses may occur in this case. (Sun, 2006) In order to control the shear locking of linear solid elements, a reduced integration is often proposed with one Gauss point. The reduced integration element is more flexible to shape deformations. The problems is that the elements might have a too high tolerance against distortions, which is called hourglassing. This hourglassing needs to be limited and can be controlled in most FE-programs. (Sun, 2006)

In Figure 3.10 the deformation of a first order element under bending can be seen. That element has one integration point (where red dotted lines intersect) and while deforming, the dotted lines stay unchanged. No stresses (normal, shear) will develop at that Gauss point, so that no strain energy is created and thereby a zero energy deformation mode occurs. This mode may give results without value, which demonstrate the hourglassing effect, i.e. a too high element shape flexibility. (Sun, 2006)

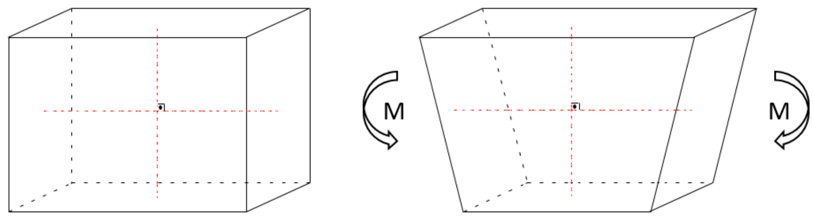

Figure 3.10: Form alteration of a first order element with reduced integration under bending.

Fully integrated solid brick (8 integration points) are exact in the constitutive law integration, but they can undergo shear locking when used for bending-dominated problems. On the contrary, solid elements with reduced integration have just one integration point within the element. That prevents shear locking, but at the same time it may lead to hourglassing, i.e. false singular modes of the stiffness matrix. Additionally, incompatible modes is another element control, where 13 degrees of freedom are added and which erase the so-called ”parasitic shear stress” in bending-dominated structures (Bursi and Jaspart, 1997b). Nodes are added inside the element to show changes inside each element. These nodes are condensed into the outer nodes so that the output looks the same but has higher accuracy. (Krolo et al., 2016)

For a 3D-FEA, eight-node hexahedrons with trilinear expansion (so called ”bricks”) are suitable according to Bursi and Jaspart (1997b). Continuing, the brick element with incompatible modes performs well in the plastic range, suitable for bending-dominated problems. While the element with reduced integration underestimate the failure load and the normal solid 3D element gives an overestimation together with the risk of introducing shear locking. Moreover, Gantes and Lemonis (2003) stated that 2D shell elements are not appropriate for a T-stub connection, based on the fact, that internal stresses in plasticity zones generate unacceptable results.

An important part of the discretization is the size of each element. Adjacent elements share boundaries and values at the boundary need to coincide for both elements, to maintain continuity within the material. Convergence in the analysis is critical, and can be achieved with a suitable mesh size (Yorgun et al., 2004).

3.3.2 Mesh

For a model to provide good results, mesh is very much dependant on the size of the object. A coarse mesh will not capture the correct stiffness and affect the stress gradients between nodes, which in turn affects the final stresses and strains Shah (2002). Redistribution of stresses are smooth with an adequate mesh density. However in a 3-dimensional mesh, interaction of mesh quality in all dimensions will influence the results. When a model require different discretization and specifically a finer mesh at certain regions, such as the connection detail in a simple frame, then partitioning of the present model is required. One should also consider that distortions in the mesh are likely to happen if too many partitions interfere at e.g. edges and thereby creating unsuitable element shapes. Users should be careful when using large corner angles for linear hexahedral elements in regions with stress concentrations (Wang et al., 2004).

Díaz et al. (2011) concludes that there should be three elements across all thicknesses to give a good representation of reality. This is also confirmed by Bursi and Jaspart (1997a) as a recommended minimum number of elements. Moreover, EN 1993-1-5 states that the size of the mesh always should be validated via a sensitivity analysis i.e. a convergence study.

3.4 Contact Interactions

Contact definition in finite element modelling are essential to give proper representation of reality. By defining contact surfaces, the analysis is prepared to consider interaction between elements and nodes in the model. Contacts are divided into two behaviours. Firstly, tangential behaviour describes the effects along the surfaces, typically shear forces and frictional coefficients. Lastly, the normal behaviour is the way the movements perpendicular to the surface are handled. Coefficient for element penetration, before adjustment, are defined under normal behaviour (Dassault Systèmes, 2014).

However, contacts are not cheap in terms of computer performance, which creates a desire to reduce the amount of contact surfaces. In rare locations, they can be supernumerary and thus be simplified. An example of this is a washer between a bolt and a plate, where the height of the head can be increased to the total thickness of head and washer, thereby merging them together. This does not interfere with the global nor local behaviour of the connection (Bursi and Jaspart, 1997a). Nevertheless, the contact surface between washer and plate is considered as normal.

The contacts properties can be assigned in different ways in different softwares, such as contact elements and contact pairs. Contact elements give the outer elements in the mesh properties to react to contacts. When assigning nodes or surfaces to each other, they can be defined as master and slave respectively, which means that one adjust according to the other (Dassault Systèmes, 2016). General contact definition applies to all exterior surface elements and preparing them for contact. This induces extra running time, but may capture effects which are easy to miss.

3.4.1 Friction

Surfaces in contact develop frictional forces dependant on type of material, smoothness of surface and the magnitude of normal force. FE modeling of this phenomena can be created with a surface penalty condition or a contact element. Surfaces to be considered in bolted connections are; contacts between plates, bolt head and bolt nut connection to plate, cylindrical surface of bushing and bolt shank. EN 1993-1-8 Table 3.7 states friction coefficients for design of slip resistance with preloaded bolts, i.e. a connection subjected to shear. These are in the range of 0.2 - 0.5 and determined based on surface class. There are no directions for the application of friction in a connection subjected to tension, but Bursi and Jaspart (1997b) state that frictional effects influence the response at larger displacements with increasing friction coefficient. However, an overall friction coefficient is recommended to 0.33 by AISC for surfaces of Class A (Swanson et al., 2002) which has the same surface dependence as in EN 1993. Moreover, scientific literature papers performing analysis of bolted steel connections, use values in the range of 0.2 up to 0.5. Their outcome is not to determine frictional influence so friction is kept consistent in each paper.

3.4.2 Normal contact

In finite element analysis the normal behaviour determines the conditions perpendicular to the surface such as collisions. Parts deform together and how the transfer between parts are approximated, is according to the software. Specimen can be allowed to penetrate the surface to an extent before adjusting and this is done by linear or nonlinear approximations (Dassault Systèmes, 2016).

3.5 Bolts

Bolts in steel joints can be numerically modelled with different parameters. A bolt is usually composed of a bolt shank, head and nut with addition of washers under bolt head or/and nut. Commonly these components are all modelled as one single body in finite element programs for simplicity (Krolo et al., 2016). Idealization of bolts can be done with either solid elements or with shell elements in form of beam elements forming the bolt in a spin model (Bursi and Jaspart, 1997b)

3.5.1 Simplification

Bolt heads and bolt nuts are typically hexagons by standard, but are modelled as cylindrical in softwares, with the largest circle possible within the hexagon boundaries. Threading are often neglected and made into a cylindrical shank with or without a reduced cross-sectional area, removing the thread failure mechanism (Swanson et al., 2002). This simplification is representative when measuring tensile capacity but in addition, thread failure need to be checked. The principle behind thread failure or thread stripping was previously mentioned in Section 2.1.3.

Due to the fact that a bolt is not completely symmetric and the mentioned geometric simplifications, H. Agerskov has developed an expression for effective bolt length L_{bolt}, which takes the irregularities into account (Gantes and Lemonis, 2003).

$$L_{bolt} = \frac{A_s}{A_b} \cdot (K_1 + 2K_4) \tag{3.3}$$

In Equation 3.3, A_s represents the tensile stress area corresponding to the threaded bolt part and A_b the gross cross-section. The effective bolt length can be determined with Figure 3.11, and Equation 3.4, where K_1 and K_4 are bolt geometry parameters.

$$\begin{aligned} K_1 &= l_s + 1.43 \cdot l_r + 0.71 \cdot l_n \\ K_4 &= 0.1 \cdot l_n + 0.2 \cdot l_w \end{aligned} \tag{3.4}$$

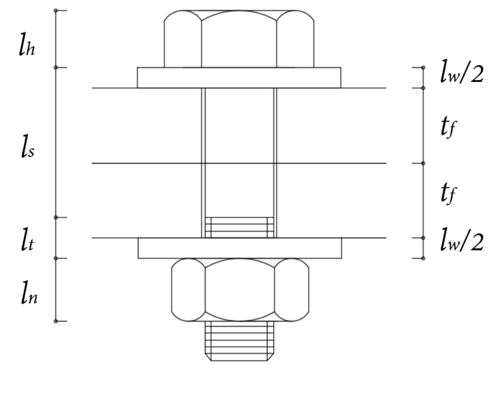

Figure 3.11: Geometrical properties for Agerkov's model (Gantes and Lemonis, 2003).

However, Agerskov's expression for equivalent bolt length may lead to inadequate results for maximum displacements of a T-stub model. Gantes and Lemonis (2003) performed a parametric analysis of the bolt length and proved that the bolt length expression is greatly dependent on pretension level and the governing failure mechanism.

3.5.2 Preloading

As a bolt is pretensioned, an elongation of the bolt shank is introduced which is equivalent to the plate shortening, i.e. compression of the plates. The elongation is small and induces an initial stress in the shank (Moore and Wald, 2003). The cross-section of the bolt is marginally changed thinner when elongated due to contraction, which also explains why an applied force on top of the bolt head and under the nut does not represent the behaviour correctly, as the bolt shank would be slightly larger due to compression. The principle behind preloading of bolts can be studied in the Figure 3.12.

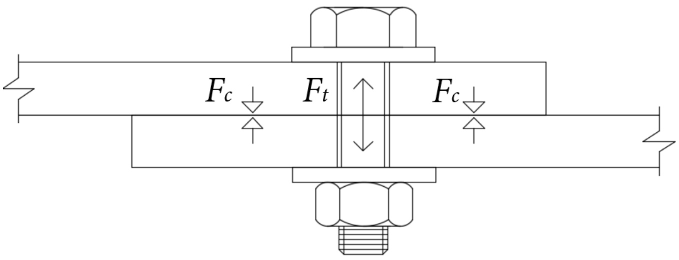

Figure 3.12: Principle of bolt pretensioning.

The constant contact between bolts and plates make frictional coefficient for the surfaces of importance. Preloading of bolts significantly influence the initials stiffness of a joint, creating reduced deformations initially (Jaspart and Maquoi, 1995). However, the strength is unaffected, leading to a similar ultimate capacity with and without preloading (Swanson et al., 2002).

There exists different preloading levels in literature. Krolo et al. (2016) uses 70 % of the ultimate bolt strength as EN1993-1-8 suggests. Despite this, Swanson et al. (2002) pretension the bolts to 65 % of ultimate strength of the bolt and Chin et al. (2017) uses a pretension level of 70 % of the bolt's yield strength to maintain elastic strain.

Pretensioned bolts in finite element software can be created in different ways. Krolo et al. (2016) presents a guideline for FE- modelling preloading bolts in structural connections, where two different preloading techniques "bolt load" and "inital stress" are introduced, both created before external load is applied. In the "bolt load" technique, the preloading is done by fixation of the bolt shank ends while a load in form of force or deflection is added. Before applying the external load, the fixations are released creating the pretensioned bolt behaviour. Whereas for the "intial stress" method, the pretensioning is applied as stress in the bolt shank directly.

4 Methods

The upcoming chapter introduces the different methods used throughout the project, to reach the goal of an accurate, time efficient FE-model. Firstly, two T-stub models are replicated according to the origin from scientific literature (Bursi and Jaspart, 1997a) and (Gantes and Lemonis, 2003). This is done to get a good image of FE-modelling of T-stub components in tension and to obtain a validated FE-model, as a base for further studies.

Moreover, one of the models is further used for a parametric study with focus on time efficiency and ultimate load accuracy of selected FE-parameters. Additionally, a geometrical parameter study is performed, in order to compare the change in running time with changing geometry. Transition of failure modes are also determined for the changing geometries.

4.1 Numerical approach - Finite element model

As a smooth launch into FE-modelling of bolted steel connections, the different components of a bolted joint were modelled to prevent set-up problems at a later stage. An arbitrary T-stub was modelled without a bolt, but with a bottom plate and reasonable boundary conditions to represent a bolt before the complete models were recreated.

Two benchmarks were chosen because of their descriptive models and results. Both consist of standard profiles attached together with four bolts each loaded in tension. The provided information regarding FE-parameters was adopted according to the research papers, while the theory from Chapter 3 was kept in mind. Three symmetry planes were utilized for simplicity which reduced the amount of elements, calculations and contact planes etc. These planes can be identified in Figure 4.1.

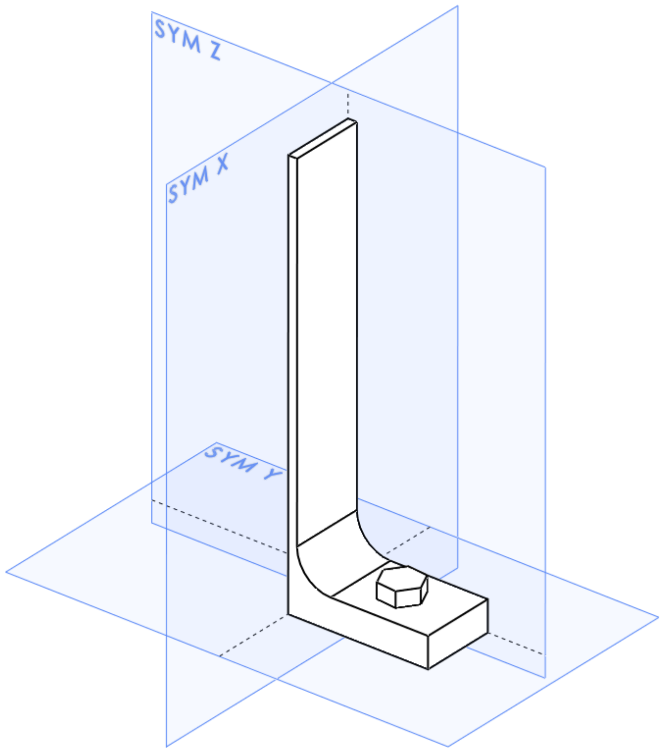

Figure 4.1: Model visualization with three symmetry planes.

4.1.1 Benchmark replication

The set-up of the finite element models for both benchmarks were precisely documented in this subsection with information regarding geometry, element discretization, material model, loading and boundary conditions, contact interaction and bolt modelling.

The first remodel was taken from Bursi's and Jaspart's journal article *"Benchmarks for Finite Element Modelling of Bolted Steel Connections"*. It consisted of two T-stubs of profile IPE300 which were attached with four M12 bolts of strength class "8.8". Joint is further named to "IPE300" in the paper. Geometry together with dimensions and appearance can be found subsequently.

While the second remodel of a T-stub consisting of HEB220 was taken from from C.J. Gantes publication *"Influence of equivalent bolt length in finite element modeling of T-stub steel connections"*. Two T-stubs are likewise attached with four M12 bolts of strength class "8.8" and this joint is further mentioned as "HEB220".

Model geometry

The following Figures 4.2 and 4.3 provide an overview of the two different remodelled T-stub models IPE300 and HEB220. The distance d corresponds to the height of the modelled web and was taken to obtain the same model geometry as in literature.

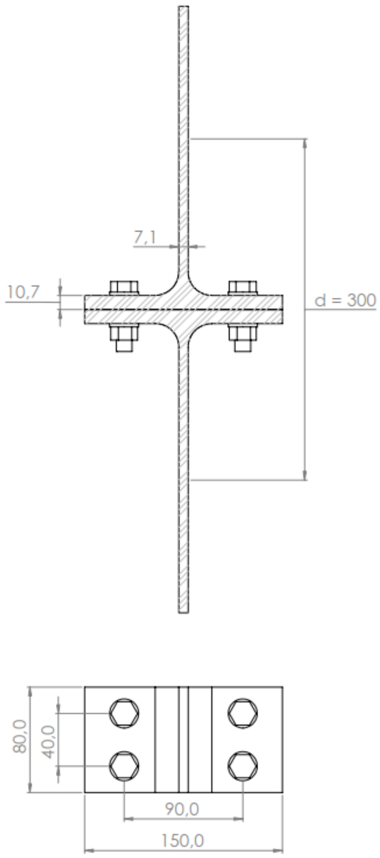

Figure 4.2: Geometry of FE-model T-stub IPE300.

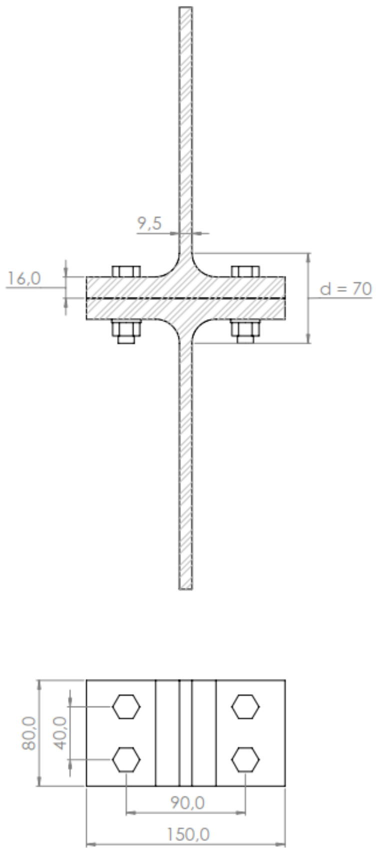

Figure 4.3: Geometry of FE-model T-stub HEB220.

Overall Set-up & Boundary conditions

First of all symmetry was utilized according to Figure 4.1 into a quarter of a T-stub, with corresponding symmetry boundary conditions. Since only this reduced model was analyzed, the bolt shank was halved in accordance with Agerskov's expression in Section 3.5.1, and thereby boundary conditions at the halved bolt shank were introduced. The vertical translation of the bolt-shank-end area was prevented, while a simple bottom plate was introduced for both models to create the required interaction plane. The plates were fixed in all translational directions at the contact surface to prevent rigid body motion of the entire T-stub model. The bolt hole in bottom plate was created sufficiently large so that it wouldn't interfere with the bolt shank behaviour and only work as contact surface. Moreover, non-linear geometry was also used because of the relation between specimen size and deformation.

Element discretization

For both remodelled T-stubs linear solid three-dimensional elements with 8 nodes (so called "bricks") were chosen. These 8-node brick elements are called "C3D8" in Abaqus and use full integration, i.e. eight integration (Gauss-) points, as previously explained in Section 3.3. The element shape was chosen to be hexahedrons and hex-dominated in the fillet area of the flange.

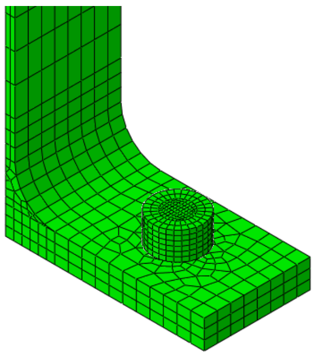

Figure 4.4: Mesh density of FE-model T-stub IPE300.

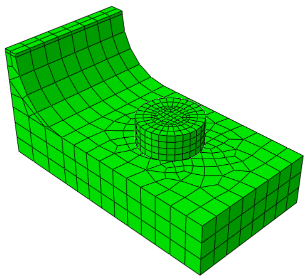

Figure 4.5: Mesh density of FE-model T-stub HEB220.

Mesh density for both models was extracted from their research papers respectively. The HEB220 was chosen for a mesh convergence study according to EN 1993-1-5 and Section 5.1. Idea was to verify whether the selected mesh in literature was made sufficient, and this was made through a general change of size for all elements in the model from 16 mm to 4 mm. The final selected mesh density of both models can be studied in Figures 4.4 and 4.5 and was adopted in accordance with both benchmark models. Nevertheless, the mesh in the bolts and in the flange fillet was adjusted to fit the curvatures better.

Material models

The material behavior of both T-stubs were extracted as elastic-plastic with strain-hardening in form of true stress-strain curves created by Bursi and Gantes. The true-stress strain law was previously explained in Section 3.2 and the relationship for the remodels can be found in Figures 4.6 and 4.7 respectively. In both papers the true stress-strain values were presented graphically together with experimental results of the tested T-stub specimens. From these graphs the values were extracted via measuring them true to scale. The same applies for the Young's modulus, measured to $E = 200$ GPa.

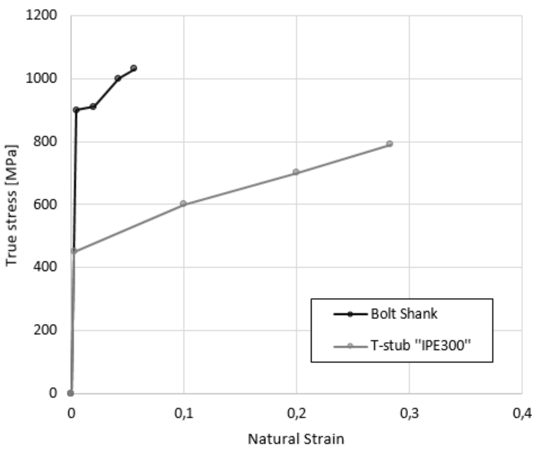

Figure 4.6: True stress-strain relationship for model IPE300.

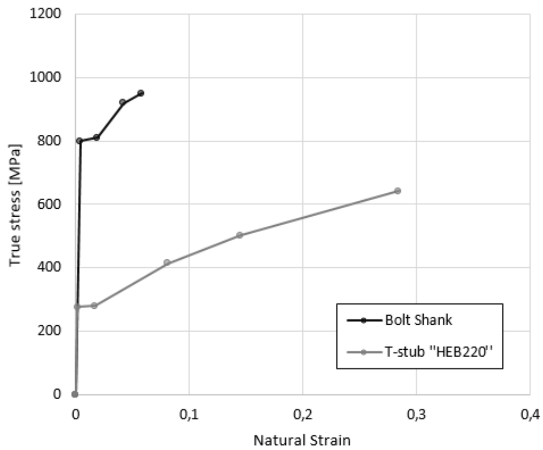

Figure 4.7: True stress-strain relationship for model HEB220.

Loading procedure

The external pulling force on the end of the web plate was applied in different load increment manners. Bursi used a deformation-induced loading in form of a prescribed displacement at the web end for the T-stub IPE300, whereas Gantes chose a force-controlled loading. The selected method for solving all load steps, including necessary iterations, was the Newton-Raphson method.

The simulations in Abaqus were performed with automatic increments, with a restriction on the maximum allowed step size, so that the step size was rather fixed. This was chosen too get small enough load steps (displacement or force) to get a finer image of the plastic region, i.e. first point of yielding and the curvature of strain-hardening.

For the case where loads were applied in a displacement-induced manner, as in T-stub IPE300, the displacement was applied in increments of size 0.5% of the total applied deflection of 20 mm. Moreover, the minimum step size was set to 0.001% of the applied deflection as a tolerance for convergence. On the other hand, for the model HEB220, load was applied as force increments of size 0.5% of the total load of 100 kN on the modelled T-stub quarter.

There was a difference in post-processing of both load increment methods. The deformation-induced method require extraction of reaction forces compared to the displacement while the load-induced method simply compare the applied load with the displacement.

Interaction

In the set-up of original model IPE300, a LAGAMINE software package was used which inter alia defines contact elements. That finite element package was developed at MSM Department of the University of Liège to simulate metal forming (Bursi and Jaspart, 1997a). The benchmark of model HEB220 used a MSC/Nastran software package to define gap elements (Gantes and Lemonis, 2003).

However, the contact in both remodelled benchmarks were defined via general contact in Abaqus. The interaction properties in both T-stubs were chosen to be friction-less in the tangential direction and hard contact in the normal direction. This was applied for all surfaces, except between bolt head and plate where the exception was that the tangential behaviour had a penalty coefficient of 0.25, according to contact properties by Bursi and Gantes.

Bolt modelling

The provided bolt lengths are 55 mm (IPE300) and 40 mm (HEB220). Additional bolt properties, such as effective diameter for hex cap screws either fully threaded or partially threaded were taken from standardized tabular DIN 933 (fully threaded) and DIN 931 (threaded). Nut dimensions are taken from DIN 934, while DIN 125/ISO 7089 was used for flat washer.

When the Y-axis symmetry was utilized the bolts were halved. As a results of asymmetry in the bolts, the Agerskov expression, as introduced in Section 3.5.1, was used to take irregularities into account. The corresponding effective bolt length for both models can be seen in Tables 4.1 and 4.2. Furthermore, the bolt head was assumed to be cylindrical with the radius of 19 mm, which corresponds to the largest circle to fit inside the hexagon shape, which was taken from before mentioned standards.

While the model IPE300 has a washer on the nut- and bolt head side, the model HEB220 has just one washer attached to the bolt nut. Regardless of the mentioned difference, the washers were considered to be attached to the head, respectively to the bolt nut, with the same diameter as the bolt head/nut and without defining contact planes.

Threads were neglected in both benchmarks by modelling the bolt shanks cylindrical with an effective area, $A_s = 84.3$ mm^2, which corresponds to the tensile strength of a threaded bolt. Thread failure was calculated based on Bursi and Jaspart (1997a) expression, Equation 2.6, with three active threads in the nuts. This was a recommendation to be selected between 3 and 6 for standard bolts and is in that way conservative. The values were calculated to 259 kN for IPE300 as well as 230 kN for HEB220, see Appendix III.

Table 4.1: Summarized parameters of remodelled benchmark IPE300.

Parameters	
Element type	Linear solid brick ”C3D8”
Material model	True-stress strain model acc. to Bursi
Bolt Type	M12 8.8
Bolt Length	55 mm
Bolt Equivalent bolt length (Agerskovs model)	15 mm
Loading Type	Deformation-induced
Iteration solver	Newton-Raphson
Friction	Tangential behavior between bolt head/nut & plates Hard contact in normal direction
Friction coefficient	0.25

Table 4.2: Summarized parameters of remodelled benchmark HEB220.

Parameters	
Element type	Linear solid brick ”C3D8”
Material model	True-stress strain model acc. to Gantes
Bolt Type	M12 8.8
Bolt Length	45 mm
Equivalent bolt length (Agerskovs model)	20 mm
Loading Type	Load-induced
Iteration solver	Newton-Raphson
Friction	Tangential behavior between bolt head/nut & plates Hard contact in normal direction
Friction coefficient	0.25

4.1.2 Parametric study of benchmark model "HEB220"

The study was executed with the remodel of Gantes' benchmark model "HEB220" as reference and the set-up of that remodel was described in Section 4.1.1 and summarized in Table 4.2. This model was set as standard and the impact of the parameters were investigated w.r.t. running time and ultimate load accuracy individually. The comparison was limited to a one-directional, in which obtained results were only opposed to the set reference T-stub model. The time factor is related only to the computational time of the FE-software since model-assembling time is more user-dependant.

For the model HEB220, the governing failure mode together with the corresponding ultimate capacity was identified according to EN 1993-1-8. While FEA does not explicitly give governing failure mode as EN 1993-1-8, but registers the mechanical behaviour and provides the ultimate capacity. Furthermore, the cylindrical bolt from Agerskov's expression makes thread stripping failure undetectable in FEA which requires a separate condition. The capacity of this was calculated to 230 kN seen in Appendix III and is plotted in each one of the resulting figures.

Element size

The first parameter study was performed with respect to the amount of element in each direction of the flange to see their single influence. Figure 4.8 illustrates the original mesh from model HEB220 with dimension directions to be changed. The sub-studies were divided into the following parts; Elements per thickness, elements per length and elements per width according to figure. Respectively, they were changed from the original model while running time and ultimate load was extracted.

Additionally, a model with coarse mesh, seen in Figure 4.9, were created to get an insight of multiple dimensional changes for the flange mesh. This model was run with the number of elements per thickness chosen to one, per width to be two and per length five.

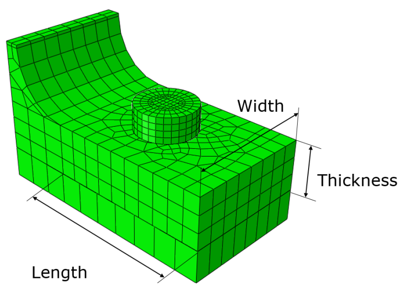

Figure 4.8: HEB220 with mesh from Gantes including dimensions to be changed.

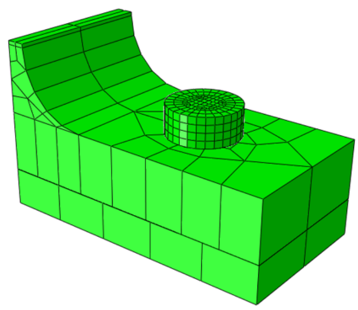

Figure 4.9: HEB220 with coarser flange mesh.

Element types

Adjustment from the normal brick elements with full integration were performed to other types. Both linear (8-nodes) and non-linear elements (20-nodes) were used together with both full and reduced integration. The element type affects how the program calculates in terms of number of nodes and integration points, which contributes to an alternated running time. The mesh was consistent throughout the changes. Moreover, the abbreviations for the different treated element types according to Abaqus were: C3D8I, C3D8R, C3D20, C3D20R and further explanation can be read in Section 3.3.1.

Material models

Material models were chosen from recommendations for FE-implementation by Eurocode and a researcher Diaz. Models were previously described in Section 3.2 and were applied with f_y and f_u extracted from the true stress-strain graphs in Section 4.1.1. Diaz tri-linear material model and the elastic-plastic material model from EN 1993 account for strain hardening which was required to capture real plastic behaviour.

Friction

During the contact interaction, the tangential properties for contact between plates and bolt head were changed. In Gantes original set-up all surfaces were frictionless except the bolt head and bolt nut connected with the plates. This friction coefficient was originally 0.25 but was changed with tangential penalty of 0.1 up to 0.5.

Moreover, general friction coefficient for all exterior surfaces was also investigated and compared separately to get an idea of the influence of including friction between flange and bottom plate.

Stepping

Automatic stepping was used for the FEA in Abaqus, which lets the software choose step length (also increment size) based on previous load step. Inputs provided by the user were the initial step in percent of applied load, the maximal and minimal step size. The minimum step size or increment size (in terms of applied load) sets the convergence tolerance and was set relatively low (0.001%) in order to get an accurate converged result.

The initial step was calibrated in a structured way to find the quickest running time, which was inter alia done through setting no limit on the maximum step size in Abaqus. When initial step was determined, the maximum step size was calibrated accordingly. Maximum step size was changed from the initial value and up until convergence is reached while initial step size was changed from 0.5% up to 25%.

Additional parameter

The last parameters included in the parameter study were put together as selective parameters as they are chosen to be used or not. They were checked separately to see how much they relate to ultimate load and computational time. The investigated parameters were deformation-induced loading and Quasi-Newton iteration method. Applied deformation was set to 10 mm and displacement was registered at collapse while the force-deflection curves were achieved by extracting the reaction forces compared to the deflection.

Time optimized HEB220 model

Finally, in order to see the outcome of the one-directional comparisons and to see the action of multiple changes, a time optimized model was created. Results from the study was extracted and implemented together with the FE-parameter theory from Chapter 3 in mind.

4.1.3 Geometrical study of benchmark model ”HEB220”

In order to see the correlations between changes in geometry and running time, the geometrical parameter study was performed. Additionally, ultimate capacity and governing failure mode progression based on model geometry changes, were determined. However, changes were performed within defined boundaries by EN 1993-1-8 regarding edge distances.

The specimen HEB220 as seen in Figure 4.10, was chosen for the study, which originally fails in a combined failure according to EN 1993-1-8. Geometrical adjustments were made to induce flange or combined failure which gives the flange a higher utilization ratio. The M12 bolts in the model had a thread stripping capacity of 230 kN, which applies for all changes, and are seen in each graph respectively.

The FE-parameters were kept constant according to Gantes HEB220 model during this study which resulted in that the only change made were the size of elements since the amount of elements were kept.

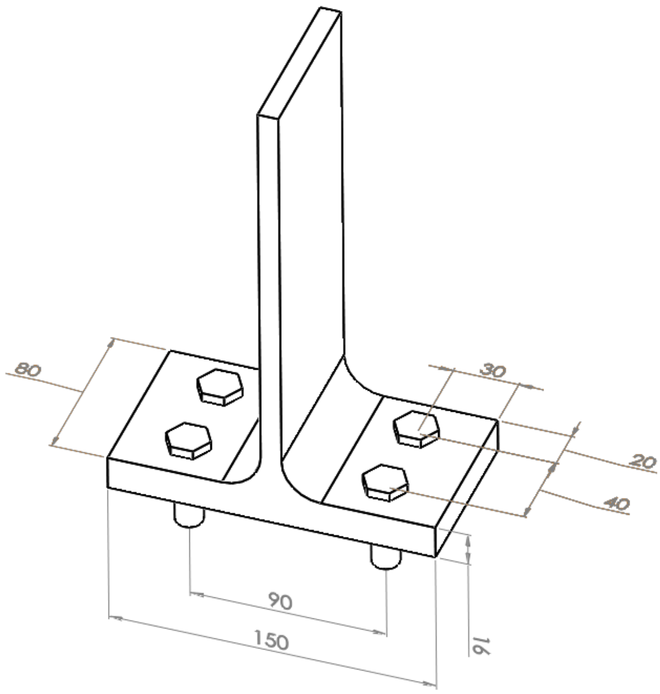

Figure 4.10: HEB220 with original dimensions.

Force-deflection curve for remodelled HEB220 were taken from previous section and used as reference in the study. Two geometrical changes were done per chosen geometric parameter and presented in force-deflection curves. Simultaneously, hand calculation for each specimen, with geometrical changes were performed.

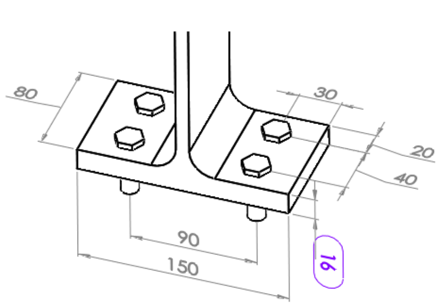

Figure 4.11: Geometrical change: Flange thickness t_f.

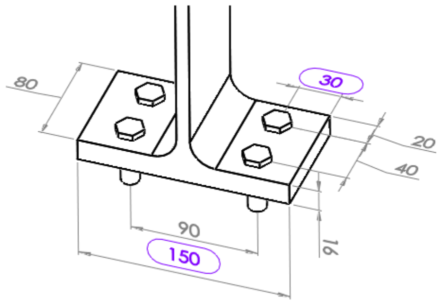

Figure 4.12: Geometrical change: End distance e_1.

Change 1: Flange thickness (t_f)

Firstly, the thickness of the flange was reduced in two steps from the original model to 14 mm and 12 mm. The adjusted thickness can be seen marked in Figure 4.11 while the rest were kept constant. With changing thickness, the formulation of Agerskov's bolt length changes. It was recalculated to L_{bolt} = [18 16] mm for t_f = [14 12] mm respectively.

Change 2: End distance (e_1)

Then, the distance from center bolt hole to outer edge in load direction was changed both up to 40 mm and down to 20 mm. The total dimensions of the plate were changed and distances to nearby bolt holes in both directions were kept. Concerned dimensions can be seen marked in Figure 4.12.

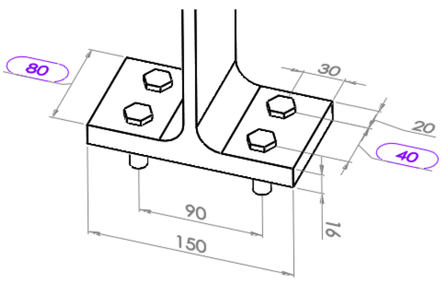

Figure 4.13: Geometrical change: Bolt-row distance p.

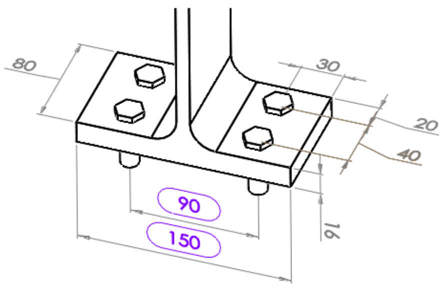

Figure 4.14: Geometrical change: Bolt distance w.

Change 3: Bolt row distance (p)

Next, dimension between bolt row holes was adjusted, which influences the combined strength of two bolt rows in the T-stub. p was adjusted to 35 and 50 mm and all dimensions that are affected can be seen marked in Figure 4.13.

Change 4: Bolt-web distance (w)

Lastly, distance from web to bolt was adjusted by the symmetric dimension w. e_1 and e_2 i.e. location of bolt hole in comparison to outer edges were kept. Adjusted dimensions can be seen marked in Figure 4.14 while the rest were kept constant.

4.2 Analytic approach - Equivalent T-stub

The Equivalent T-stub method presented earlier in Section 2.5, was used in order to calculate the ultimate capacity and to determine the critical failure mode for the benchmarks processed in Section 4.1, as well as the geometrically modified specimen in Section 4.1.3. In the design process, checks of end-, edge- and space-distances according to Table 3.3 in EN 1993-1-8 were included to make sure that the following design procedure, Equivalent T-stub in tension, could be applicable. Moreover, the suggested safety factor of 1.25 for connections was used, which makes results from EN 1993 automatically conservative.

Moreover, the T-stubs were designed with a combined action of bolt rows to account for their interacting behaviour which explicitly mean that the capacity of two single-row T-stubs can not simply be multiplied by two. The effective length the joint with combined bolt rows were calculated with Equation 4.1 - 4.2 below, taken from Table 6.4 in EN 1993-1-8, where flanges are unstiffened and failure happens with either a circular or non-circular pattern.

$$\text{Circular:} \qquad min(\pi m + p, 2e_1 + p) \tag{4.1}$$

$$\text{Non-circular:} \qquad min(2m + 0.625e + 0.5p, e_1 + 0.5p) \tag{4.2}$$

When plastic moment resistance of the plates, together with the effective length of the yield lines were determined the critical failure mode and ultimate capacity were denoted. Calculations for IPE300 and HEB220 including geometrical changes for the parameter study can be seen in Appendix I and Appendix II.

5
Results

The results from the methods previously described are presented here, mainly in form of load-deflection curves with associated tables. First, results of the two provided benchmarks from (Bursi and Jaspart, 1997b) and (Gantes and Lemonis, 2003) with comparison to the analytic method ”Equivalent T-stub” by EN 1993-1-8 are presented. This shown in graphs, together with figures of events during loading for both specimen.

After that, the outcome of the FE-parameter study, with the previous studied benchmark ”HEB220” as reference, are presented. Tables present running time in seconds, time difference with respect to the reference in %, ultimate load in kilo-Newtons and load difference with respect to the reference in absolute %.

Lastly, results from the geometrical parameter study of HEB220 are shown, where the tables display dimension change and the difference in running time from the reference shown in %.

5.1 Remodelling of benchmarks

5.1.1 Mesh convergence

The verification of mesh density chosen by previous authors was made with model HEB220 as representation for both models due to their similar geometry. Results can be seen in Figure 5.1, where the original HEB220 is seen as "HEB Remodel" as the black curve in the graph. General mesh size of 16 and 12 mm, which correspond to one element per thickness, gave a lower value for ultimate capacity of below 200 kN, while mesh of size 8 mm with 2 elements per thickness resulted in a closer value to "HEB remodel". Mesh orientation according to HEB remodel (Gantes) gave a difference of 0.4% compared to the mesh with overall size 4 mm. Thereby it can be said that the mesh density provided by Gantes is appropriate to for further application within this section.

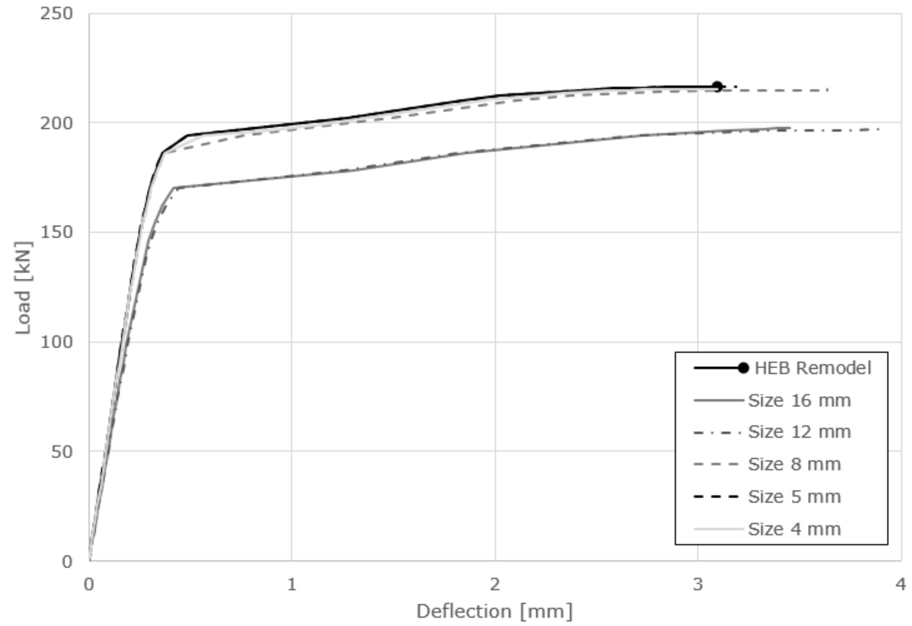

Figure 5.1: Mesh convergence study of HEB220.

5.1.2 FE-model "IPE300" and comparison to EN 1993-1-8

The force-deflection curve showing the behavior of the remodelled specimen with respective ultimate load, together with Bursi's numerical model and the value obtained by the Equivalent T-stub method (dashed line) can be seen in Figure 5.2. The different stages of stress developments, i.e when yielding is first reached, when a part is completely yielded trough or when the ultimate stress is reached etc., are shown in the Figures 5.3, 5.4 and 5.5 with same notations as in Figure 5.2.

In the T-stub specimen IPE300 happened first that the flange started to yield at a load of 94 kN at the fillet and at top side of the bolt hole. Simultaneously at the same load magnitude, the bolt started to yield at the side showing to the web. These

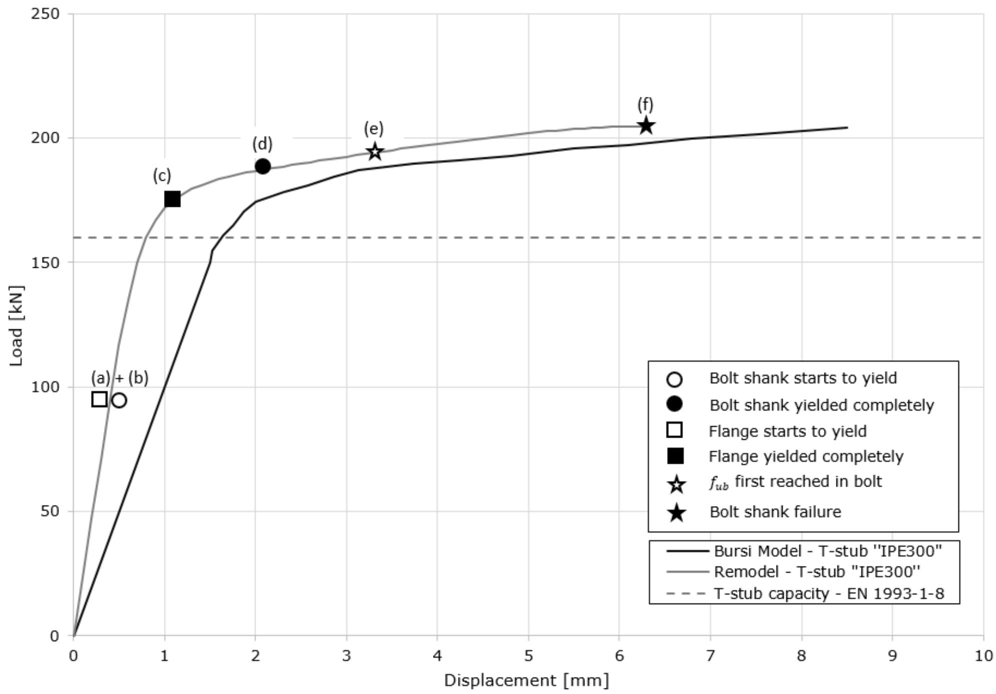

Figure 5.2: Force-deflection curve of benchmark model ”IPE300”.

two effects together with their stress distributions can be seen as stage ”a” and ”b” in Figure 5.3. Next occurred complete yielding through the flange at fillet and bolt hole level, as seen in stage ”c” in Figure 5.4, followed by the complete yielding of the bolt indicated with stage ”d”. The bolt reached the ultimate strength f_u for the first time at stage ”e” followed by the rupture of the bolt in stage ”f” at the force of 204 kN.

Further, it can be observed that the F-d curve from the remodelled and Bursi's model diverged in terms of linear stiffness. The remodelled specimen shows smaller deflections at same load magnitudes, e.g. for a applied load of 150 kN on the T-stub the remodelled T-stub display a deflection of 0.8 mm, while Bursi's has 1.5 mm. Nevertheless, the obtained ultimate load of both models shows the same value of 204 kN.

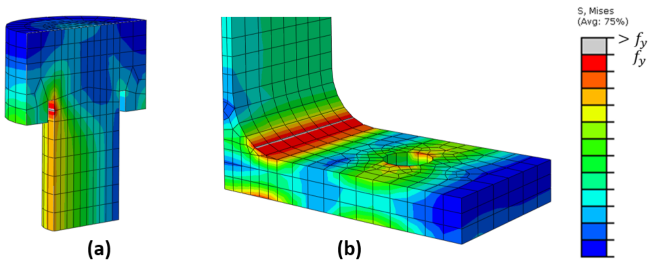

Figure 5.3: T-stub ”IPE300”: Start of yielding in bolt shank (a) and in flange at fillet/bolt hole (b).

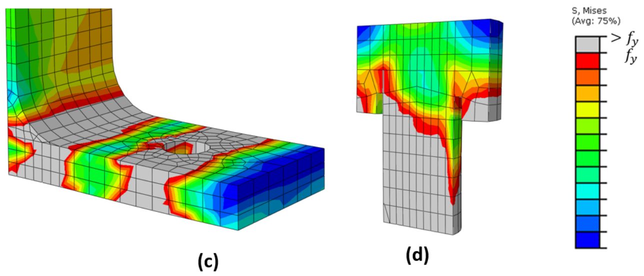

Figure 5.4: T-stub "IPE300": Complete yielding in flange at fillet/bolt hole (c) and of bolt shank (d).

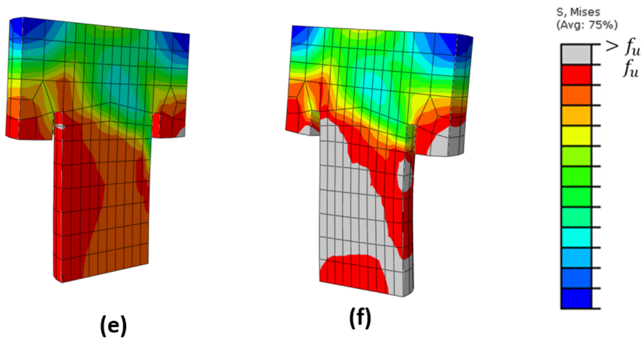

Figure 5.5: T-stub "IPE300": f_u reached in bolt shank (e) and complete rupture of shank (f).

When the connection by Bursi is designed with respect to EN 1993-1-8, seen in Section 4.2, the governing failure mode is flange failure. The ultimate load calculated correspond to 160 kN and full calculations can be seen in Appendix I.

The simplified bolt shank without threading in correspondence to Agerkov's expression, as previously explained in Section 3.5.1, removed the thread failure phenomena in the model. The thread failure occurrence was calculated separately to a value of 259 kN, as shown in Appendix III, and is not shown in the graph since its not governing.

5.1.3 FE-model "HEB220" and comparison to EN 1993-1-8

Likewise is the Force-deflection curve shown in Figure 5.6 for the benchmark T-stub HEB220 comparing the remodelled specimen, the values provided by Gantes and the capacity determined by the Equivalent T-stub method according to EN 1993-1-8. The different stages of stress distribution within the force-deflection curve are demonstrated in the Figures 5.7, 5.8 and 5.9.

The first point of yielding for HEB220 was also in the flange at the fillet, bolt hole and yielding in the bolt shank, seen in Figure 5.7 at a force of 134 kN. Next was the complete yielding of the bolt shank (c) at a load of 195 kN and complete yielding in

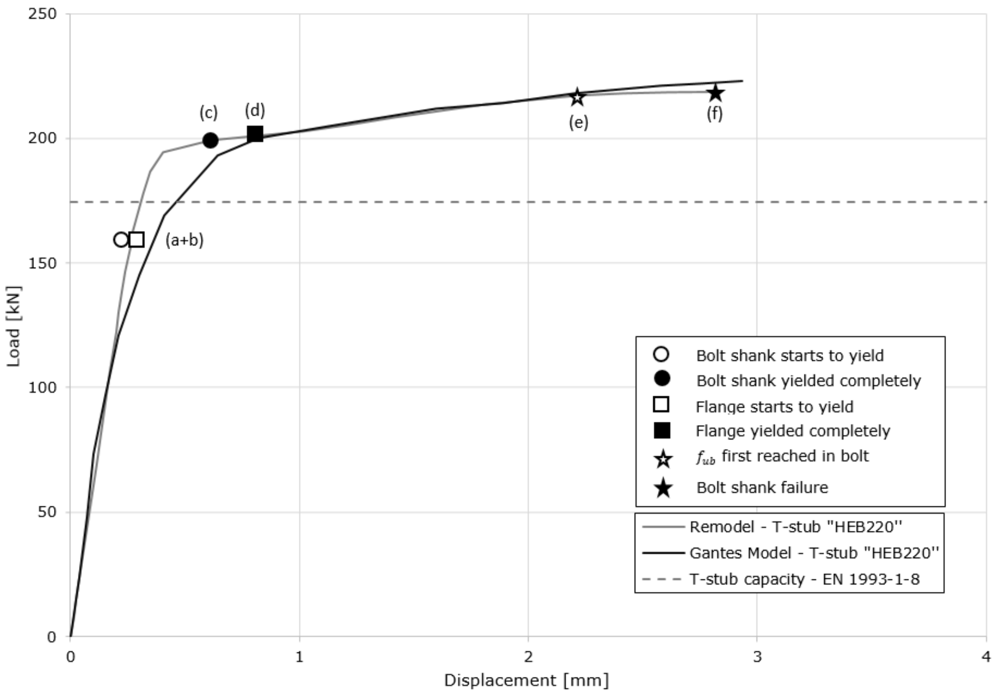

Figure 5.6: Force-deflection curve of benchmark model "HEB220".

flange at fillet (d) for a load of 199 kN. Followed by the shank reaching f_u (e) and fracture of the bolt shank (f) at a load of 220 kN, see Figures 5.8 and 5.9.

The F-d curve in Figure 5.6 has initially a similar behavior in the elastic range until a load of circa 125 kN is reached. After that the remodelled specimen was deflecting less a the same amount of load. The remodelled T-stub has a deflection of 0.40 mm for a load of 194 kN while the one from Gantes deflects 0.64 mm. Later during strain hardening the curves coincide again to end with a similar ultimate load of 220 kN.

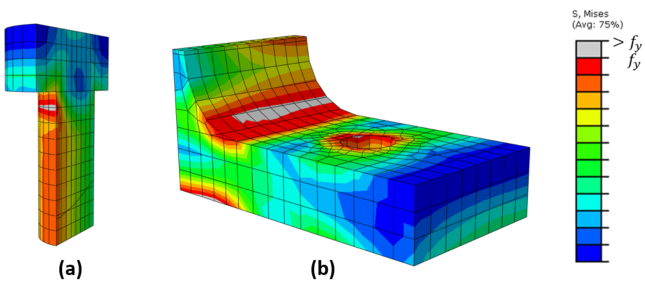

Figure 5.7: T-stub "HEB220": Start of yielding in bolt shank (a) and and in flange at filled / bolt hole (b).

For the joint by Gantes, the governing failure mode is a combined failure according to EN 1993-1-8. The ultimate load was calculated corresponding to 174 kN, seen in Figure 5.6. The calculation can be reviewed in Appendix II.

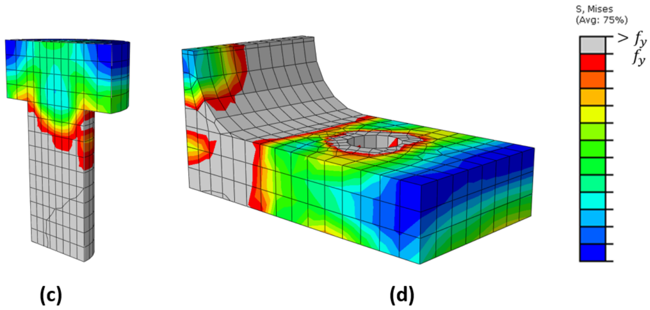

Figure 5.8: T-stub "HEB220": Complete yielding of bolt shank (c) and in flange at fillet (d)).

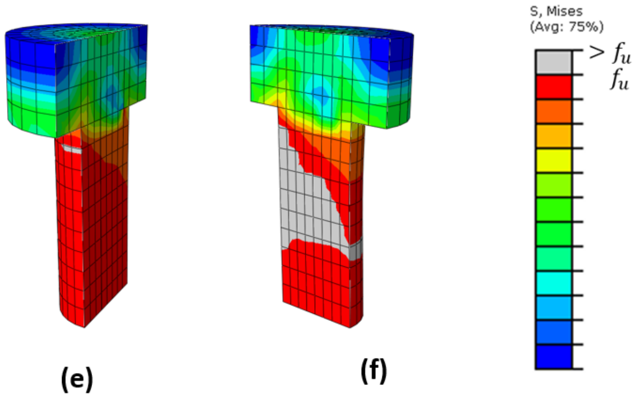

Figure 5.9: T-stub "HEB220":f_u reached in bolt shank (e) and complete rupture of shank (f).

Additionally, thread stripping occurs at load magnitude of 230 kN, which is above the capacity of the T-stub specimen.

5.2 Numerical FE-parameter study

For each studied finite element parameter change, a load-deflection (F-d) curve including the thread failure of the HEB220 model is displayed. Additionally, in agreement with the objective for a time efficient and accurate FE-model, the percentage change in ultimate load and computation time has been denoted in comparison to the standard set-up, provided by the HEB220 remodel, for every changed parameter. That comparison was executed in Tables 5.1 to 5.11. The tables are arranged in order of running time, so that the fastest model is placed at the top and the difference in time compared to the original model is seen in percentage, where a negative number indicates a faster analysis. Ultimate load is displayed and difference in ultimate load is shown as absolute percentage.

In the different subsections below, the change in behaviour of the F-d curves, as well as the impact on computational time and difference in load, can be studied for every change. Graphical and tabular outputs are developed to easily understand the accuracy and time of each FE-solution.

5.2.1 Element size

As an orientation help, the Figure 4.8 under Section 4.1.2 defines the three orientations "thickness", "length" and "width" for the present HEB220 model. The element sizes, i.e. the amount of elements per direction was the first finite element parameter to be changed and documented. The following Tables 5.1, 5.2 and 5.3 show the comparison of change in ultimate load and change of computational time in the T-stub models in percentage compared to the HEB remodel. Within the study of element sizes in directions, the results were compared with the "coarse" set-up model explained in Section 4.1.2, Figure 4.9.

Firstly, for a change of elements per thickness, it can be clearly seen in the F-d curve in Figure 5.10 that there is no perceptible difference in the behaviour of the curve from two, three (HEB), four and six elements per thickness. Roughly the same ultimate load of around 220 kN and deflection of 2.9 mm is reached. In contrast, the model "Coarse" evince an earlier and slightly stronger bending of the curve, which led to a collapse load reached at a lower level of circa 204 kN and a deflection of 3.4 mm. This was also the case for using one element per thickness (1E).

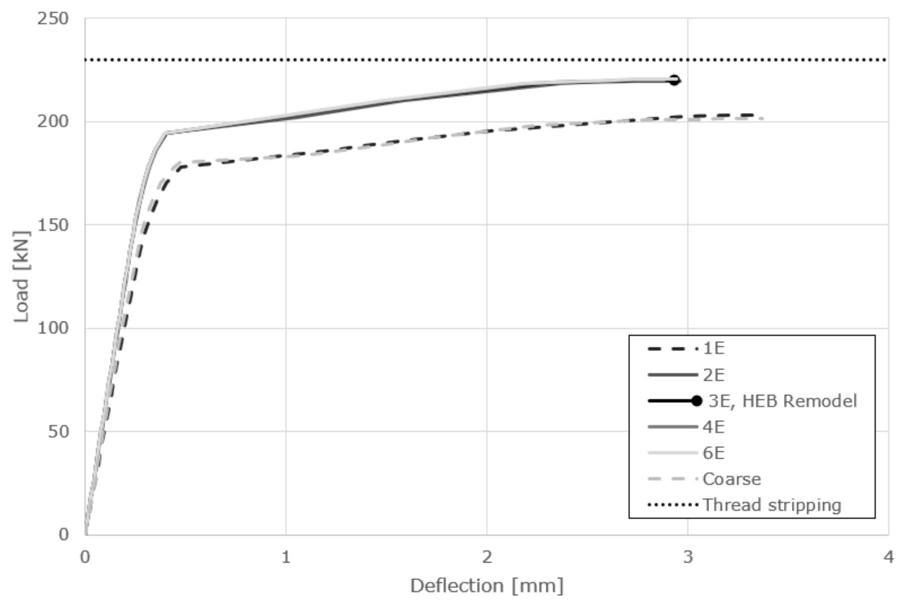

Figure 5.10: Force-deflection graph - Different elements per plate thickness.

With a closer look at Table 5.1, it can be seen that the needed time differs. A decrease from the original discretized flange with three elements to two elements per thickness led to a time gain of 9.3%, while an increase to six elements drove the computation time up with 30.6%. On the other hand, the ultimate load was barely influenced by changes in element size for alteration from "3E" to "2E", "4E" and "6E" with maximum up 0.3%. Diverging values can be seen in "Coarse" and 1E, which clearly had an impact on the ultimate load with a change of up to 8.5%.

Table 5.1: Parameter - Element amount per thickness.

Parameter -	Time [s]	Time diff. [%]	Ultimate Load [kN]	Load diff. [|%|]
1E	96	-11.1	203.1	7.7
2E	98	-9.3	219.7	0.1
Coarse	99	-8.3	201.3	8.5
3E	108	0	220.0	0
4E	110	1.9	220.4	0.2
6E	141	30.6	220.6	0.3

Secondly, for an alteration of elements in plate length, it can be observed that there is no noticeable difference in the F-d curve, seen in Figure 5.11 for the different elements per plate length, apart from a slight larger deformation for ”7E” before collapse. The model ”Coarse” is the same as in the previous study and evince the same behavior.

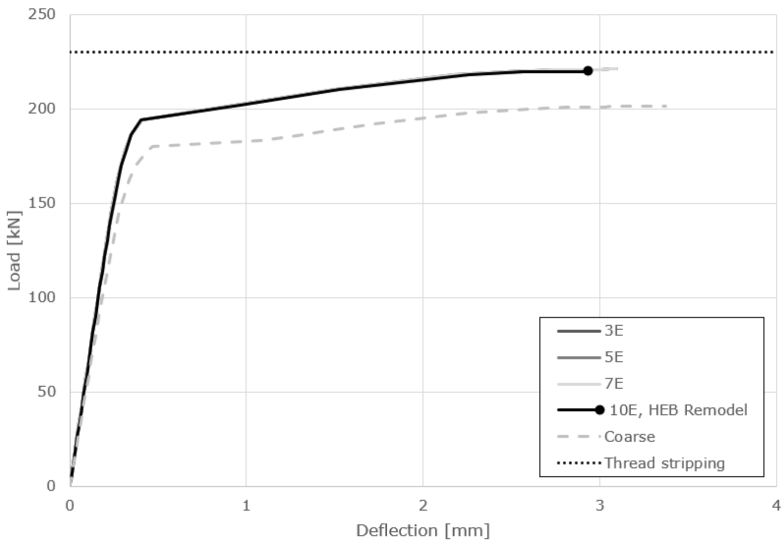

Figure 5.11: Force-deflection graph - Different elements per plate length.

As seen in Table 5.2, the deviated element quantity of five elements per length ”5E” led to a time gain of 27%, while the ultimate load was affected with 0.2%. Changing to ”7E” gave a slight time gain of 1% for a difference in load of 0.5%.

Table 5.2: Parameter - Amount of elements per length.

Parameter -	Time [s]	Time diff. [%]	Ultimate Load [kN]	Load diff. [|%|]
5E	79	-26.9	220.5	0.2
Coarse	99	-8.3	201.3	8.5
7E	107	-0.9	221.1	0.5
10E	108	0	220.0	0
3E	110	1.9	221.1	0.5

Thirdly, for a change of element quantity in plate width direction, Figure 5.12 shows no conspicuous deviation. Moreover, Table 5.3 demonstrate that all changes from the original model set-up lead to a time gain of computation. By reducing the elements to four, 30% gain in time and a load accuracy of 1% was reached, whereas an element quantity of two had 31% decrease in time with a load change of 1.4%. Additionally, an element increase to ten led also to slightly faster FE-model with 7.4%.

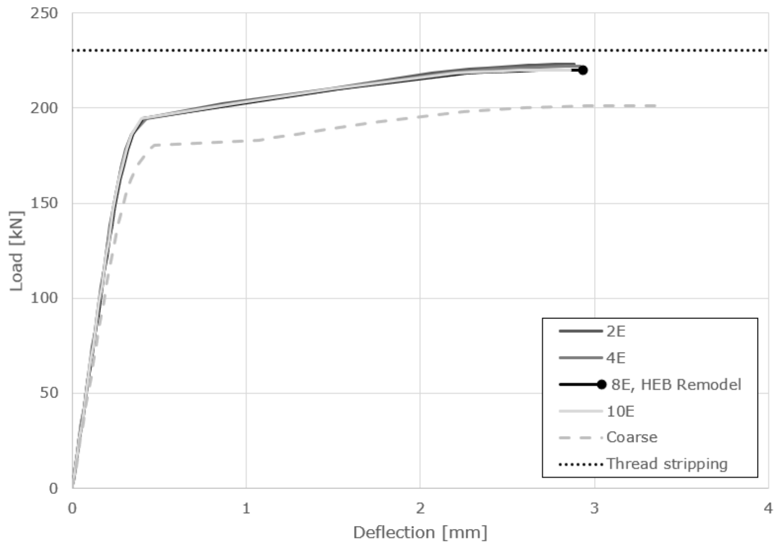

Figure 5.12: Force-deflection graph - Different elements per plate width.

Table 5.3: Parameter study - Elements per width.

Parameter	Time	Time	Ultimate	Load
-	[s]	diff. [%]	Load [kN]	diff. [|%|]
2E	74	-31	223.0	1.4
4E	76	-30	222.2	1.0
Coarse	99	-8.3	201.3	8.5
10E	100	-7.4	220.2	0.1
8E	108	0	220.0	0

5.2.2 Element types

For a change in element types, it can be observed that the Force-deflection curves, as seen in Figure 5.13, demonstrate a similar overall performance. All curves with modified element types evinced a force-deflection curve, which was slightly under the curve/values of the remodelled set-up with full integration "C3D8" elements. All alterations had a ultimate load accuracy within 2.8%, as seen in Table 5.4.

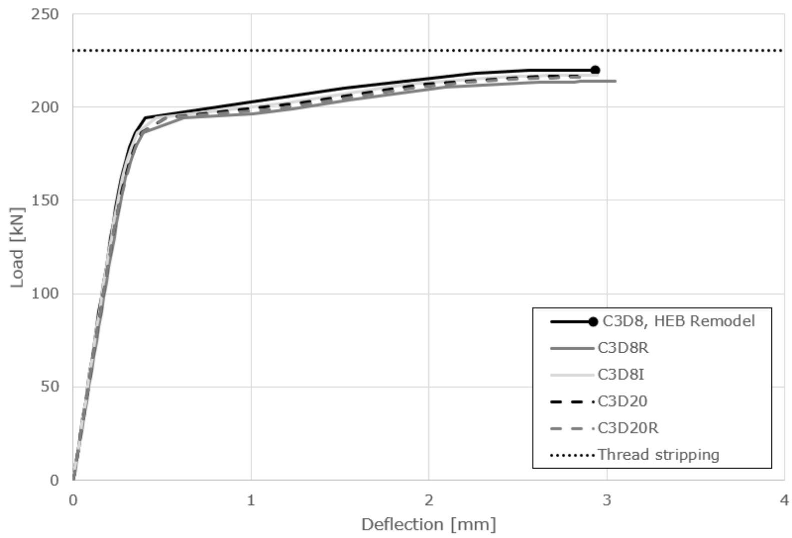

Figure 5.13: Force-deflection graph - Different element types.

There was a great deviation in running time for the different element types, compared to the HEB remodel with set-up by Gantes. While the C3D8R elements with reduced integration induced a gain in time of 19.4%, the other element types showed an increase in computation time up to 522%.

Table 5.4: Parameter study - Element types.

Parameter	Time	Time	Ultimate	Load
-	[s]	diff. [%]	Load [kN]	diff. [|%|]
C3D8R	87	-19.4	213.8	2.8
C3D8	108	0	220.0	0
C3D8I	143	32.4	217.2	1.3
C3D20R	636	488.9	216.0	1.5
C3D20	672	522.2	216.6	1.8

5.2.3 Material model

When the material model of the T-stub specimen HEB220 was changed, significant difference in the Force-deflection graph, as seen in Figure 5.14, was determined. The tri-linear material model by Diaz deviated in its behavior in terms of a higher ultimate load, governed by thread failure at 230 kN and an earlier reached failure deflection-wise. The elastic-plastic material model with strain hardening by Eurocode showed a quite similar behavior, compared to the true-stress relation of the HEB remodel. The collapse load was reached at a slightly higher value of 2.4% difference, as shown in Table 5.5.

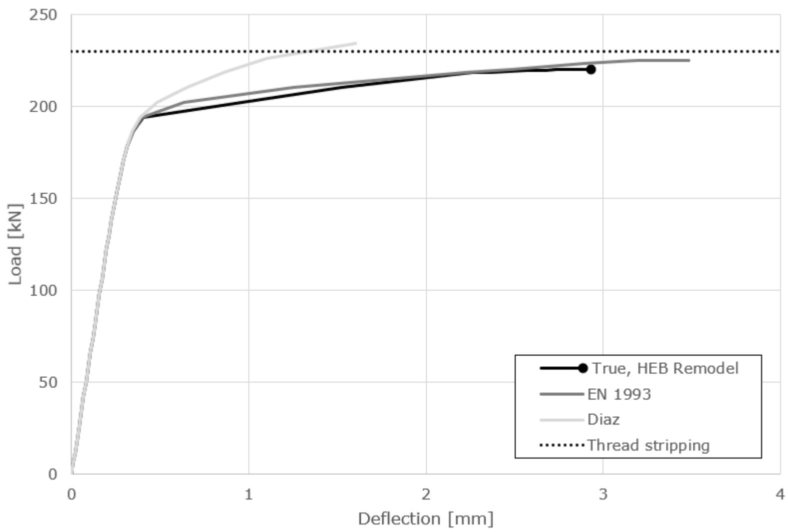

Figure 5.14: Force-deflection graph - Different material models.

The computation time varied from 3.7% time gain and a load difference of 2.4% with the bi-linear Eurocode model, to a time increase of 7.4% and 6.5% deviation in load with Diaz material representation.

Table 5.5: Parameter study - Material model.

Parameter	Time	Time	Ultimate	Load
-	[s]	diff. [%]	Load [kN]	diff. [|%|]
EN 1993	104	-3.7	225.3	2.4
True	108	0	220.0	0
Diaz	116	7.4	230.0 (234.3)	6.5

5.2.4 Contact interactions

Firstly, when changing the tangential-behaviour properties of the bolt head and plate surface interaction, the effect was very marginal on the ultimate load with a maximum discrepancy of 0.06%, as seen in Figure 5.15 and Table 5.6. The needed time on the other hand were able to drop down to 10.2% for a friction coefficient of 0.2.

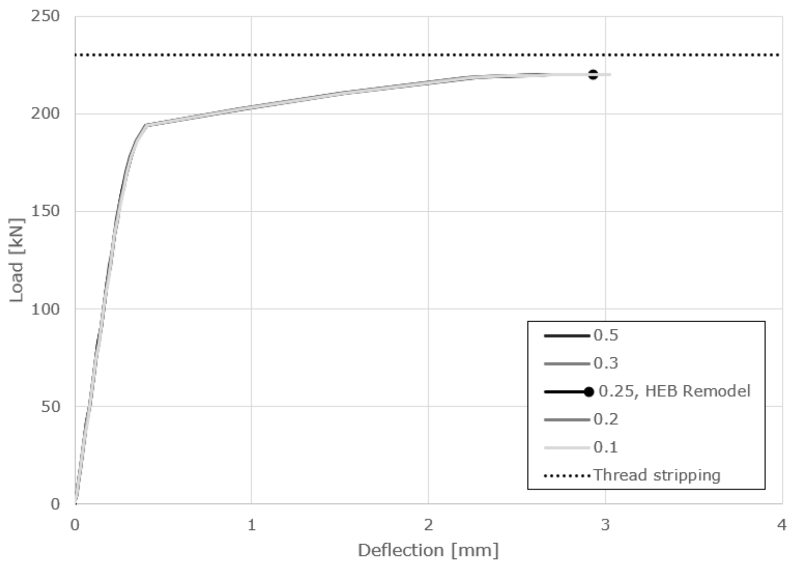

Figure 5.15: Force-deflection graph - Different tangential friction coefficients for bolt head interaction with plate.

Table 5.6: Parameter study - Bolt friction.

Parameter -	Time [s]	Time diff. [%]	Ultimate Load [kN]	Load diff. [|%|]
0.2	97	-10.2	220.1	0.03
0.1	99	-8.3	220.1	0.05
0.3	104	-3.7	220.1	0.06
0.25	108	0	220.0	0
0.5	110	1.9	220.1	0.06

Secondly, general contact was adopted for every exterior surface. There was no perceptible divergence between the different load-deflection curves seen in Figure 5.16. However, the ultimate load differed with up to 3.2%, as shown in Table 5.7, from the set-up of remodelled HEB. Moreover, the time deviation was decreased with 27.8% with a general friction coefficient of 0.1 and increased up to 8.3% for a value of 0.5.

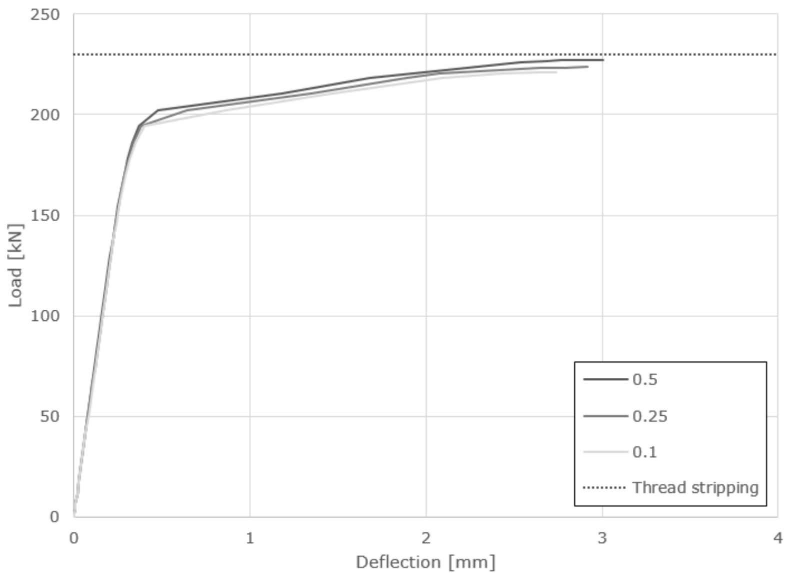

Figure 5.16: Force-deflection graph - Different general tangential friction coefficients.

Table 5.7: Parameter study - General friction.

Parameter -	Time [s]	Time diff. [%]	Ultimate Load [kN]	Load diff. [|%|]
0.1	78	-27.8	221.2	0.6
0.25	93	-13.9	223.6	1.7
0.5	117	8.3	227.2	3.2

5.2.5 Stepping

Results from change in initial step can be seen in Figure 5.17. Only selected series were plotted due to the small change, but all data can be studied in Table 5.8. Results point out that for the case with 6% of all applied load as initial load gave the lowest running time with a 39.8% difference. Nevertheless, the ultimate capacity was barely influenced by the change of initial step seen in Table 5.8.

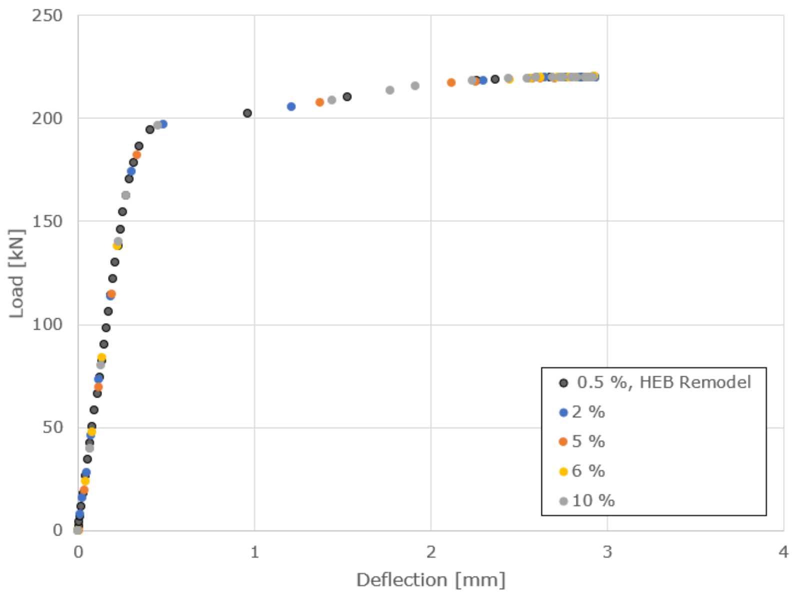

Figure 5.17: Force-deflection graph - Varying initial step.

Table 5.8: Parameter study - Initial step.

Parameter [%]	Time [s]	Time diff. [%]	Ultimate Load [kN]	Load diff. [|%|]
6	65	-39.8	220.1	0.05
5	70	-35.2	220.0	0.01
4	77	-28.7	220.0	0.01
8	82	-24.1	220.1	0.02
2	85	-21.3	220.0	0.01
10	91	-15.7	220.0	0.01
25	99	-8.3	220.0	0.02
0.5	108	0	220.0	0

For the alteration of maximum load step, the initial step was set to 6%, based on the outcome of the previous study. Results can be seen in Figure 5.18 and showed that with a small maximum step, the analysis was forced to take smaller steps than it would have done which made the analysis take longer time. For maximum step limit of 40% the time was 65s, with largest step 20.25% with accuracy of 0.05% seen in Table 5.9.

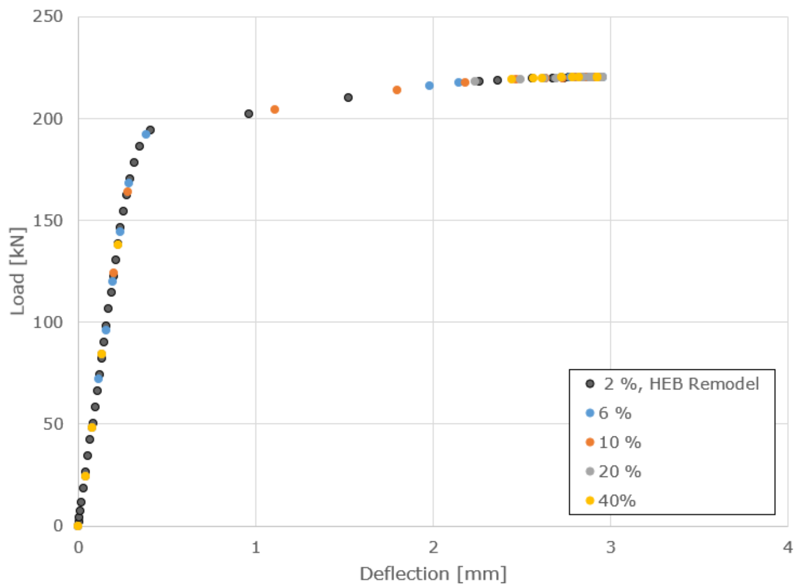

Figure 5.18: Force-deflection graph - Varying maximum step.

Table 5.9: Parameter study - Maximum step.

Parameter [%]	Time [s]	Time diff. [%]	Ultimate Load [kN]	Load diff. [|%|]
50	65	-39.8	220.1	0.04
40	65	-39.8	220.1	0.05
25	72	-33.3	220.1	0.04
20	73	-32.4	220.2	0.06
30	82	-24.1	220.1	0.05
6	82	-24.1	220.1	0.06
10	90	-16.7	220.1	0.06
2	108	0	220.0	0

5.2.6 Additional parameters

Outcome of the study of additional parameters showed a slight change in running time for the models seen in Table 5.10. The largest difference was identified for analysis with Quasi-Newton iteration method. The reduction reach 7.4% while ultimate capacity is untouched seen in Table 5.10.

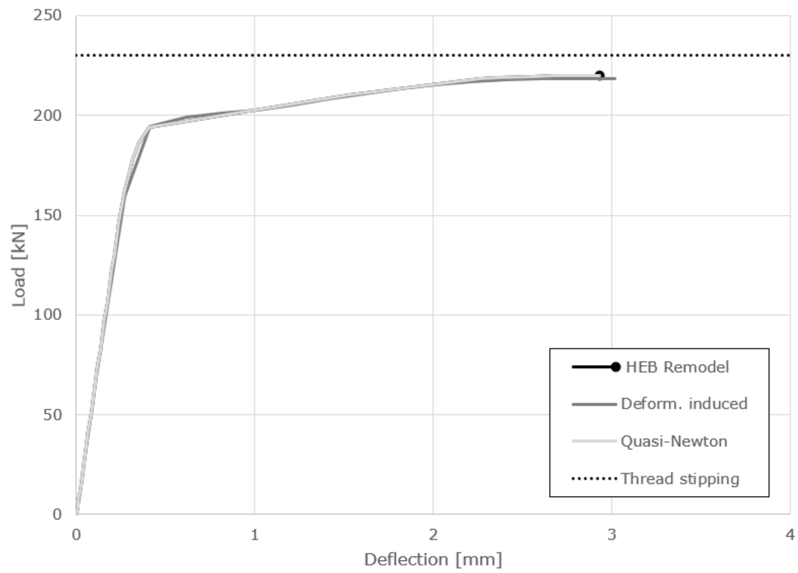

Figure 5.19: Force-deflection graph - Additional parameters.

Table 5.10: Parameter study - Additional parameters.

Parameter -	Time [s]	Time diff. [%]	Ultimate Load [kN]	Load diff. [|%|]
Quasi-Newton	100	-7.4	220.0	0
Deform. ind.	105	-2.8	218.6	0.6
HEB Remodel	108	0	220.0	0

5.2.7 Time efficient HEB220

From the previously mentioned results regarding time and accuracy, together with input from literature regarding mesh density, the following model was set up and analyzed as the time efficient model. Parameters adjusted from the HEB model were: C3D8R, 0.1 tangential friction at bolt head, stepping (init. 6% / min. 0.1% / max. 40%) and Quasi-newton iteration method. This together with a mesh density of three elements per thickness, five per length and four per width gave the following results:

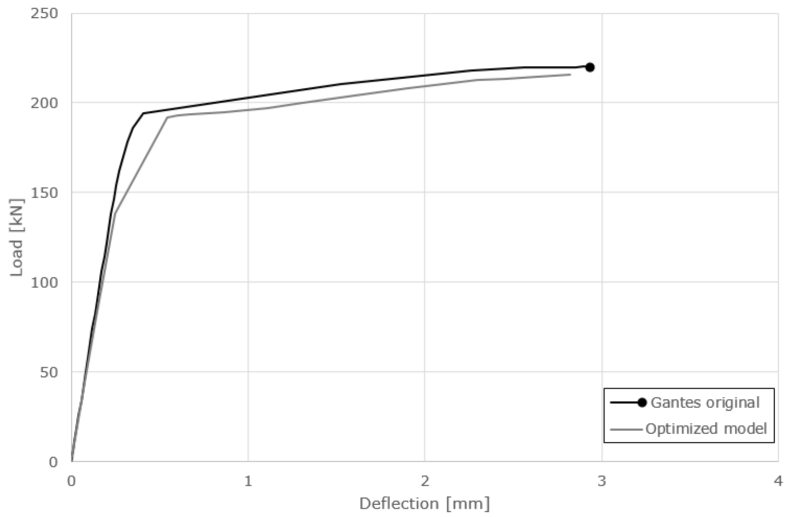

Figure 5.20: Force-deflection curve for time optimized model.

The optimization showed a reduced running time of 57.4% with a difference in ultimate load of 2.0% seen in Table 5.11. The optimized model has a sharper curve at the transition to the more flatten out part of the curve seen in Figure 5.20.

Table 5.11: Summary optimized model.

Parameter	Time	Time	Ultimate	Load
-	[s]	diff. [%]	Load [kN]	diff. [|%|]
Optimized	46	-57.4	215.7	2.0
HEB Remodel	108	0	220.0	0

5.3 Geometrical study of HEB220

Lastly, the geometrical changes made with the remodelled HEB220 came to the following results, as illustrated below. Tables display change in dimension as % and the difference in running time from the reference shown in %.

Ultimate load can be extracted from the graphs for the different alterations and the events of bolt yielding, plate yielding and bolt failure are identified in the figures below, i.e. how failure in the respective specimen with alternating dimension develops. Additionally, hand calculated values can be seen in each figure respectively, as well as thread stripping failure which was considered for the cases where F-d curve reached that level. Curves were cut when f_{ub} was reached across the entire bolt shank diameter. The hand calculation with the Equivalent T-stub method according to EN 1993, as well as the bolt thread capacity, can be seen in Appendix II, respectively in Appendix III

Change 1: Flange thickness (t_f)

Results of first geometrical change are seen in Figure 5.21 where the ultimate loads are marked as stars when bolt failure happens. All numerical models showed a higher ultimate capacity than analytical calculation according to EN 1993. The difference was largest for $t_f = 12$ mm and smallest for 14 mm with a small margin. For $t_f = 12$ mm failure occurs at more than double the deflection compared to others and flange yielding took place in the end of the linear part before plasticity. However, $t_f = 16$ mm starts with bolt yielding and follows the linear elastic curve longer.

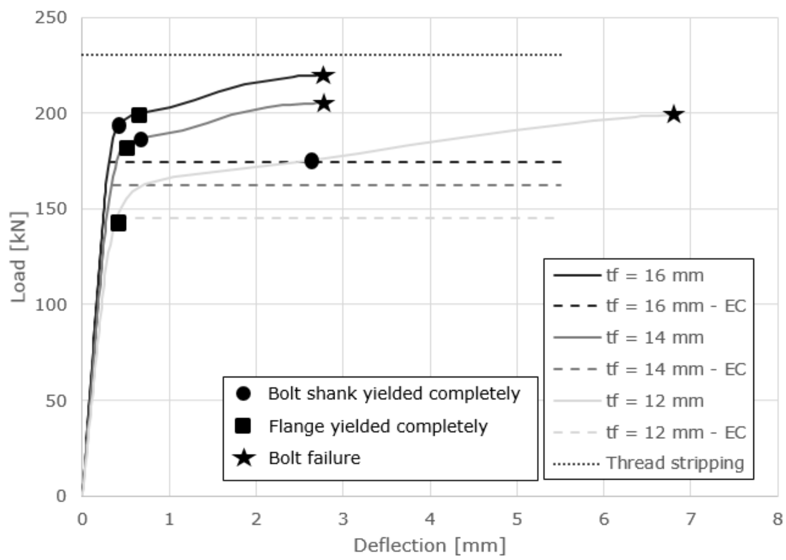

Figure 5.21: Geometrical parameter study of t_f.

Table 5.12 shows an increase in running time from the original model for both changes with up to 8.4%.

Table 5.12: Relation of t_f-change and running time.

Dimension [mm]	Change [%]	Time difference [%]	Ultimate load [kN]
16	0	0	220.0
14	-12.5	8.4	205.6
12	-25	6.9	199.3

Change 2: End distance (e_1)

Increasing the end distance increased the ultimate capacity, seen in Figure 5.22. The curve $e_1 = 40$ mm just reached thread stripping before complete tension failure. Event progression was barely affected by the change and of e_1, as bolt starts to yield first at the marked circles.

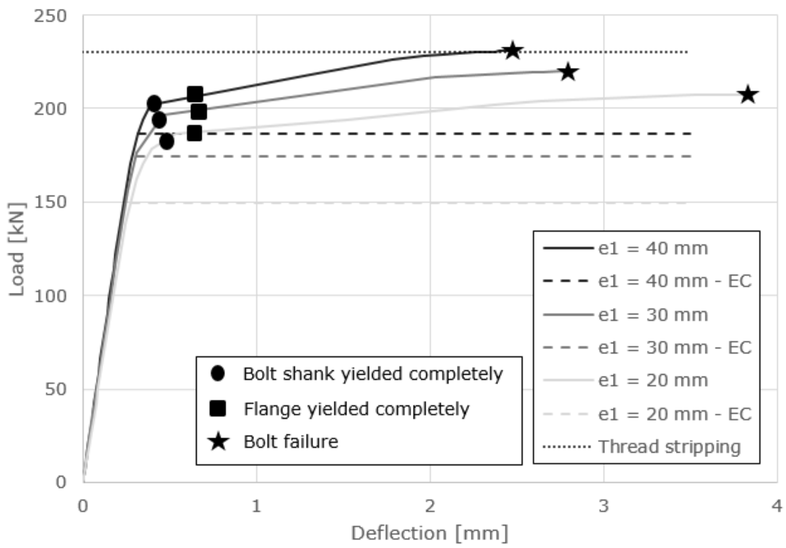

Figure 5.22: Geometrical parameter study of e_1.

The relation of geometrical change and running time is shown in Table 5.13, where it can be seen that the geometrical change of 33.3% influences the time to a small extent.

Table 5.13: Relation of e_1-change and running time.

Dimension [mm]	Change [%]	Time difference [%]	Ultimate load [kN]
20	33.3	-8.3	207.5
30	0	0	220.0
40	-33.3	3.7	230.0 (230.7)

Change 3: Bolt row distance (p)

Increased distance between bolts slightly raised the ultimate capacity and lowered the deflection until failure. Ultimate capacities according to EN 1993-1-8, marked in dashed in Figure 5.23, were less than the numerical values with 20% for all changes. Yielding happened simultaneously for bolt and flange for p = 35 mm, while bolt yielded earlier for the other changes. There was a minor difference in running time from the models seen in Table 5.14.

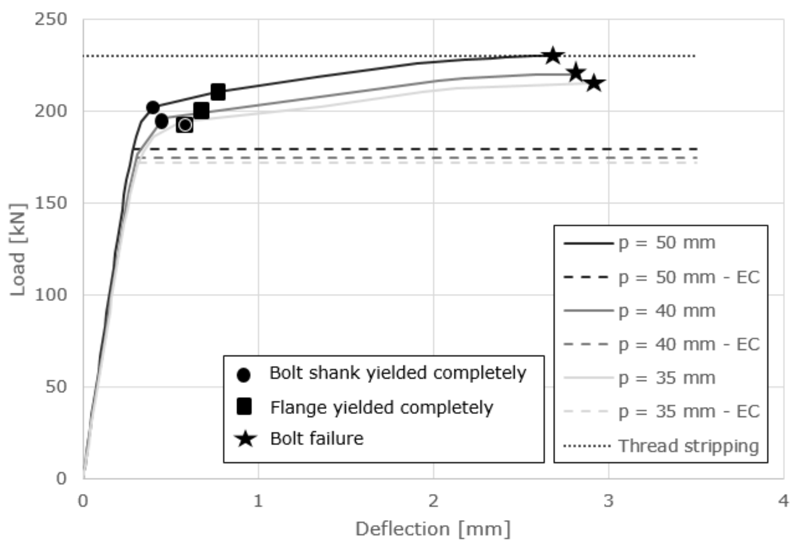

Figure 5.23: Geometrical parameter study of p.

Table 5.14: Relation of p-change and running time.

Dimension [mm]	Change [%]	Time difference [%]	Ultimate load [kN]
35	-12.5	-1.9	215.3
40	0	0	220.0
50	25	5.6	229.8

Change 4: Bolt-web distance (*w*)

There was a significant increase in ultimate load with reducing distance from web to bolt seen in 5.24, where $w = 70$ mm reached bolt thread stripping just after the linear elastic part. Moreover, adjustment of w changed linear stiffness of the T-stub seen as the varying inclination of the linear elastic part. However, the behaviour was remained for all changes where bolt yielding happened close to the plate yielding followed by bolt fracture at a higher load.

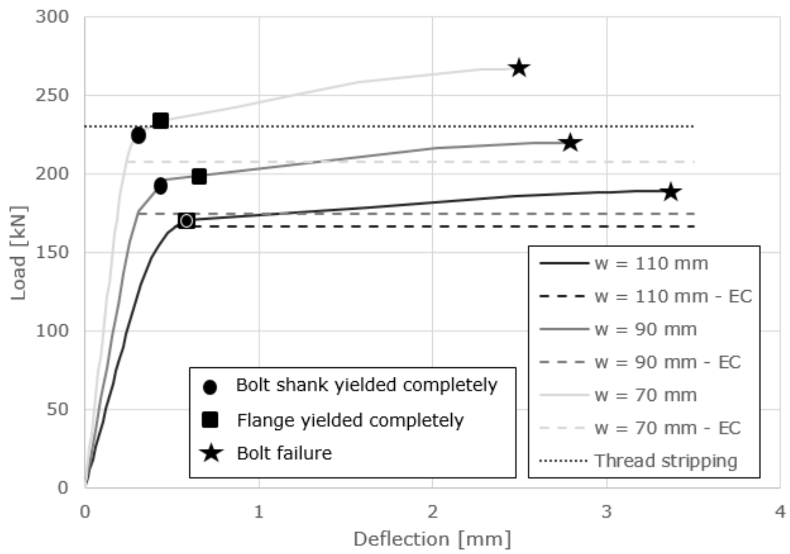

Figure 5.24: Geometrical parameter study of w.

Relation between running time and geometrical change for all changes can be seen in Table 5.15.

Table 5.15: Relation of w-change and running time.

Dimension [mm]	Change [%]	Time difference [%]	Ultimate load [kN]
70	-22.2	-3.7	230.0 (267.2)
90	0	0	220.0
110	22.2	0.9	188.9

6 Discussion

Since previous research related to time influence of FE-parameters was not found, a validation and comparison between the results of this study and previous research was not possible. However, the change of ultimate load with respect to FE-parameters has been performed in previous research mainly through comparison between FE-modelling and real experiments, which allow direct comparison opportunities. Geometrical influence on time was not found either, but ultimate capacity as well as failure mode transition could be verified with EN 1993 formulations.

The studies were carried out in a structured and successive way, where a predicted result based on literature and expectation was registered at each step. This procedure provides consistent validation in addition to the final results, which makes the results trustworthy. Furthermore, the results may be used as comparison for further research within the topic.

All analyses were made in Abaqus/CAE using a local stationary computer with server license acquired through VPN from Chalmers which might affect running time, but the time relation between results should be kept unaffected, generating valuable outcome.

6.1 Remodelling of benchmarks

The results from remodelling of benchmarks yielded in an understanding of FE-modelling, knowledge regarding failure mode progressions and led to a reference model to be used for further analyses.

The understanding of how meshing influences the overall behaviour of a T-stub is complex but crucial to achieve an accurate ultimate load. The mesh convergence study of model HEB220 showed that the mesh of the remodelled HEB was sufficient to be continued during the rest of the analyses. General mesh with element sizes 5 and 4 mm together with remodelled HEB were in the span of 1% load accuracy. All those three meshes were also made with at least 3 elements per thickness, which was also recommended by previous scientific papers. 2 elements per thickness, in form of general mesh of 8 mm, also gave a fair representation due to the selected element type of 8 nodes with full integration. The coarser mesh had a larger difference of up to 10% and as mentioned a too coarse mesh is fatal for the outcome of the FEA due to not capturing stiffness and missing high stressed areas (Shah, 2002). However, a "too fine" mesh does not provide any additional information and will just generate longer running time which creates a threshold and shows the importance of the sensitivity analysis, which confirms the theory mentioned in Section 3.3.2.

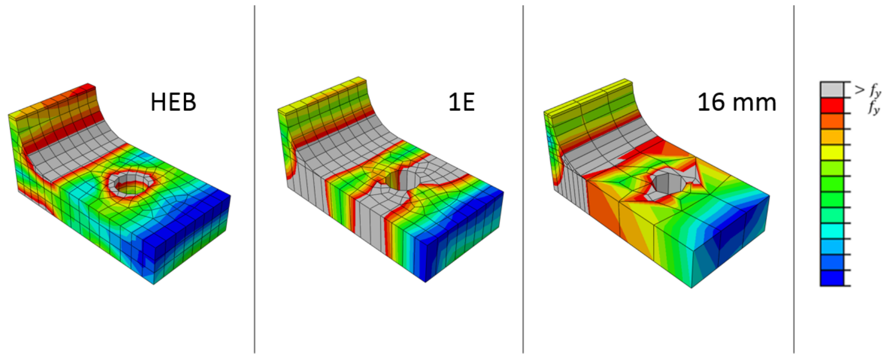

Figure 6.1: T-stub behaviour for different meshes at the same amount of applied load corresponding to 162.25 kN.

In Figure 6.1 the mesh from HEB is shown together with 1 element per thickness from the parameter study and the case with 16 mm from the mesh convergence study. The yield spread for an applied load of 162.25 kN can be identified and it can clearly be seen that the flange at the fillets are completely yielded for the cases with coarser mesh. Using 1 element per thickness makes the top and bottom of the plate yield almost simultaneously and by that the plastic hinge is created almost instantly. A complete second plastic moment hinge on the level of bolt hole is also created with one mesh, which indicates a flange failure. The formed plastic hinge induces plastic deformations in plate which in hand creates rotation in the bolt, reduces its capacity which cause earlier failure from combined action of bending and tension. Additionally, shank bending can be confirmed by the inclined von Mises stress distribution seen in Figure 6.2, where the ultimate strength f_{ub} is reached first on the tension-side.

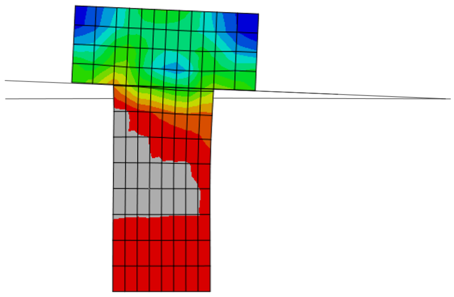

Figure 6.2: Interaction of bending in the bolt shank where the gray region indicate stress above the ultimate capacity f_{ub}.

During the mesh convergence study of the HEB220 specimen, it was discovered that the mesh in the fillet was crucial for the overall behavior of the T-stub model. Curvature represented by too few elements generate a larger model than the actual specimen, leading to inaccurate results. Because of that, the mesh density was kept as in the set-up of the created HEB remodel during the convergence study of the flange. This was also applied for the bolt head and shank as the flange was the main objective of investigation. A mesh of 16 mm is rather small in normal context, but in a plate with thickness 16 mm its representation is not sufficient.

Results from both benchmarks reached the expected limit of ultimate capacity and are about 25% over the capacity according to EN 1993, which was expected and confirm that Eurocode is conservative in terms of predicting ultimate capacity. To be noted is that the "Equivalent T-stub method" in Eurocode included safety factor of 1.25 on the results, which thereby led to a lower capacity and a conservative value. Regardless of that, results from Eurocode were still taken with safety factors since it is the way how to apply this code. This was also done later in the geometrical study. Moreover, flange failure by the ”Equivalent T-stub” method in EN 1993 is defined, when m_{pl} is reached along the yield lines in the flange, i.e. by forming a plastic hinge. Thereby redistribution of stresses above yielding are not accounted for. This redistribution in the plastic range is characteristic for steel in general, as mentioned under Theory of plasticity in Section 2.3.1. Also Lubliner (2008) states that the load capacity is higher due to strain hardening from the point on when plastic stress redistribution occurs, i.e. plastic deformation. The categorization of failure modes is strictly determined by EN 1993, see Section 2.5.2, but it changes gradually within a FEA, which can be seen in the F-d curves of both remodels, Figures 5.2 and 5.6. Deflections occur earlier in the linear-elastic part when the flange starts to yield and thereby a more bi-linear behaviour at the yield point when bolts yield first. The thicker flange in HEB220 provides more stiffness and causes the bolt to yield before the flange, creating only one plastic hinge in the flange at the fillet before bolt fracture. The thickness of the plate directly influences the plastic moment resistance, which in turn affects how much dissipated energy that is needed to create the plastic hinge. Conversely for IPE300, where complete yielding of the flange is reached before complete yielding of the bolt shank, which creates two plastic hinges in the flange and thereby bending in the plate at both fillet and bolt hole, before rupture of the bolt.

As seen in F-d graph of the IPE300 model, Figure 5.2, the remodelled T-stub and Bursi's model show a significant difference in the initial stiffness, but stop at similar ultimate load. Deflection at failure deviates about 2 mm between the original and remodelled T-stub due to the different initial stiffness. The reason of the error in IPE300 model remains undefined with a hypothesis that it may be something implicit that has been omitted by previous authors or how the LAGAMINE contact package has been processed.

However, the F-d curve of the HEB220 remodel on the other hand fits the original benchmark model regarding initial stiffness. This was achieved after troubleshooting as for the IPE300 model, which e.g. was concerning wrongly assumed bolt length with the Agerskov expression. Besides, the HEB220 model deviates a bit at the beginning of the plastic region before coinciding with the original model again. Moreover, an unexpected event occurred while modelling benchmark HEB220. Web was modelled with a height of 200 mm but the F-d curve together with stress-strain relation indicated web yielding at a load of 210 kN with large deflections as result. Deflections were progressing and upcoming stages were denoted later than expected. This was identified and adjusted by remodelling the T-stub with a small web of 1 mm after the fillet radius end. This was only cryptically mentioned in the report by Gantes in form of the dimension d but not further commented on.

In terms of the two different performed load increment methods, it can be stated that for the IPE300 a displacement increment of 0.5% from total applied 20 mm corresponds to 1.6% of the displacement at failure, which is post-calculated from the results. Whereas for the HEB220 an applied load of 400 kN and an increment step of 0.5% instead corresponded to a calculated value of 0.91% of the ultimate load. The ultimate capacity is unknown in the beginning of an analysis, which creates concern deciding step size. Moreover, there was a great difference in post-processing of both load increment methods. More effort was required for extracting the sum of nodal reaction forces in the web end, compared to a rather fast and direct extraction of the load for the force-induced loading.

Altogether, the creation of both benchmarks was not easy due to lack of expertise and lack of information that may be obvious to the authors. This resulted in a lot of learning by modelling of the benchmarks, as well as FE-application of parameters discovered in literature. Agerskov's bolt expression provided inadequate results for displacements according to Gantes and Lemonis (2003), which does not affect the thesis goal of time and ultimate capacity and is the reason why Agerskov still was considered. Moreover, minor differences between remodels and original can be expected from measuring of stress-strain relations from scientific documents. However, the figures were imported into a computer software, scaled and digitally measured to prevent errors.

6.2 FE-parameter study

Overall it can be stated that the study of different model parameters with respect to time efficiency and load accuracy opens up an interesting and wide discussion. The parametric study helped to clarify and confirm assumptions made during this thesis project, while simultaneously opening up more complex relations to investigate.

First of all, the influence of changes in element size, i.e. element quantity in a single direction, has barely an impact on the overall force-deflection curve assuming a not too coarse mesh being chosen, seen in F-d curves Figures 5.10, 5.11 and 5.12. This is due to the performed one-directional change of the mesh density. The mesh density in the other two directions were kept constant and thereby a good enough representation was still achieved. In comparison to the mesh convergence study in Section 4.1.1 where general size of all elements were changed a larger effect can be seen on the overall behaviour. The impact of coarse elements can be seen on the overall F-d curves in Figure 6.3, in which HEB220 remodel is shown as the black curve containing a fine mesh, confirmed trustworthy by the performed convergence study. Second curve is the mesh with 16 mm general size which yields quite early at the fillet and the last curve is with one element (1E) per thickness, while mesh in other two directions were kept, taken from the parameter study about elements per thickness, as shown in Figure 5.10. With a coarser mesh, the curve bends earlier, i.e. plastic region is reached at a earlier stage force-wise leading to a lowered ultimate capacity. As mentioned by Shah (2002), result depends on the mesh quality interaction in all directions, as well as a too coarse mesh will have significant effect on the final stresses and strains; both is hereby confirmed with this sub-study.

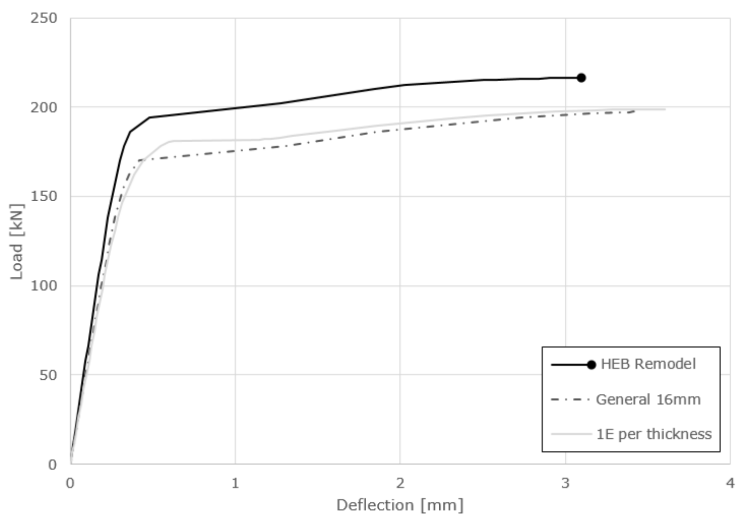

Figure 6.3: HEB220 with meshes from convergence study (16 mm), parameter study (1E) and final mesh.

That computation time is linked to the amount of elements, can be observed. A densified mesh provides the same output as a coarser mesh but with longer running time, which makes the convergence study of importance when choosing an appropriate mesh. In general it can be said that the fewer elements, the higher time gain. This is however not always the case, as seen in Table 5.2, where the decrease from 10 elements to 3 elements gives about the same computation time with the marginal difference of 1.9%. Also, the "Coarse" model, as introduced in Section 5.2.1, is in some cases more time consuming even though the amount of elements are fewer. That shows also how yield spreading within elements affect the running time in form of amount of iterations required. Brick elements perform best, when they are of similar size in all directions, which make the shape of elements affect the spread (Wang et al., 2004). The study was disturbed by the bolt hole that influenced the way the software created the mesh. Amount of elements was selected along the outer boundaries but closer to the bolt hole in the model the mesh was reoriented and more elements were created to fit the hole diameter.

Díaz et al. (2011) conclusion of three required elements per thickness to accurately capture bending moment, is verified and can be seen in the mesh convergence study and in this parameter study. Three elements per thickness is sufficient to give a good representation and more elements provide the same output with a longer running time. However, it is of importance to remember the parameters that influence how the mesh performs. For reduced integration elements (C3D8R) with one integration point per element a distribution of three elements per plate thickness is sufficient, when looking in one direction. By having this said, the F-d curve for elements per thickness, Figure 5.10, shows a marginal difference in behaviour for 2 elements per thickness when run with 8 node elements with 8 integration points, which shows that the bending of the flange at the fillet is represented accurately with the element type and mesh. However, for a representation with the "Coarse" mesh, multiple directions of the mesh density were changed, which then led to a large influence on the overall behaviour. As the parameter study contained single parameter changes, no discrete information regarding impact of multiple changes with the exception of the "Coarse" model can be made. However, there is a large correlation between mesh density and element types that need further investigation. A study with several changes at the same time would have been more extensive though.

A good element discretization can be achieved by different set-ups and is strongly related to how the mesh set-up is performed. As an example, a certain amount of linear 8-node full integration "brick" (C3D8) elements or alternatively quadratic 20-node (C3D20) elements with 27 integration points are sufficient respectively for different mesh densities. In other words, first-order elements might require a finer mesh to obtain an accurate result, than a quadratic element for the same specimen, as previously described in Section 3.3.1. For the HEB220 model with a fixed mesh density, the element gives an increased running time of 522%, compared to the linear C3D8 element type. So the geometrical order of each element, together with the large amount of nodes is the cause of the longer running time.

The performance of different element types might differ. As mentioned by Bursi and Jaspart (1997b) in Section 3.3.1, the C3D8 elements provide an overestimation of ultimate capacity while C3D8R gives an underestimation and the incompatible mode, C3D8I, is quite exact for cases where plasticity is involved. No experimental data from model HEB220 was present, but the obtained results from this study indicate the same trend. This can be studied in Figure 5.13, where ultimate loads obtained had the same rank as mentioned. On the other hand, the difference in running time is evident. The element C3D8R is the only element type with a time gain due to its reduced integration points, which require less calculation time. The other studied 8-node element C3D8I has an increased time of 32.4% due to 13 added dofs, which are condensed to the outer nodes. Whereas the second-order 20-node elements C3D20 and C3D20R are even costlier in terms of time due to their increased number of nodes and integration points.

For problems governed by bending, the shear locking phenomena may appear with first-order elements with full integration (C3D8), as described under Section 3.3.1. The geometrical set-up of HEB220 is governed by a combined failure which corresponds to bending of the flange. Additionally, the plate both at the fillet and bolt is subjected to bending, which is displayed in terms of von Mises stresses. However, there were no traceable effects of shear locking, in terms of false displacement or stresses, found during analysis.

Material models have a much greater impact on the behavior of the Force-deflection curve than expected, as seen in Figure 5.14 under Section 5.2 and compared to the other studied finite element parameters. The model with bi-linear elastic-plastic material from EN 1993 shows a similar response as the F-d curve with true stress-strain by Gantes, except from a slight increased deformation capacity before failure. Whereas with the bi-linear material model, a time gain of 3.7%, as found in Table 5.14, was achieved. An assumption is that this is due to the linear stress-hardening compared to the true formulation. In contrast, with Diaz tri-linear material representation a different behavior can be observed. The initial stiffness in the elastic region is similar, while the performance deviates in the plastic region, leading to ultimate load capacity governed by bolt thread failure at 230 kN with a small ultimate displacement. By that point, a divergence in ultimate load of 6.5% and an increased time of 7.4% was obtained. The running time is affected by the needed amount of iterations in each load step. A larger strain hardening coefficient as in Diaz model causes more yield spreading in each load step, which can induce longer running times. However, the reason for the climbed ultimate load is due to the predicted inclination of $E/30$ at strain hardening in the model, as previously shown in Figure 3.6, which is not accurate with reference to the true stress-strain curve. This difference in ultimate capacity is much larger, which indicates for the case of no provided material properties, an assumption regarding material is needed. It is essential to select a model with proper strain hardening inclination to represent the behaviour after yielding, provided that the plastic region is of importance in the analysis.

A change in the tangential friction coefficient of the bolt head - plate interaction did not effect the overall F-d curve, as seen in Figure 5.15, but conversely a time decrease of up to 10.2% was obtained. The reason for the non-diverging ultimate loads lay in small impact of tangential contact behaviour in general regarding the failure load of a T-stub in tension (Bursi and Jaspart, 1997b). This tangential was introduced within the framework of the benchmarks replication accordingly to the authors. Moreover, all other surfaces were selected to be friction-less, while the only affected surfaces were between plates and the envelope surface in the bolt hole. The applied "hard contact " in normal direction kept the surfaces to each other and prevented penetration without resistance. The contact surface at bolt nut and washer was reduced throughout all analyses according to Krolo et al. (2016), so no information regarding the influence can be made regarding amount of interaction surfaces, as they were consistent.

Within the second interaction substudy with general contact of all exterior surfaces, the difference in time compared to the original set-up, is up to 28%, as seen in Table 5.7, for a friction coefficient of 0.1. In fact it can be said, that running time decrease with a decreased coefficient. Furthermore, it can also be confirmed that the ultimate capacity of the HEB220 model is increased, when the tangential contact for every surface is implemented. The ultimate load is increased by e.g. 3.2% for a friction coefficient of 0.5. This is mainly due to introduced friction between both plates, where the upper plate is now "sliding" with a harder resistance on the lower one while the T-stub specimen is being pulled up. The enhanced T-stub resistance with an increased friction was indeed expected, which is in agreement with Bursi and Jaspart (1997b) results from his journal. Thus, the impact of friction in a connection in tension, is rather small when comparing to slip-resistant connections subjected mainly to shear. On the other hand, EN 1993 provides only friction values for the design of slip resistance with preloaded bolts, as previously mentioned in Section 3.4, which is interpreted as an indication of the importance of friction in shear connections.

The finite element parameter of load steps/increment in a FEA has among others, the highest impact on computation time for the finite element model of HEB220. Nevertheless, both induced changes of initial load step and maximum load step are having a negligible influence on the ultimate load accuracy with a maximum divergence of 0.06 %, as seen in Tables 5.8, 5.9. This is reasonable since both initial and maximum load step decide about how load is applied early in the analysis, while the final converged value is governed by the minimal step. Minimal step size sets the tolerance about how small a load increment can be and decides about the time until convergence and the deviation of ultimate capacity. Thereby, the minimum step affects both ultimate load accuracy and running time in contrast to the initial step and maximum allowed step, which only influence time. However, all three depend on that the "correct" ultimate capacity is represented by the other model parameters. Another benefit of the maximal load step is that it can be used as a tool to obtain a finer stepping and therefore a good illustration of stress distribution, by choosing a small value. Moreover, based on the initial step, the software calculates the following step, and so on, which mean that the initial step determines the amount of steps along the linear region as the steps are increasing in the beginning, seen in Figure 6.4. The converged value of the ultimate load is also seen in Figure 6.4 as 55% of the applied load which corresponds to 220 kN.

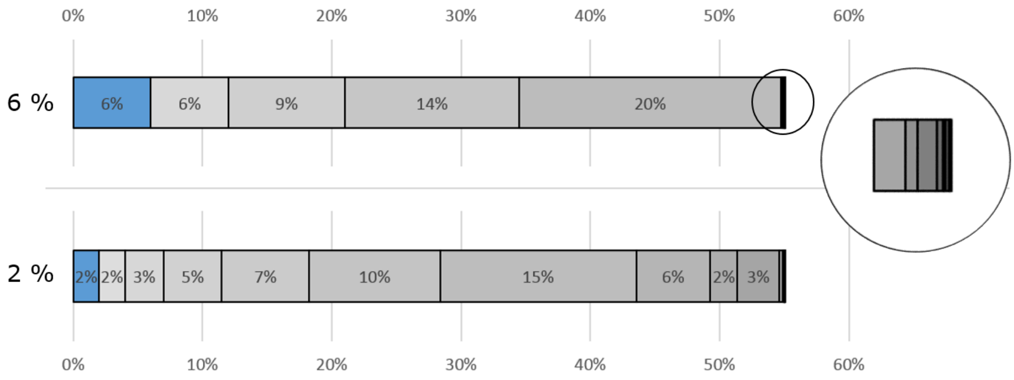

Figure 6.4: Visualized automatic load stepping procedure - Chosen initial steps 6% and 2%.

The way load is applied in terms of increments or steps, in particular with initial step and maximum step, is crucial for the impact on time of the FEA. Larger load steps normally generate a faster analysis which is good when the ultimate capacity is striven for. But when plastic behaviour is accounted for, more steps are required to cover for the geometrical changes of the specimen. Initial step is most time efficiently placed at 6% of the applied load, corresponding to an initial load increment of 24 kN or 11% in terms of the T-stub capacity. That gives a decrease in time of 39.8%, as seen in Table 5.17 under Results. For the studied maximum allowed load step, the result shows that setting the step to 40 or 50% gives the same time reduction of 39.8%. The largest chosen load step by Abaqus, with a maximum allowed step of at least 40%, was 20.25%. Furthermore, maximum allowed step size of 100% thereby give the same results as max step 40%, as it was used for the initial step study with 6%, seen in Figure 6.4. To determine the reason of 20.25% being the largest step, further investigation needs to be performed by looking into how Abaqus uses the automatic stepping technique. Overall it can be stated that selecting the maximum allowed step size to 100% of the applied load is easiest, since the FE-software automatically chooses load stepping. Nevertheless, for programs without automatic stepping it is good to know that a step cannot be taken too large due to the risk of missing the plastic region.

Stepping is a percentage of the applied load, which directly connects stepping with the load increment method, i.e. if load is applied as prescribed displacement or as actual load, as explained in Section 3.1.1. For all performed FEA within the frameworks of this model parameter study, apart from the substudy about maximum load step itself, the maximum allowed load increment was restrained to 2% to cover the plastic region in a good way. Thereby many small load steps were also applied in the elastic region of the F-d curve. That is not essential since the relation is linear and no significant changes are happening in this region. On the other hand, a deformation-induced technique applies displacement increments and thereby covers the elastic range much faster due to the relatively small elastic deformations before yielding. At the same time the plastic region is also well represented. This is resulting in a slight time decrease of the FE-model with a deformation-induced loading, as seen in Table 5.10, compared to the load-induced manner as in remodelled HEB220. Moreover, complications can occur while trying to select proper stepping, when the ultimate capacity and plastic deformations are still unknown. A small size is conservative, but will generate longer running time. If an accuracy of 0.5% is needed, fixed increments of 0.5% does not provide this due to that the fixed increments are based on the applied load and not the ultimate load of the model. Automatic stepping however adjust the stepping to a precise converged result while taking necessary steps along the way. Abaqus can also automatically reduce the first step size, if the size is defined too large, as in the "25% initial step", where no solution could be found during eight iterations. The first step was then reduced to 6.25% automatically and the procedure continued.

Adjusting to Quasi-Newton iteration method gave a noticeable difference in time. A reduction in running time of 7.4% was achieved while the ultimate load was kept unaffected, as seen in Table 5.10. This corresponds to the theory discussed under FE-parameters, Section 3.1.1, in which it is mentioned that the normal Newton method has the highest convergence rate, though not automatically the fastest running time due to its stiffness update and inverting in each iteration step. Quasi-Newton on the other hand performs the inversion once in the first load step and then just updates the stiffness matrix based on previous steps. This is most likely the reason for the time gain.

Regardless of whether load or displacement is applied, it has a rather small impact on time and ultimate load. Adjusting the Gantes set-up to a deformation-induced loading, the F-d curve was limited to the selected applied deflection and will continue to that defined limit. To be noted is that registered F-d values after the occurred bolt failure were cut away along the curve, but the selected running time on the other hand was still from the point where a converged solution was found. With this performed procedure in mind, the running time might be larger than originally, but that's not the case, as it is 2.8% faster. Despite that, the total applied deflection could be lowered, hence the related initial step and the maximum step should have been adjusted, to make a difference. Most important, if the applied deflection is set too low, nothing can be stated regarding the ultimate capacity.

The time efficient model was created based on the results from the performed sub-studies. That means that this optimization is limited to this HEB220 specimen and specific values for model parameter cannot be directly applied to any other type of steel connection in tension. The taken parameters for the optimized model can be reviewed in Section 5.2.7. To be noted is that the mesh was designed coarser than the remodelled HEB, but sufficiently to still perceive bending in the flange. This was done in particular with respect to the selected reduced element type (C3D8R). Moreover the limit of convergence, i.e. the minimal load step was also adjusted to 0.1% in this final model as an attempt to decrease the time. The 0.1% minimum step limit is equivalent to 0.4 kN, which is a deviation of 0.2% to the ultimate capacity by the HEB model, assuming an error in load accuracy of at least that value.

The optimized model is a result from merging time efficient parameters based on both time and accuracy. The load difference from HEB is 2.0%, while the influence on time is computed to a time gain of 57.4%, as shown in Table 5.11. That was performed without being able to foresee the degree of interaction between multiple changes. On the other hand, a time decrease of 39.8% for the "step setting" substudy was achieved with just a change of how load was applied, while the time efficient model is a result of merging different time optimized model parameters. That clearly emphasizes the crucial importance of the way of load application in a FE-model in terms of computing time and that the different FE-parameters influence each other. In addition, the plastic region in the optimized model, as seen in F-d curve in Figure 5.20, is not sufficient for a stress analysis as the steps are too coarse. This is influencing events along the curve, but for sought ultimate load this is sufficient.

6.3 Geometrical study

The results from the geometrical parameter study revealed mainly predicted results together with some exceptions worth discussing.

First of all, FE-parameters including mesh density were consistent during the geometrical studies, which means that the change within all performed substudies affected only the element size, not the amount of elements. By this, the amount of integration points remain the same and the difference in calculation were only the new geometries for the elements. The expectation of having the same running time for all of the geometrical changes were partly correct since the obtained difference was less than 10%. The difference occur from calculation complexity i.e. the difficulty to solve, which generates an altering amount of iterations. The largest deviation was an increase of 8.4% for $t_f = 14$ mm, while for $t_f = 12$ mm it has shrunk to 6.9%, making it hard to predict the change in running time. Larger plastic region generate longer running time as seen when the solver takes more iterations to find equilibrium. Furthermore, for the changed parameters e_1, p and w. As seen in Tables 5.13, 5.14 and 5.15, the computing time is decreasing down to a maximum of 8.3% for a reduced geometry (33%), while the opposite occurs similar for the increased dimensions. Nevertheless, it can be said that the geometry of a specimen should not influence the running time to a large extent, making the running time almost independent of geometrical changes, which opens up for applications to joints with other dimensions as long as FE-parameters are kept and mesh is sufficient.

Ultimate load was significantly influenced by geometrical changes which changed the behaviour of the T-stub, as expected. It is known that ultimate load changes with dimension, but the impact selected properties made, was remarkable. Decreasing thickness of the flange (t_f) from 16 mm to 12 mm is a thickness reduction of 25% and simultaneously it lead to a lower ultimate load with a deviation of 20 kN, equivalent to roughly 10%. Swanson and Leon (2000) stated that thickness is the most important factor, however results show that the distance from web to bolt hole is just as important. The distance from web to hole (w) had the largest impact on ultimate load, when comparing 90 mm to 70 mm with an increase of capacity for the smaller number of w, i.e. the shortest lever arm, with about 47 kN. This case led to bolt stripping (230 kN) just after linear elastic part, which indicates low utilization ratio of both flange plate and bolt shank, so that thinner dimension of plate could be used with similar results, but more likely that a larger bolt could have been used so that the overall capacity could be increased. The dimension w influence the distance between applied load and bolt, which plays a big role in terms of the resulted moment, see Figure 6.5. The flange thickness t_f contributes to the plastic moment resistance, W_{pl}, and by that affects the flange behaviour directly.

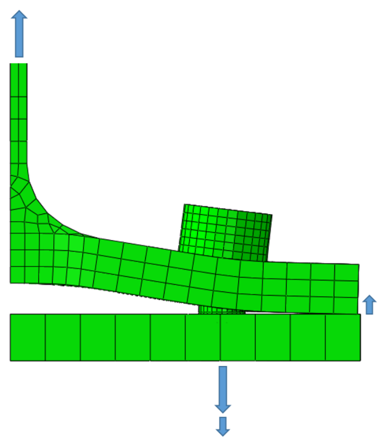

Figure 6.5: Force equilibrium on IPE300 close to failure.

The distance e_1 also affects the moment equation by distance to resultant of the prying force, while the dimension p affects more the degree of interaction between the two bolt rows, i.e. how much the capacity is reduced due to a combined interaction of two bolt rows acting as a group. The larger the dimension p, the more each bolt-row acts individually and thereby the strength is increased. The overall influence of p on the ultimate load is roughly the same, as for the other studied dimensions.

Furthermore, the analytical results follow the same trend as the FEA of how geometry is influencing the ultimate load capacity, seen in Figures 4.11, 4.12, 4.13 and 4.14. The obtained capacities are below the numerical solutions, which indicates the conservatism of Eurocode and confirms the expectation.

During the studied failure mode progression, geometry was changed in order to see the impact of these changes on the failure modes, both in accordance to finite element analysis and EN 1993-1-8. Easiest visualized is the change in flange thickness, which is related to the plastic moment behaviour of the flange. With a thin flange, see Figure 5.21 for t_f = 12 mm, the flange yielded much faster than the bolt and therewith generating deflections in the flange. Same behaviour is seen in remodelled benchmark IPE300, Figure 5.2, where the smooth transition between linear and plastic region in the f-d graph is shown. EN 1993 determine both these models as flange failure and both include two plastic hinges, one at the fillet and one at the bolt hole.

For the case with $t_f = 16$ the failure is "combined" by EN 1993 formulation and the curve behave linear until complete yielding of the bolt shank occur. That happens before the flange has completely yielded and thereby creates a sharper and more clear yield point. Flange yields at the fillet and no complete yielding takes place around the bolt hole. Illustration of the difference is displayed in Figure 6.6, where the yield spread is much more extensive at the bolt hole, forming the second plastic hinge, for the case with 12 mm flange thickness.

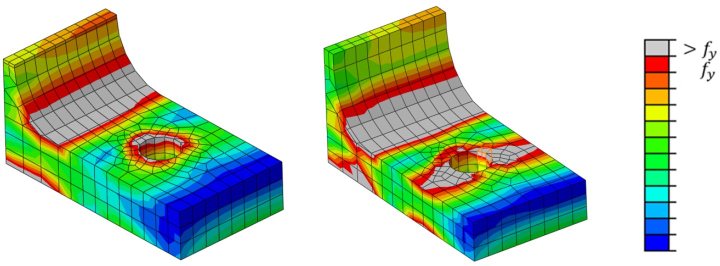

Figure 6.6: Yield spread for HEB with $t_f = 16$ on the left and $t_f = 12$ on the right.

It can be seen that both cases, seen in Figure 6.6, categorized with different failures by EN 1993, finally fail in a bolt failure at a higher load. Plastic deformations occur in the T-stub and the higher the deflection is, the more force is taken by normal force in the flange with the same reasoning as large deformations in the string example mentioned in Section 2.2. Simultaneously the bolt head experience rotation induced by the flange, reducing its capacity due to interaction of bending and tension in the shank. Likewise, the theory can be applied for much thicker flanges, where no bending occurs in plastic hinges and thereby also no rotation in the bolts. This leads to a failure of complete tension failure in the bolt shanks, categorized as bolt failure by EN 1993-1-8. Moreover, the formulation according to EN 1993 determines failure when a plastic hinge is created and thereby it does not take the redistribution of stresses above yielding into account. Thereby the full potential of steel with its good ability for plastic redistribution of stress, as previously introduced in Section 2.3.1, is not utilized.

The changes of other dimensions e_1, p and w do not influence the failure mode progression significantly, but some things can be identified:

- Variations of dimension e_1 does not change the failure mode progression, but the resulting plastic deformation before failure is increased with a decreased end distance e_1. This is due to a smaller counterbalancing flange part on the outside of the bolt and thereby a larger rotation angle at the bolt, which enables a larger displacement capacity before the governing bolt failure is reached. The overall principle can be better visualized with Figure 6.5, that shows the forces acting in equilibrium on the T-stub.
- Additionally, the distance perpendicular to the load direction (p) does not significantly change the overall failure progression seen in Figure 5.23. However, an indication can be seen that the flange yields later with increasing value of p while complete yielding of flange and bolt happens simultaneously for $p = 35$ mm. Shorter distances for the bolt-row distance were not chosen due to the limitation of the "distance to edge"-formulation by Table 3.3 in EN 1993-1-8.
- Lastly, change of w shows a significant increase in initial stiffness for bolts placed closer to the web, directly connected to the lever arm between applied force (web) and reaction force (bolt). The linear region in Figure 5.24 ends with bolt yielding in all cases followed by flange yielding, just as the other models with "combined" failure.

Thread stripping governs failure for a few geometrical changes. Bursi and Jaspart (1997a) provided an expression for the bolt thread failure, as previously mentioned in Section 2.1.3. The amount of active threads could have been chosen in a range from 3 to 6, where an increased number of threads leads to a higher thread capacity. On the safe side, the minimum number of active threads possible (3) was assumed for all analyses performed. With the chosen three active threads, the capacity was indicated in all F-d curves, as seen in Figure 5.12 to 5.15 and additionally displayed in the graphs within the parametric study, as in Section 5.2. For same cases of changed dimensions, thread failure occurs before actual bolt rupture. If more active threads had been chosen, this phenomena, as seen in some F-d relations, would have not occurred. Moreover, thread stripping is normally prevented by choosing standard bolts and nuts, i.e. without varying strength properties, as mentioned under Section 2.1.3.

Additionally, the Agerskov expression, more precisely the effective bolt length, should have been verified since Gantes and Lemonis (2003) stated before that it might lead to inadequate results for maximum displacements of a T-stub model. This verification could have been performed trough modelling the whole T-stub connection, without making using of symmetry planes. The outcome from that could be directly compared to the present obtained outcome and thereby the correctness of the Agerskov's expression within the field of T-stubs in tension, can be be judged.

Finally, it has to be noted that the time-optimized model, as introduced in Methods 4.1.2 and through performed sub-studies assembled in Section 5.2.7, was supposed to be further used for this geometrical study. The idea was to have a fast model and still get accurate enough results. This intend failed though, when the first geometrical dimension "flange thickness" was performed, since it lead to ultimate load values deviating much from capacities provided in the now performed substudy, which are based on the benchmark set-up of the HEB220. The cause was probably the coarser mesh used in the time efficient model, which only gave quick and accurate result for t_f = 16 mm, while deviating more and more for 14 and 12 mm. However, the choice to run the geometrical study with the HEB220 set-up was made due to the fact that the relation between geometric change and running time is expected to be consistent, if the same model set-up is used throughout all changes in dimensions.

7 Conclusion

It is hard to justify, whether a FEA is advantageous because of its user dependence. However, the presented facts can prevent errors in modeling with finite elements via understanding of how phenomena are represented, which increases the reader's basic knowledge and opens up the possibility to create their own models. Moreover, it can generally be said that FE-parameters influence on ultimate load is marginal and that the influence on time can be large.

The following conclusions can be drawn for knowledge regarding FE-modelling and the related model parameters:

- Sensitivity analysis of mesh should always be performed.
- Mesh should be made with three elements per shortest length and remain of similar size in all directions.
- Mesh density clearly has an effect on the T-stubs behavior in terms of stress appearance.
- Interaction of mesh size and element type should be considered while setting up an appropriate mesh.
- If plastic deformations are considered, the strain hardening within the material model should be carefully selected.
- Bolt asymmetry can be simplified with Agerskov's expression.
- Way of load application needs to be established in accordance with amount of applied load or deflection, to achieve the desired output.
- Friction should be considered in a shear-connection.

For the influence of model parameters on computing time and ultimate load accuracy, the subsequent can be concluded:

- Amount of nodes and integration points increase the running time, while maintaining a sufficient load accuracy.
- Friction has a minor impact on a T-stub component in tension w.r.t. ultimate capacity while computational time decreases with decreasing friction coefficient.
- Way of applying load has the largest impact on running time.
- Load incrementation (Stepping) does not contribute to the ultimate capacity thereby relying on other parameters representation.
- Quasi-Newton iteration scheme leads, while maintaining load accuracy, to a slight time gain, despite a lower convergence rate.

For the influence of geometrical changes both on time and ultimate load, as well on the overall behavior of the T-stub specimen, the following can be concluded:

- Geometrical changes have a slight impact on computing time due to more iterations when having more extensive yielding.
- Mainly lever-arm related dimensions affect the T-stub's overall behaviour.
- With increasing dimensions t_f, p and e_1 the ultimate load increases, while increasing w, leads to an ultimate load decrease.
- Plastic deformation of the flange induces rotation of the bolt head, which in hand leads to bolt failure by combined bending and tension.
- EN 1993 defines failure at the formation of a plastic hinge, neglecting strain hardening.
- EN 1993-1-8 provides only a sharp transition about the definition of governing failure mode for a T-stub in tension.
- Thread failure is governed by the amount of active threads.

Altogether, it must be said that the before mentioned conclusions and recommendations can be only applied to T-stubs in tension with similar geometry. Nevertheless, the following Figure 7.1 provides a quick overview about what needs to be considered for the FE-model of a bolted steel connection in tension.

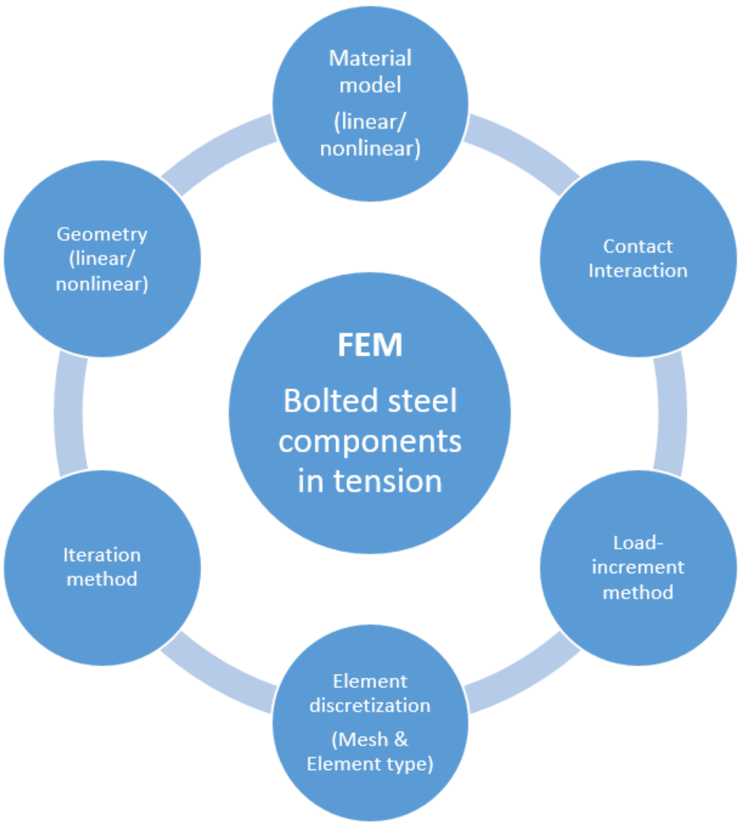

Figure 7.1: Work-chart - FE-model set up.

8
Future studies

During this study, several interesting relations and questions arose, which could be further investigated. Mainly regarding computational time, ultimate load accuracy and mechanical behaviour of T-stubs, but also practical implementation. These can be summarized as follows:

- Combined interaction of FE-parameters with respect to load and accuracy.
- Automatic step techniques.
- Loop program with generalized set-up model to be used for multiple analyses.
- Dynamic loading - Fatigue and Eigenfrequency.
- Temperature depending material models - Fire design.
- Make use of Yield line method to create a general estimation tool for ultimate load including the effect of bending in bolts.
- Probabilistic evaluation of partial safety factors.
- FE-implementation of connections subjected to shear.

Bibliography

Al-Emrani, M., Engström, B., Johansson, M., and Johansson, P. (2011). *Bärande konstruktioner Del 2*.

Alverne, A. and Deus, E. (2012). Determination of the reinforced concrete slabs ultimate load. *Latin American Journal of Solids and Structures*, 9(9):69–93.

Bandyopadhyay, J. N. (2008). *Design of concrete structures*. Prentice-Hall of India.

BCSA (2003). *Steel Buildings*. Number 35.

Bursi, O. S. and Jaspart, J. P. (1997a). Benchmarks for Finite Element Modelling of Bolted Steel Connections. *J. Construct. Steel Res*, 43(3):17–42.

Bursi, O. S. and Jaspart, J. P. (1997b). Calibration of a Finite Element Model for Isolated Bolted End-Plate Steel Connections. *J. Construct. Steel Res*, 44(3):225–262.

CEN (2005). EN 1993-1-8: Eurocode 3: Design of steel structures - Part 1-8: Design of joints. Technical report.

CEN (2006). EN 1993-1-5: Eurocode 3-Design of steel structures-Part 1-5: Plated structural elements. Technical report.

CEN (2009). EN 1993-1-1: Eurocode 3: Design of steel structures - Part 1-1: General rules and rules for buildings. Technical report.

Chakrabarty, J. (2006). Stresses and Strains. In *Theory of Plasticity (Third Edition)*, chapter 1, pages 1–55.

Chakrabarty, J. (2012). Foundations of Plasticity. In *Theory of Plasticity (Third Edition)*, chapter 2, pages 56–126.

Chin, S. C., Al Fakih, K., and Doh, S. (2017). Finite Element Analysis of Beam to Column Bolted Connection – A Review. *Indian Journal of Science and Technology*, 10(8):1–9.

Collette, Q., Wouters, I., and Lauriks, L. (2011). Evolution of historical riveted connections: joining typologies, installation techniques and calculation methods. pages 295–306.

Dassault Systèmes (2014). Abaqus/CAE User's Guide.

Dassault Systèmes (2016). Abaqus/CAE 2017.

Demonceau, J.-F., Weynand, K., Jaspart, J.-P., and Muller, C. (2010). Application of Eurocode 3 to Steel Connections with Four Bolts per Horizontal Row. Technical Report January 2010.

Díaz, C., Victoria, M., Martí, P., and Querin, O. M. (2011). FE model of beam-to-column extended end-plate joints. *Journal of Constructional Steel Research*, 67(10):1578–1590.

Engström, B. (2014). *Design and analysis of slabs and flat slabs*. Göteborg, Sweden.

Francken, D. (1910). La construction civile. Les matériaux et leur mise en œuvre. Technical report.

Gantes, C. J. and Lemonis, M. E. (2003). Influence of equivalent bolt length in finite element modeling of T-stub steel connections.

Gilbert, M., He, L., and Pritchard, T. . (2015). The yield-line method for concrete slabs: automated at last. The yield-line method for concrete slabs: automated at last. Technical report.

Grimsmo, E. L., Aalberg, A., Langseth, M., and Clausen, A. H. (2016). Failure modes of bolt and nut assemblies under tensile loading. *Journal of Constructional Steel Research*, 126:15–25.

Jaspart, J. and Maquoi, R. (1995). Effect of bolt preloading on joint behaviour. In *Proceedings of the First European Conference on Steel Structures*, pages 219–226, Athens, Greece.

Jaspart, J.-P. and Demonceau, J.-F. (2008). European design recommendations for simple joints in steel structures. *Journal of Constructional Steel Research*, 64(7-8):822–832.

Kelly, P. (2013). Yield Criteria in Three Dimensional Plasticity. In *Solid Mechanics Part II*, chapter 8, pages 259 –280.

Kennedy, G. and Goodchild, C. (2004). Practical Yield Line Design. Technical report, © The Concrete Centre, Blackwater, United Kingdom.

Kirby, B. (1995). The behaviour of high-strength grade 8.8 bolts in fire. *Journal of Constructional Steel Research*, 33(1-2):3–38.

Krishnamurthy, N. and Durwood, E. (1976). Correlation between 2- and 3-dimensional finite element analysis of steel bolted end-plate connections. *Computers and Structures*, 6(4-5):381–389.

Krolo, P., Grandić, D., and Bulić, M. (2016). The Guidelines for Modelling the Preloading Bolts in the Structural Connection Using Finite Element Methods. *Journal of Computational Engineering*, 2016:1–8.

Leon, R. and Swanson, J. (2000). Tests On Steel T-Stub Connections. Technical report.

Lubliner, J. (2008). *Plasticity Theory.* Pearson Education, Inc, revised (p edition.

Lundh, H. (2000). *Grundläggande Hållfasthetslära.* Instant Book AB.

McLain, T. (1998). Connectors and fasteners: Research needs and goals. In *Wood Engineering in the 21st Century: Research Needs and Goals*, pages 56–69.

Meyboom, J. (2002). Limit analysis of reinforced concrete slabs. Technical report.

Moore, D. and Wald, F. (2003). Design of Structural Connections to Eurocode 3 - Frequently asked questions. Technical report.

Neves, L., Cruz, P., and Henriques, A. (2001). Reliability analysis of steel connection components based on FEM. *Engineering Failure Analysis 8*, 8:20.

Pisarek, Z. and Koz, A. (2008). Effective length of end plate in moment connections with four bolts in the row. page 10.

Prager, W. (1955). The Theory of Plasticity : A Survey of Recent Achievements. page 17.

Santiago, A., da Silva, L. S., Latour, M., Rizzano, G., and Trezza, S. (2013). Theoretical and Experimental Analysis of T-Stubs With Four Bolts. Technical report.

SCI and BCSA (1995). Joints in Steel Construction: Moment Connections. Technical report.

Shah, C. (2002). Mesh Discretization Error and Criteria for Accuracy of Finite Element Solutions. Technical report.

Singulani, A. P. (2014). Advanced Methods for Mechanical Analysis and Simulation of Through Silicon Vias.

Sun, E. Q. (2006). Shear Locking and Hourglassing in MSC Nastran , ABAQUS , and ANSYS. *MSC Software Users Conference*, pages 1–9.

Swanson, J. A., Kokan, D. S., and Leon, R. T. (2002). Advanced finite element modeling of bolted T-stub connection components. *Journal of Constructional Steel Research*, 58:17.

Swanson, J. A. and Leon, R. T. (2000). Bolted Steel Connections: Tests on T-Stubs Components. *Journal of Structural Engineering*, 126(1):50–56.

Vrouwenvelder, A. C. W. M. and Witteveen, J. (2003). The plastic behaviour and the calculation of plates subjected to bending. page 111.

Wang, E., Nelson, T., and Rauch, R. (2004). Back to Elements - Tetrahedra vs . Hexahedra. *Ansys*, (9):15–16.

Yorgun, C., Dalci, S., and Altay, G. A. (2004). Finite element modeling of bolted steel connections designed by double channel. *Computers and Structures*, 82:2563–2571.

Zienkiewicz, O. C. and Taylor, R. L. (2003). *Finete Element Method - Solid Mechanics (Volume 2)*. Elsevier.

Appendices

I
Appendix

Calculation - T-stub Benchmark 1

12/5 -2019
Felix Dubrefjord
Ole Netek

Master Thesis:
Recommendations for finite element modelling of bolted T-stubs in tension

Design of ultimate capacity for T-stub according to EN 1993-1-8

Benchmark 1

- O. Bursi *"Calibration of a Finite Element Model for Isolated Bolted End-Plate Steel Connections"*

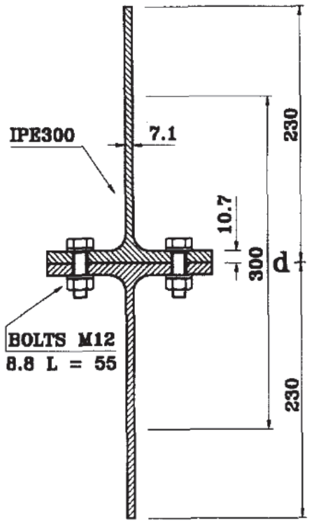

Flange in bending with prying forces,
Lowest value from *EN3-1-8 Table 6.2*
Mode 1: Complete yielding of the flange
Mode 2: Bolt failure with yielding of the flange
Mode 3: Bolt failure

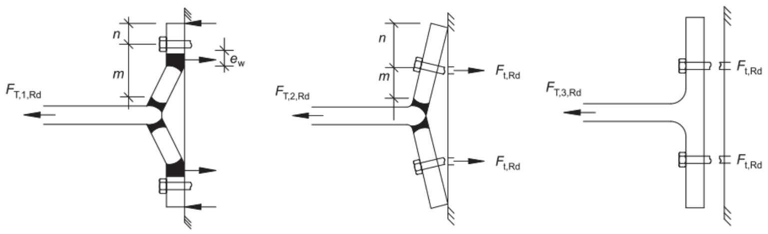

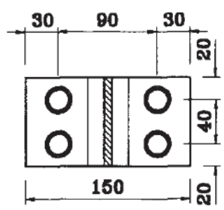

Bursi True stress-strain

Plate yield strength $f_y := 450\ MPa$

Plate ultimate strength $f_u := 790\ MPa$

Bolt yield strength $f_{yb} := 900\ MPa$

Bolt ultimate strength $f_{ub} := 1040\ MPa$

Bolt dimensions

Hole diameter M12 $d_0 := 13\ mm$

Effective thread area
[Nodic Fastening Group] $A_s := 84.30\ mm^2$

Bolt head diameter
[DIN 931] $d_w := 19\ mm$

Effective diameter of bolt $d := 2\sqrt{\frac{A_s}{\pi}} = 10.36\ mm$

Distance from bolt center to plastic hinge $e_w := \frac{d_w}{4} = 4.75\ mm$

Plate dimensions

Distance between holes $w := 90\ mm$
Width flange $b_p := 150\ mm$
Thickness flange $t_f := 10.7\ mm$
Thickness web $t_w := 7.1\ mm$
Radius, web and flange $r := 15\ mm$

Distance to end $e_1 := \frac{b_p - w}{2} = 30\ mm$

Distance to edge, transverse $e_2 := 20\ mm$

Distance between bolt-rows $p := 40\ mm$

Check of edge distances [EN 1993-1-8 Table 3.3]

$e_{min.edge} := 1.2 \cdot d_0 = 15.6\ mm$
$e_{min.bolt.x} := 2.2 \cdot d_0 = 28.6\ mm$
$e_{min.bolt.y} := 2.4 \cdot d_0 = 31.2\ mm$

$e_{max.edge} := 4 \cdot t_f + 40\ mm = 82.8\ mm$
$e_{max.bolt.x} := min\left(200\ mm, 14 \cdot t_f\right) = 149.8\ mm$
$e_{max.bolt.y} := min\left(200\ mm, 14 \cdot t_f\right) = 149.8\ mm$

$e_{min.edge} < e_1 = 1$ $e_{max.edge} \geq e_1 = 1$

$e_{min.edge} < e_2 = 1$ $e_{max.edge} \geq e_2 = 1$

$e_{min.bolt.y} < p = 1$ $e_{max.bolt.y} \geq p = 1$

Capacity one bolt row

EN3-1-8 Table 6.2, 6.4
- 1 bolt row
Column flange bending

Bolt distances

Figure 6.2; Distance from camfer/ fillet to center hole	$m := \frac{w - t_w - 2 \cdot 0.8 \cdot r}{2} = 29.45\ mm$
Figure 6.8; Shortest distance to outer edge in load direction	$e_{min} := min\left(e_1\right) = 30\ mm$
Figure 6.8; e is the same as e_1	$e := e_1 = 30\ mm$
Table 6.2; Distance to plastic hinge	$n := min\left(e_{min}, 1.25 \cdot m\right) = 30\ mm$

Effective length for END bolt row; Bolts act individually

Table 6.4; Circular patterns	$l_{eff.cp} := min\left(2 \cdot \pi \cdot m, \pi \cdot m + 2 \cdot e_1\right)$
Table 6.4; Non-circular patterns	$l_{eff.nc} := min\left(4 \cdot m + 1.25 \cdot e, 2 \cdot m + 0.625 \cdot e + e_1\right)$
Mode 1	$l_{eff.1} := min\left(l_{eff.cp}, l_{eff.nc}\right) = 107.65\ mm$
Mode 2	$l_{eff.2} := l_{eff.nc} = 107.65\ mm$

Partial safety factor for connections [EN1993-1-8 Table 2.1]	$\gamma_{M2} := 1.25$
Table 6.2; Moment capacity	$M_{pl.1.Rd} := \frac{l_{eff.1} \cdot {t_f}^2 \cdot f_y}{4 \cdot \gamma_{M2}} = 1.109\ kN \cdot m$
Table 6.2; Moment capacity	$M_{pl.2.Rd} := \frac{l_{eff.2} \cdot {t_f}^2 \cdot f_y}{4 \cdot \gamma_{M2}} = 1.109\ kN \cdot m$
Table 3.4; Bolts not countersunk	$k_2 := 0.9$

Table 3.4; Tension resistance for one bolt

$$F_{t.Rd} := \frac{k_2 \cdot f_{ub} \cdot A_s}{\gamma_{M2}} = 63.124 \ kN$$

Amount of bolts in active row

$$n_{bolt} := 2$$

Table 3.4 Punching shear per bolt

$$B_{p.Rd} := \frac{0.6 \cdot \pi \cdot d_w \cdot t_f \cdot f_u}{\gamma_{M2}} = 242.19 \ kN$$

Failure modes from Table 6.2

Flange yielding

$$F_{T.1.Rd} := \frac{\left(8 \cdot n - 2 \cdot e_w\right) \cdot M_{pl.1.Rd}}{2 \cdot m \cdot n - e_w \cdot (m + n)} = 172.219 \ kN$$

Combined failure

$$F_{T.2.Rd} := \frac{2 \cdot M_{pl.2.Rd} + n \cdot \sum_{i=1}^{n_{bolt}} F_{t.Rd}}{m + n} = 101.024 \ kN$$

Bolt failure

$$F_{T.3.Rd} := \sum_{i=1}^{n_{bolt}} F_{t.Rd} = 126.248 \ kN$$

Critical load; Combined failure

$$F_{T.single.Rd} := min\left(F_{T.1.Rd}, F_{T.2.Rd}, F_{T.3.Rd}\right) = 101.024 \ kN$$

$$B_{p.Rd} \cdot n_{bolt} = 484.379 \ kN$$

Can be applied for both bolt row 1 and 2 separately
---> Check combined

Combined row 1 & row 2

EN3-1-8 Table 6.2, 6.4
- 2 bolt rows
Column flange bending

Bolt distances

Figure 6.2; Distance from plastic hinge to center hole

$$m = 29.45 \ mm$$

Table 6.2; Distance from end of plate to center hole $n = 30\ mm$

Thickness of flange $t_f = 10.7\ mm$

Figure 6.10; Distance between bolt-row holes $p = 40\ mm$

Figure 6.8; e is the same as e_1 $e := e_1 = 30\ mm$

Figure 6.8; Shortest distance to outer edge in load direction $e_{min} := min\left(e_1\right) = 30\ mm$

Effective length for END bolt row; Bolts act in group

Table 6.4; Non-circular patterns $l_{eff.nc} := min\left(2 \cdot m + 0.625 \cdot e + 0.5 \cdot p, e_1 + 0.5 \cdot p\right)$

Table 6.4; Circular patterns $l_{eff.cp} := min\left(\pi \cdot m + p, 2 \cdot e_1 + p\right)$

Effective length for row 2 is the same as row 1

Table 6.4; Non-circular $\sum_{i=1}^{2} l_{eff.nc} = 100\ mm$

Table 6.4; Circular $\sum_{i=1}^{2} l_{eff.cp} = 200\ mm$

Mode 1 $l_{eff.1} := min\left(\sum_{i=1}^{2} l_{eff.nc}, \sum_{i=1}^{2} l_{eff.cp}\right) = 100\ mm$

Mode 2 $l_{eff.2} := \sum_{i=1}^{2} l_{eff.nc} = 100\ mm$

Partial safety factor for connections [EN1993-1-8 Table 2.1] $\gamma_{M2} := 1.25$

Table 6.2; Moment capacity $M_{pl.1.Rd} := \dfrac{l_{eff.1} \cdot {t_f}^2 \cdot f_y}{4 \cdot \gamma_{M2}} = 1.03\ kN \cdot m$

Table 6.2; Moment capacity

$$M_{pl.2.Rd} := \frac{l_{eff.2} \cdot {t_f}^2 \cdot f_y}{4 \cdot \gamma_{M2}} = 1.03\ kN \cdot m$$

Table 3.4; Bolts not countersunk

$$k_2 := 0.9$$

Table 3.4; Tension resistance for one bolt

$$F_{t.Rd} := \frac{k_2 \cdot f_{ub} \cdot A_s}{\gamma_{M2}} = 63.124\ kN$$

Amount of bolts in active row

$$n_{bolt} := 4$$

Table 3.4 Punching shear per bolt

$$B_{p.Rd} := \frac{0.6 \cdot \pi \cdot d_w \cdot t_f \cdot f_u}{\gamma_{M2}} = 242.19\ kN$$

Failure modes from Table 6.2

Flange yielding

$$F_{T.1.Rd} := \frac{(8 \cdot n - 2 \cdot e_w) \cdot M_{pl.1.Rd}}{2\ m \cdot n - e_w \cdot (m+n)} = 159.981\ kN$$

Combined failure

$$F_{T.2.Rd} := \frac{2 \cdot M_{pl.2.Rd} + n \cdot \sum_{i=1}^{n_{bolt}} F_{t.Rd}}{m+n} = 162.08\ kN$$

Bolt failure

$$F_{T.3.Rd} := \sum_{i=1}^{n_{bolt}} F_{t.Rd} = 252.495\ kN$$

Critical load; Combined column flange bending

$$F_{T.combined.Rd} := min\left(F_{T.1.Rd}, F_{T.2.Rd}, F_{T.3.Rd}\right) = 159.981\ kN$$

$$B_{p.Rd} \cdot n_{bolt} = 968.759\ kN$$

Capacity of T-stub according to EN 1993-1-8

$$F_{T.Rd} := min\left(2 \cdot F_{T.single.Rd}, F_{T.combined.Rd}\right) = 159.981\ kN$$

II

Appendix

Calculation - T-stub Benchmark 2

Master Thesis:
Recommendations for finite element modelling of bolted T-stubs in tension

3/5 -2019
Felix Dubrefjord
Ole Netek

Design of ultimate capacity for T-stub according to EN 1993-1-8

Benchmark 2

- C. Gantes *"Influence of equivalent bolt length in finite element modeling of T-stub steel connections"*

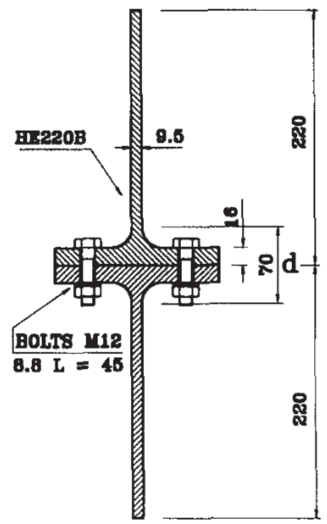

Flange in bending with prying forces,
Lowest value from *EN3-1-8 Table 6.2*
Mode 1: Complete yielding of the flange
Mode 2: Bolt failure with yielding of the flange
Mode 3: Bolt failure

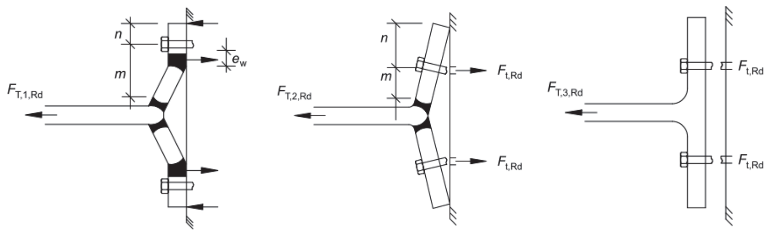

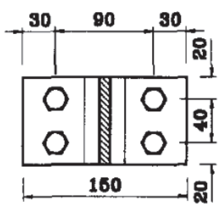

Gantes True stress-strain

Plate yield strength $f_y := 276\ MPa$

Plate ultimate strength $f_u := 642\ MPa$

Bolt yield strength $f_{yb} := 800\ MPa$

Bolt ultimate strength $f_{ub} := 950\ MPa$

Bolt dimensions

Hole diameter M12 $d_0 := 13\ mm$

Effective thread area [DIN 931] $A_s := 84.30\ mm^2$

Bolt head diameter [DIN 931] $d_w := 21.1\ mm$

Effective diameter of bolt $d := 2\sqrt{\dfrac{A_s}{\pi}} = 10.36\ mm$

Distance from bolt center to plastic hinge $e_w := \dfrac{d_w}{4} = 5.275\ mm$

Plate dimensions

Distance between holes $w := 90\ mm$

Width flange $b_p := 150\ mm$

Thickness flange $t_f := 16\ mm$

Thickness web $t_w := 9.5\ mm$

Radius, web and flange $r := 18\ mm$

Distance to end $e_1 := \dfrac{b_p - w}{2} = 30\ mm$

Distance to edge, transverse $e_2 := 20\ mm$

Distance between bolt-rows $p := 40\ mm$

INACTIVE:
For geometrical study, the following parameters are changed:

$t_f := 10\ mm$ $t_f := 13\ mm$ thickness

$e_1 := 20$ $e_1 := 40$ n-distance

By chaning b_p = 130, 170

$w := 70\ mm$ $w := 110\ mm$ m-distance

$b_p := 130\ mm$ $b_p := 170\ mm$

Still e_1 =30

Check of edge distances [EN 1993-1-8 Table 3.3]

$e_{min.edge} := 1.2 \cdot d_0 = 15.6\ mm$
$e_{min.bolt.x} := 2.2 \cdot d_0 = 28.6\ mm$
$e_{min.bolt.y} := 2.4 \cdot d_0 = 31.2\ mm$

$e_{max.edge} := 4 \cdot t_f + 40\ mm = 104\ mm$
$e_{max.bolt.x} := min\left(200\ mm, 14 \cdot t_f\right) = 200\ mm$
$e_{max.bolt.y} := min\left(200\ mm, 14 \cdot t_f\right) = 200\ mm$

$e_{min.edge} < e_1 = 1$

$e_{min.edge} < e_2 = 1$

$e_{min.bolt.y} < p = 1$

$e_{max.edge} \geq e_1 = 1$

$e_{max.edge} \geq e_2 = 1$

$e_{max.bolt.y} \geq p = 1$

Capacity one bolt row

EN3-1-8 Table 6.2, 6.4
- 1 bolt row
Column flange bending

Bolt distances

Figure 6.2; Distance from camfer/ fillet to center hole $\quad m := \dfrac{w - t_w - 2 \cdot 0.8 \cdot r}{2} = 25.85\ mm$

Figure 6.8; Shortest distance to outer edge in load direction $\quad e_{min} := min\left(e_1\right) = 30\ mm$

Figure 6.8; e is the same as e_1 $\quad e := e_1 = 30\ mm$

Table 6.2; Distance to plastic hinge $\quad n := min\left(e_{min}, 1.25 \cdot m\right) = 30\ mm$

Effective length for END bolt row; Bolts act individually

Table 6.4; Circular patterns $\quad l_{eff.cp} := min\left(2 \cdot \pi \cdot m, \pi \cdot m + 2 \cdot e_1\right)$

Table 6.4; Non-circular patterns $\quad l_{eff.nc} := min\left(4 \cdot m + 1.25 \cdot e, 2 \cdot m + 0.625 \cdot e + e_1\right)$

Mode 1 $\quad l_{eff.1} := min\left(l_{eff.cp}, l_{eff.nc}\right) = 100.45\ mm$

Mode 2 $\quad l_{eff.2} := l_{eff.nc} = 100.45\ mm$

Partial safety factor for connections [EN1993-1-8 Table 2.1] $\gamma_{M2} := 1.25$

Table 6.2; Moment capacity $M_{pl.1.Rd} := \dfrac{l_{eff.1} \cdot t_f^{\ 2} \cdot f_y}{4 \cdot \gamma_{M2}} = 1.419\ kN \cdot m$

Table 6.2; Moment capacity $M_{pl.2.Rd} := \dfrac{l_{eff.2} \cdot t_f^{\ 2} \cdot f_y}{4 \cdot \gamma_{M2}} = 1.419\ kN \cdot m$

Table 3.4; Bolts not countersunk $k_2 := 0.9$

Table 3.4; Tension resistance for one bolt $F_{t.Rd} := \dfrac{k_2 \cdot f_{ub} \cdot A_s}{\gamma_{M2}} = 57.661\ kN$

Amount of bolts in active row $n_{bolt} := 2$

Table 3.4 Punching shear per bolt $B_{p.Rd} := \dfrac{0.6 \cdot \pi \cdot d_w \cdot t_f \cdot f_u}{\gamma_{M2}} = 326.835\ kN$

Failure modes from Table 6.2

Flange yielding $F_{T.1.Rd} := \dfrac{(8 \cdot n - 2 \cdot e_w) \cdot M_{pl.1.Rd}}{2 \cdot m \cdot n - e_w \cdot (m + n)} = 259.234\ kN$

Combined failure $F_{T.2.Rd} := \dfrac{2 \cdot M_{pl.2.Rd} + n \cdot \sum_{i=1}^{n_{bolt}} F_{t.Rd}}{m + n} = 112.778\ kN$

Bolt failure $F_{T.3.Rd} := \sum_{i=1}^{n_{bolt}} F_{t.Rd} = 115.322\ kN$

Critical load; Combined failure

$$F_{T.single.Rd} := min\left(F_{T.1.Rd}, F_{T.2.Rd}, F_{T.3.Rd}\right) = 112.778\ kN$$

$$B_{p.Rd} \cdot n_{bolt} = 653.67\ kN$$

Can be applied for both bolt row 1 and 2 separately
---> Check combined

Combined row 1 & row 2

EN3-1-8 Table 6.2, 6.4
- 2 bolt rows
Column flange bending

Bolt distances

Figure 6.2; Distance from plastic hinge to center hole $m=25.85\ mm$

Table 6.2; Distance from end of plate to center hole $n=30\ mm$

Thickness of flange $t_f=16\ mm$

Figure 6.10; Distance between bolt-row holes $p=40\ mm$

Figure 6.8; e is the same as e_1 $e:=e_1=30\ mm$

Figure 6.8; Shortest distance to outer edge in load direction $e_{min}:=min\left(e_1\right)=30\ mm$

Effective length for END bolt row; Bolts act in group

Table 6.4; Non-circular patterns $l_{eff.nc}:=min\left(2\cdot m+0.625\cdot e+0.5\cdot p,e_1+0.5\cdot p\right)$

Table 6.4; Circular patterns $l_{eff.cp}:=min\left(\pi\cdot m+p,2\cdot e_1+p\right)$

Effective length for row 2 is the same as row 1

Table 6.4; Non-circular $\sum_{i=1}^{2} l_{eff.nc}=100\ mm$

Table 6.4; Circular $\sum_{i=1}^{2} l_{eff.cp}=200\ mm$

Mode 1 $l_{eff.1} := min\left(\sum_{i=1}^{2} l_{eff.nc}, \sum_{i=1}^{2} l_{eff.cp}\right) = 100\ mm$

Mode 2 $l_{eff.2} := \sum_{i=1}^{2} l_{eff.nc} = 100\ mm$

Partial safety factor for connections [EN1993-1-8 Table 2.1] $\gamma_{M2} := 1.25$

Table 6.2; Moment capacity $M_{pl.1.Rd} := \frac{l_{eff.1} \cdot t_f^{\ 2} \cdot f_y}{4 \cdot \gamma_{M2}} = 1.413\ kN \cdot m$

Table 6.2; Moment capacity $M_{pl.2.Rd} := \frac{l_{eff.2} \cdot t_f^{\ 2} \cdot f_y}{4 \cdot \gamma_{M2}} = 1.413\ kN \cdot m$

Table 3.4; Bolts not countersunk $k_2 := 0.9$

Table 3.4; Tension resistance for one bolt $F_{t.Rd} := \frac{k_2 \cdot f_{ub} \cdot A_s}{\gamma_{M2}} = 57.661\ kN$

Amount of bolts in active row $n_{bolt} := 4$

Table 3.4 Punching shear per bolt $B_{p.Rd} := \frac{0.6 \cdot \pi \cdot d_w \cdot t_f \cdot f_u}{\gamma_{M2}} = 326.835\ kN$

Failure modes from Table 6.2

Flange yielding $F_{T.1.Rd} := \frac{(8 \cdot n - 2 \cdot e_w) \cdot M_{pl.1.Rd}}{2\ m \cdot n - e_w \cdot (m + n)} = 258.073\ kN$

Combined failure $F_{T.2.Rd} := \frac{2 \cdot M_{pl.2.Rd} + n \cdot \sum_{i=1}^{n_{bolt}} F_{t.Rd}}{m + n} = 174.496\ kN$

Bolt failure $F_{T.3.Rd} := \sum_{i=1}^{n_{bolt}} F_{t.Rd} = 230.645\ kN$

Critical load; Combined column flange bending

$$F_{T.combined.Rd} := min\left(F_{T.1.Rd}, F_{T.2.Rd}, F_{T.3.Rd}\right) = 174.496\ \boldsymbol{kN}$$

$$B_{p.Rd} \cdot n_{bolt} = 1307.34\ \boldsymbol{kN}$$

Capacity of T-stub according to EN 1993-1-8

$$F_{T.Rd} := min\left(2 \cdot F_{T.single.Rd}, F_{T.combined.Rd}\right) = 174.496\ \boldsymbol{kN}$$

III
Appendix

Calculation - Effective bolt length and thread stripping load

Master Thesis:
Recommendations for finite element modelling of bolted T-stubs in tension

7/5 - 2019
Felix Dubrefjord
Ole Netek

Calculation of Agerskov's effective bolt length
[C. Gantes , *"Influence of equivalent bolt length in finite element modeling of T-stub steel connections"*]

Calculation of bolt thread stripping load
[O. Bursi , *"Benchmarks for Finite Element Modelling of Bolted Steel Connections"*]

Gross cross-sectional area of bolt $A_b := (6 \cdot 6 \cdot \pi)\ mm^2 = 113.097\ mm^2$

Effective cross-sectional area of bolt
[Nodic Fastening Group] $A_s := 84.30\ mm^2$

Dimensions for Agerskovs models are taken based on standard DIN 931 and DIN 934

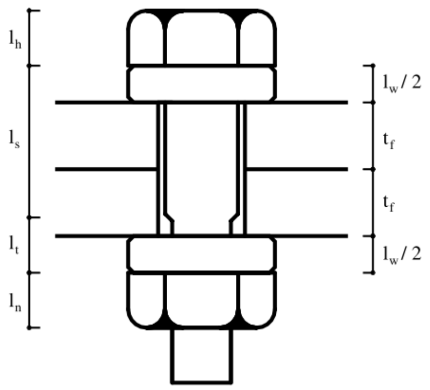

Inative regions, activate right model

Benchmark IPE300

$Model := \text{"IPE300"}$
$l_w := 5\ mm$
$l_s := (55 - 30)\ mm$
$l_t := ((2 \cdot 2.5 + 2 \cdot 10.7)\ mm - l_s) = 1.4\ mm$
$l_n := 10\ mm$
$f_{yb} := 900\ MPa$

Benchmark HEB220

$Model := \text{"HEB220"}$
$l_w := 2.5\ mm$
$l_s := (45 - 30)\ mm$
$l_t := ((1 \cdot 2.5 + 2 \cdot 16)\ mm - l_s) = 19.5\ mm$
$l_n := 10\ mm$
$f_{yb} := 800\ MPa$

Parameters, bolt geometry $K_1 := l_s + 1.43 \cdot l_t + 0.71 \cdot l_n = 49.985\ mm$

Parameters, bolt geometry $K_4 := 0.1 \cdot l_n + 0.2 \cdot l_w = 1.5\ mm$

Effective bolt length $L_{bolt} := \frac{A_s}{A_b} \cdot (K_1 + 2 \cdot K_4) = 39.494\ mm$

Symmetric half $L_{bolt.SYM} := \mathrm{Ceil}\left(\frac{L_{bolt}}{2}, 1\ mm\right) = 20\ mm$

Bolt thread failure
DIN931 - M12 characteristics

Thread pitch $p := 1.75\ mm$

Effective thread dimater $d_1 := \sqrt{\left(\frac{A_s}{\pi} \cdot 4\right)} = 10.36\ mm$

Effective thread height $h := \frac{7}{8}\ p$

Effective shear area ratio $\frac{5}{6}$

Amount of active threads are between 3 and 6 (Giovannozzi, R.) $z := 3$

Bolt stripping load per bolt $B_s := \frac{5}{6} \cdot \frac{f_{yb}}{\sqrt{3}} \cdot h \cdot \pi \cdot d_1 \cdot z = 57.549\ kN$

Summary: Bolt length and thread stripping load

$Model = \text{“HEB220”}$
$L_{bolt.SYM} = 20\ mm$
$4 \cdot B_s = 230.194\ kN$

IV
Appendix

Calculation - Example of infinitesimal strain theory

7/5 -2019
Felix Dubrefjord
Ole Netek

Master Thesis:
Recommendations for finite element modelling of bolted T-stubs in tension

Calculation example of infinitesimal strain teory

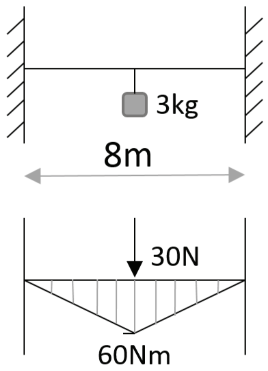

$$\sigma = \frac{N}{A} + \frac{M}{W}$$

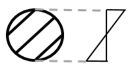

Young's modulus	$E := 210\ GPa$
Span length	$L := 8\ m$
Force from weight	$F := 30\ N = 30\ N$
Moment	$M := \frac{F \cdot L}{4} = 60\ N \cdot m$

Wire properties

Radius of wire	$r := 2.5\ mm$
Cross-sectional area	$A := r \cdot r \cdot (\pi) = 19.635\ mm^2$
Moment of inertia	$I := \frac{1}{4} \cdot \pi \cdot r^4 = \left(3.068 \cdot 10^{-11}\right)\ m^4$
Flexural strength	$W := \frac{I}{r} = 12.2718\ mm^3$
Yield strength	$f_y := 355\ MPa$
Ultimate strength	$f_u := 490\ MPa$

Without changing geometry, these are the results

Stress from load taken by bending moment	$\sigma := \frac{M}{W} = 4889.24\ MPa$
Utilization ratio of ultimate strength	$\frac{\sigma}{f_u} = 9.978$
Deflection	$\delta := \frac{F \cdot L^3}{192 \cdot E \cdot I} = 12.417\ m$

However, if load is simply hung vertically in two wires
i.g. taken by normal force.

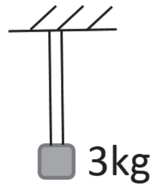

$$\sigma := \frac{30\ N}{2 \cdot A} = 0.764\ MPa \qquad \frac{\sigma}{f_u} = 0.002$$

Non-linear geometry lets the deflection change loading from moment to normal force until equilibrium